KTH Electrical Engineering

Control of Dynamically Assisted Phase-shifting Transformers

Nicklas Johansson

Royal Institute of Technology
School of Electrical Engineering
Division of Electrical Machines and Power Electronics

Stockholm 2008

Submitted to the School of Electrical Engineering in partial fulfillment of
the requirements for the degree of Licentiate.

Stockholm 2008

ISBN 978-91-7178-879-5
ISSN 1653-5146
TRITA–EE 2008:008

This document was prepared using LaTeX.

Preface

The work presented in this thesis was carried out at the Division of Electrical Machines and Power Electronics, School of Electrical Engineering, Royal Institute of Technology (KTH). This project is financed from the Elforsk ELEKTRA foundation.

The main contributions of this work can be summarized as follows:

- A simple generic system model comprising only two rotating machines has been proposed to serve as a basis for control design for Controlled Series Compensators (CSC) and Dynamic Power Flow Controllers (DPFC) for power oscillation damping and power flow control in power grids susceptible to oscillations of one dominating frequency mode.

- Estimation routines for estimation of the system model parameters using the step response in the locally measured line power when a series reactance change is executed at the FACTS device have been derived.

For a power system which can be accurately described by the proposed system model it has been shown that:

- Damping of inter-area oscillations of the above type can be achieved by insertion of a series reactance in one discrete step at a suitable location in the power system at a carefully selected time instant determined from the locally measured line power. The necessary step reactance magnitude can be determined with knowledge of the generic system model parameters.

- It is possible to achieve damping of all inter-area power oscillations and determine the power flow on the FACTS line by extending the controller to modify the line reactance in two discrete steps separated in time.

The above results have lead to that:

- An adaptive time-discrete Model Predictive Controller (MPC) for power oscillation damping and power flow control intended for control of CSC and DPFC has been designed and verified by means of time-domain simulation of power systems with different complexities with good results.

Abstract

In this thesis, controllers for power oscillation damping, transient stability improvement and power flow control by means of a Controlled Series Compensator (CSC) and and a Dynamic Power Flow Controller (DPFC) are proposed. These devices belong to the group of power system components referred to as Flexible AC Transmission System (FACTS) devices. The developed controllers use only quantities measured locally at the FACTS device as inputs, thereby avoiding the risk of interrupted communications associated with the use of remote signals for control.

For power systems with one dominating, poorly damped inter-area power oscillation mode, it is shown that a simple generic system model can be used as a basis for damping- and power flow control design. The model for control of CSC includes two synchronous machine models representing the two grid areas participating in the oscillation and three reactance variables, representing the interconnecting transmission lines and the FACTS device. The model for control of DPFC is of the same type but it also includes the phase shift of the internal phase-shifting transformer of the DPFC.

The key parameters of the generic grid models are adaptively set during the controller operation by estimation from the step responses in the FACTS line power to the changes in the line series reactance inserted by the FACTS device. The power oscillation damping controller is based on a time-discrete, non-linear approach which aims to damp the power oscillations and set the desired power flow on the FACTS line by means of two step changes in the line reactance separated in time by half an oscillation cycle.

A verification of the proposed controllers was done by means of digital simulations using power system models of different complexities. The CSC

and DPFC controllers were shown to significantly improve the small-signal- and transient stability in one four-machine system of a type commonly used to study inter-area oscillations. The CSC controller was also tested for 18 different contingencies in a 23-machine system, resulting in an improvement in both the system transient stability and the damping of the critical oscillation mode.

Keywords

- Thyristor Controlled Series Compensator
- Thyristor Switched Series Compensator
- Controlled Series Compensator
- Dynamic Power Flow Controller
- Phase-Shifting Transformer
- Power Oscillation Damping
- Transient Stability
- Power Flow Control
- Adaptive Control

Acknowledgement

Many people have a part in this work. First of all, my advisors, Prof. Hans-Peter Nee and Prof. Lennart Ängquist should be thanked for supporting my thesis work. Hans-Peter has helped me to refine my ideas during the course of my work and he has encouraged me many times with his positive attitude. He has allowed me to work independently at the location of my choice, which was essential for the progress of my work. Lennart has devoted generous amounts of his time at KTH to discussions with me. His knowledge in the field of FACTS has been of great importance numerous times during the process of my work.

Many thanks also to all the staff at EME and EPS and all of the colleague Ph.D. students for contributing to the nice atmosphere at the department.

Outside of KTH, Bertil Berggren at ABB Corporate Research should be thanked for patiently answering my questions and Peter Lundberg at ABB FACTS receives gratitude for his support during the project. Thanks also to Tomas Jonsson at ABB Corporate Research for getting me involved in the project.

Sincere gratitude goes to my family, Josefin and Julia, for immense support during the ups and downs of the project.

Last, but not least, Elforsk and the Elektra foundation should be thanked for financial support.

Nicklas Johansson

Stockholm, December, 2007

Contents

1 Introduction **1**
- 1.1 Scope of the thesis . . . 2
- 1.2 Terminology . . . 3
- 1.3 List of publications . . . 4
- 1.4 Outline of the thesis . . . 5

2 Mathematical Modeling of Power Systems **7**
- 2.1 Classical model for a single-machine system . . . 8
- 2.2 Classical model for a multiple-machine system . . . 10
- 2.3 Structure preserving model for a multiple-machine system . . . 13
- 2.4 The dynamics of the power system . . . 15
- 2.5 Stability of the power system . . . 16
  - 2.5.1 Frequency instability . . . 17
  - 2.5.2 Transient instability . . . 17
  - 2.5.3 Voltage instability . . . 18
  - 2.5.4 Small-signal instability . . . 19

3 FACTS devices and their control **21**
- 3.1 Power electronic converters . . . 21
- 3.2 Shunt-connected FACTS devices . . . 22
- 3.3 Series-connected FACTS devices . . . 23
- 3.4 Combined shunt- and series-connected FACTS devices . . . 27
- 3.5 Previous work on control issues for PST and TCSC/TSSC . . . 29
  - 3.5.1 Phase-shifting transformers . . . 30
  - 3.5.2 Thyristor Controlled - and Thyristor Switched Series Capacitors . . . 36

4 System identification **43**
- 4.1 System model for control of CSC . . . 44

4.1.1 Power flow control by means of CSC 44
4.1.2 System model 46
4.1.3 Theory 49
4.1.4 Parameter estimation 55
4.1.5 Estimation of the power oscillation mode characteristics 58
4.1.6 Estimation of the parameter X_{eq} 60
4.1.7 Estimation of the parameter X_i 62
4.2 System model for control of a DPFC 63
4.2.1 Power flow control by means of a DPFC 63
4.2.2 System model 64
4.2.3 Parameter estimation 65

5 Principles for control of CSC **69**
5.1 Power oscillation damping and fast power flow control 69
5.1.1 Power oscillation damping in one time-step 69
5.1.2 Power oscillation damping and power flow control in two time-steps 74
5.1.3 Combining parameter estimation and power oscillation damping 78
5.2 Transient Stability Improvement 79
5.2.1 Proposed transient stability improvement strategy . . 84
5.3 The general control approach 90

6 Principles for control of the DPFC **93**
6.1 Power oscillation damping and fast power flow control 94
6.2 Transient stability improvement 96
6.3 The general control approach 96

7 Results and discussion **99**
7.1 Test systems 99
7.1.1 Four-machine system 99
7.1.2 Twenty-three machine system 101
7.2 CSC controller results 103
7.2.1 Controller implementation 103
7.2.2 Simulation results 109
7.3 DPFC controller results 129
7.3.1 Controller implementation 129

7.3.2 Simulation results 130

8 Conclusions and future work **139**

References **143**

A Parameter estimation in the DPFC system model **147**
A.1 Estimation of the parameter X_{eq} 147
A.2 Estimation of the parameter X_i 149

B Derivation of the control law in the DPFC system model **153**

List of Acronyms **157**

List of Symbols **159**

1 Introduction

Not very long ago, the operation of a transmission grid was relatively straight-forward. The grid was designed to supply electrical energy to the consumers in the country where it was built and to support the neighboring countries occasionally, in times of need. Large cross-border transmission capability was not necessary, since most of the electrical energy used in the country was supplied nationally. However, major changes in how transmission systems are operated came with the deregulation of the electricity market in recent years. Now, the power flows go from producer A to consumer B, not necessarily located in the same country. A and B have signed a deal that states that B buys a certain amount of energy from A:s production. The contractual path of the electricity is a straight line from A to B while the physical path of the power flow can be a number of parallel power flows which may flow in different countries. Since the national power grids were not designed for these parallel flows, some lines will get overloaded in the process, limiting the national power flows.

The phenomenon of loop power flows leads to power lines being operated closer to their stability limits and results in a power system which may be operated far from its optimal state in terms of losses and security margins. Such a system may for example be more prone to inter-area power oscillations and have a smaller margin to transient instability in some N-1 fault cases.

The construction of new power lines to relieve the overloaded ones is very expensive, time-consuming and often complicated by legal and land proprietary issues. Fortunately, the advances in power electronics offer new solutions to the problems. Many Flexible AC Transmission (FACTS) devices have been introduced in the last decades. These are devices which can be used to control power flows and improve the stability in a power grid by

for example injecting reactive power in selected nodes, modifying the line impedance for critical lines or shifting the voltage phase angles at certain nodes. These devices are based on high-power electronic devices like the thyristor and the Insulated Gate Bipolar Transistor (IGBT).

This thesis concerns the control of a novel FACTS device recently introduced by ABB under the name of Dynamic Flow Controller (DynaFlow). In this work the device is also referred to as Dynamic Power Flow Controller (DPFC). The device is actually a combination of two previously known devices: the Phase-Shifting Transformer (PST) and the Thyristor Switched Series Capacitor (TSSC) or the Thyristor Switched Series Reactor (TSSR). The PST is a slow device which can control active power flow on a line whereas the TSSC is a power flow controller with a much higher speed of control. These two devices can work together in order to create a very versatile device which can be used for power flow control, power oscillation damping, transient stability improvement, and voltage stability/recovery improvement. The device is believed to be cheaper than other FACTS devices with a similar functionality, like for example the Unified Power Flow Controller (UPFC).

Since a natural control design approach for the DPFC is to start with the design of a controller for the dynamic TSSC part of the device alone, the thesis will also include controller design and verification for a generic Controlled Series Compensator (CSC) device which may for example be a Thyristor Controlled Series Capacitor (TCSC) or a stand-alone TSSC.

1.1 Scope of the thesis

This work is concentrated on the functions provided by the TSSC part of the DPFC. Most of the work has been towards developing an adaptive controller for Power Oscillation Damping (POD) and power flow control. The equations governing the dynamics of the power system are non-linear and the structure of the power system is commonly not known in detail when a fault has occurred. This means that the design of a POD controller is a

challenge and a controller which can adapt to the current situation in the power grid is thus attractive.

The work has yielded a controller which can be used for control of DPFC as well as for controlling other CSC devices. The controller uses only locally available signals at the DPFC or CSC location as inputs, thereby eliminating the need for long-distance communication of control signals.

The system model for the controller has been chosen as simple as possible in order to gain knowledge of the basic relations governing control of DPFC and CSC in a power system with many unknown parameters. Also, a simple system model with few unknown parameters simplifies the implementation of the controller in a power system. The model is restricted to work for systems which exhibit one dominating (poorly damped) inter-area power oscillation mode since this is a common situation in power systems where supplementary damping is required. The system model for the DPFC has been designed to include a simple model of the PST since the phase shift of the PST has a large influence on the controllability and observability of the power oscillation mode from the DPFC location. Additionally, transient (first-swing) stability improvement by means of the CSC or the DPFC is discussed and a transient controller for the devices is included in the proposed main controller structure.

1.2 Terminology

In this thesis, controlled series compensation of transmission lines is discussed. Throughout the thesis, the term "reactance" referring to the imaginary part of an impedance variable will be used as a positive number if the reactance is inductive and a negative number if the reactance is capacitive. If a capacitor with the reactance X_C is inserted in series with a transmission line with reactance X_L, the effective reactance of the line will be decreased, $X_{Eff} = X_L + X_C$. This will be referred to as "increasing the level of compensation", "increasing the degree of compensation", or simply "increasing the (series) compensation of the line". Conversely, if a capacitor which was connected in series with a line is bypassed, it will be referred to as "decreas-

ing the level of compensation", "decreasing the degree of compensation", or simply "decreasing the (series) compensation of the line". For a controlled series compensator, "inserting a capacitive reactance step" means a step-wise increase in the level of compensation and "inserting an inductive reactance step" means a step-wise decrease in the level of series compensation. The degree of compensation, k is defined as $k = -X_C/X_L$, and it is usually expressed in per cent.

In the thesis, variables that denote the "average" active power transmitted on a transmission line or between two grid areas are frequently used. In this context, "average" means the average of the three-phase active power averaged over a full cycle of the dominating power oscillation mode. Variables denoting the "instantaneous" transmitted active power are also used. Here, "instantaneous" power refers to the the three-phase active power which flows through the transmission line or lines at a certain instant in time.

Damping of power oscillations is discussed in the text. A measure of the damping of a certain mode of power oscillation can be found from the eigenvalues of the linearized power system equations. If the real part σ of the eigenvalues corresponding to a the mode of electro-mechanical oscillations is negative, power oscillations of this frequency are likely to settle down. This is referred to as a system with "positive damping" of the oscillatory mode in the text. If, on the other hand, the real part of the eigenvalues is positive, the power oscillations are likely to grow indefinitely and the system is then said to exhibit small-signal instability with a "negative damping" of the oscillatory mode.

1.3 List of publications

Many of the results presented in this thesis have previously been published in the following papers:

1. N. P. Johansson, H-P. Nee and L. Ängquist, "Estimation of Grid Parameters for The Control of Variable Series Reactance FACTS Devices", Proceedings of 2006 IEEE PES General Meeting

2. N. P. Johansson, H.-P. Nee and L. Ängquist, "Discrete Open Loop Control for Power Oscillation damping utilizing Variable Series Reactance FACTS Devices", Proceedings of the Universities Power Engineering Conference, Newcastle, UK, September 2006

3. N. P. Johansson, H.-P. Nee and L. Ängquist, "An Adaptive Model Predictive Approach to Power Oscillation Damping utilizing Variable Series Reactance FACTS Devices", Proceedings of the Universities Power Engineering Conference, Newcastle, UK, September 2006

4. N. P. Johansson, L. Ängquist and H.-P. Nee, "Adaptive Control of Controlled Series Compensators for Power System Stability improvement", Proceedings of IEEE PowerTech 2007, July 2007

5. N. P. Johansson, L. Ängquist, B. Berggren and H.-P. Nee, "A Dynamic Power Flow Controller for Power System Stability Improvement and Loss Reduction", Submitted to Power System Computations Conference, July 2008

These papers are also included in the thesis for reference.

1.4 Outline of the thesis

Chapter 2 introduces common modeling techniques for studies of power system dynamics.

Chapter 3 gives examples of common FACTS devices and reviews earlier work in the field of CSC and PST control.

Chapter 4 introduces the system models used for design of the CSC and DPFC controllers and derives relations for parameter estimation.

Chapter 5 introduces the proposed approach of CSC control including power oscillation damping, power flow control principles, and transient stability improvement.

Chapter 6 introduces the proposed approach to DPFC control for power oscillation damping, power flow control, and transient stability improvement.

Chapter 7 includes the verification of the CSC and DPFC controllers by means of digital simulation.

Chapter 8 concludes the results and discusses possible future work.

2 Mathematical Modeling of Power Systems

In this chapter, a brief introduction to modeling of power system dynamics is given. The aim of the chapter is to review the basics necessary for understanding the approaches to system modeling and power oscillation damping described in this thesis. It is assumed that the reader is familiar with standard static load flow analysis. This topic can for example be studied in [1].

A power system consists of many different types of elements. Some of these are purely passive, like resistances, capacitances and inductances and others, like rotating machines and FACTS devices are highly complex, dynamic, and controlled devices.

A model used to describe power system dynamics usually includes the following elements:

- Synchronous machines - These are typically generator models which may include models of exciters, Automatic Voltage Regulators (AVR) and Power System Stabilizers (PSS).

- Transmission lines - These are commonly modeled as inductive elements with shunt capacitors connected at each node (a so-called π-model) to represent the distributed capacitances to ground but also more detailed models with distributed capacitances are used. The resistance of the lines may or may not be included in the model.

- Loads - These are commonly divided into active power loads and reactive power loads. These may or may not have a voltage dependence and/or a frequency dependence.

The level of detail included in a model is dependent on what the model is intended for. In a simulator, very detailed models may be used thanks to the advances in computer technology. In contrast, when a model is used as a basis for control design, a less detailed modeling approach may be adopted in order to simplify the control design or due to a limitation in computational power of the implementation platform. In the following sections, two different modeling approaches will be briefly reviewed.

In the the following, the per unit system is generally assumed to be used for expressing voltages, currents, power and impedances. We will consider only balanced (symmetrical) operation of the power systems and one-line diagrams are used to describe the three-phase systems.

2.1 Classical model for a single-machine system

The basic equations of motion for a single synchronous generator connected to an infinite bus as the system shown in Fig. 2.1 can be written as [2]:

$$\frac{2H}{\omega_0}\frac{d\omega}{dt} + D\omega = P'_m - P'_e \tag{2.1}$$

with the variables
θ = rotor angle relative to a synchronously rotating reference frame [rad],
$\omega = \frac{d\theta}{dt}$=angular frequency for rotor oscillations relative to synchronously rotating reference frame [rad/s],
H = constant of inertia [s], and the parameters
ω_0 = nominal electrical angular frequency [rad/s],
D = damping constant [p.u./(rad/s)],
P'_m = mechanical power at turbine [p.u.],
P'_e = electrical power from generator [p.u.].

The constant of inertia corresponds to the ratio between the kinetic energy W_{kin} of the machine and turbine at nominal speed and the nominal power

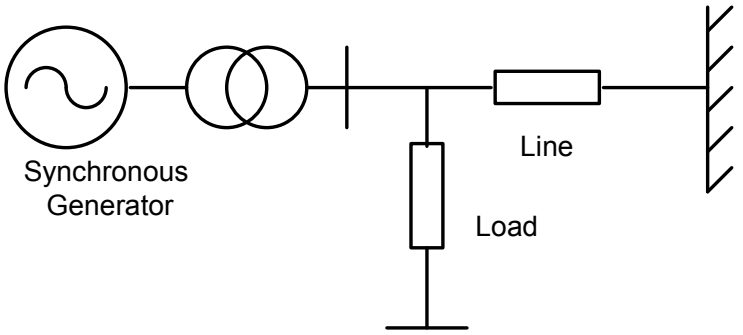

Figure 2.1: Synchronous generator connected to an infinite bus.

rating of the machine S_N,

$$H = \frac{W_{kin}}{S_N} = \frac{\frac{1}{2}\omega_{0m}^2 J}{S_N} \tag{2.2}$$

with J denoting the combined moment of inertia of generator and turbine and ω_{0m} the rated mechanical angular velocity of the machine.

In the derivation of Eq. 2.1 it was assumed that the electrical frequency of the system only deviates by small oscillations around the nominal frequency. In order to simplify the solution of Eq. 2.1 some assumptions are commonly introduced.

- The damping is neglected, that is D is set to zero.
- The mechanical power P'_m is assumed to be constant. This is plausible if the we are interested in events which happen within a time-scale of a few seconds.
- The synchronous machine is modeled as a constant voltage source behind a reactance. This reactance is usually set equal to the machine transient reactance x'_d.
- The power flow in the system is assumed to be governed by the static load flow equations.

If the load at the generator node in Fig. 2.1 is neglected and the transmission line to the infinite bus is represented as one reactance x_l, neglecting losses and shunt capacitances, the equations of motion can be written:

$$\dot{\omega} = \frac{\omega_0}{2H}(P'_m - \frac{EU}{x'_d + x_l}\sin(\theta)) \tag{2.3}$$

$$\dot{\theta} = \omega \tag{2.4}$$

Here, the voltage phasor at the generator is given as $E\angle\theta$ and the infinite bus voltage phasor is given as $U\angle 0$. The magnitudes of these voltages are assumed to be constant. Equations 2.3 and 2.4 form a system of differential equations which can be solved analytically or, more conveniently using numerical methods. The equal-area criterion [2] can be used in order to determine whether the system is transiently stable or not, given a set of initial conditions and the nature of the fault. The right hand side of Eq. 2.3 governs the system behavior after a disturbance. The stationary solution to the system of equations is given when P'_m equals P'_e. The dynamical solutions are either sinusoidal oscillations in θ and ω, so called electro-mechanical oscillations, or the angle θ grows towards infinity with time. The first case corresponds to the power oscillations which are very often seen in power systems after a disturbance and the second case results when a serious fault occurs which leads to a loss of synchronism in the system.

2.2 Classical model for a multiple-machine system

The mathematical model for the single-machine system given in the previous section is naturally of limited value when real power systems are considered. Its value lies in illustrating the principles of operation of the power system and it may be used for simplified calculations. In this section, the mathematical model is extended to include a power system with multiple machines and loads [2]. The same assumptions as in the simple case are made with the addition that the loads are considered as impedances which represent the load before the disturbance. A schematic picture of the power system is shown in Fig. 2.2.

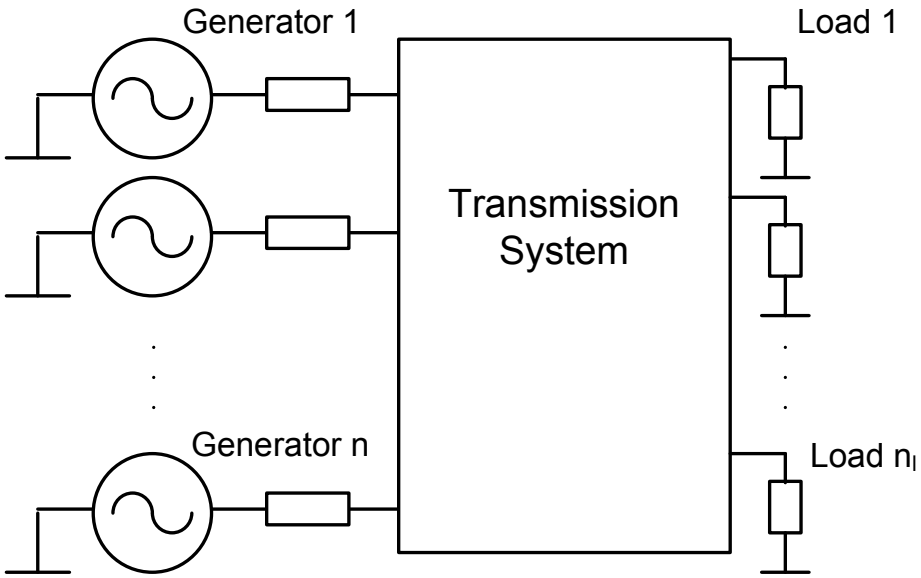

Figure 2.2: Schematic of the multiple machine power system.

The system has n sources and the injected currents at the source nodes are given by

$$\bar{I} = \bar{Y} \cdot \bar{E}, \tag{2.5}$$

with

$$\bar{I} = (\bar{I}_1, \bar{I}_2, ..., \bar{I}_n), \tag{2.6}$$

$$\bar{E} = (\bar{E}_1, \bar{E}_2, ..., \bar{E}_n). \tag{2.7}$$

Here, the admittance matrix with the impedance load representations included is given by $\bar{Y}$ with the elements

$$\bar{Y}_{ij} = Y_{ij} = G_{ij} + jB_{ij}. \tag{2.8}$$

This reduced network matrix (derived in [3]) has the dimensions n x n and describes the power grid and the loads as they appear seen from the inner voltages of the generators. The active power from generator i is given by

$$P'_{ei} = Re(\bar{E}_i \cdot \bar{I}_i^*), \tag{2.9}$$

which can be written as

$$P'_{ei} = Re(\bar{E}_i(\sum_j \bar{Y}_{ij}\bar{E}_j)^*) \tag{2.10}$$

$$= E_i^2 G_{ii} + \sum_{i \neq `j} E_i E_j (B_{ij}\sin(\theta_i - \theta_j) + G_{ij}\cos(\theta_i - \theta_j)). \tag{2.11}$$

Here, the voltage phase angles for the generator internal voltages have been introduced as θ_1 ... θ_n. The equations of motion for the whole system can now be written as

$$\dot{\omega}_i = \frac{\omega_0}{2H_i}(P'_{mi} - P'_{ei}) \tag{2.12}$$

$$\dot{\theta}_i = \omega_i. \tag{2.13}$$

where P'_{ei} is defined by Eq. 2.11. This system of equations now consists of $2n$ coupled differential equations of the first order. The system can be described by introducing the state vector

$$x = (\theta_1,...,\theta_n, \omega_1,...,\omega_n)^T, \tag{2.14}$$

which satisfies the differential equation

$$\dot{x} = f(x). \tag{2.15}$$

Solving Eq. 2.15 for systems with more than two generators is complicated and the problem is often simplified by linearizing the system around one operating point x_0. The linearized system equations are given by

$$\Delta\dot{x} = \frac{\partial f}{\partial x}\Delta x \tag{2.16}$$

with the Jacobian matrix $\frac{\partial f}{\partial x}$ whose elements are given by

$$\left(\frac{\partial f}{\partial x}\right)_{ij} = \frac{\partial f_i}{\partial x_j}. \tag{2.17}$$

The solution to the linearized system is determined by the eigenvalues and eigenvectors of the jacobian matrix. The eigenvalues give information

of the participating power oscillation mode frequencies in the system when it is subject to a disturbance. There are $n-1$ modes of electromechanical oscillation in a power system with n machines.

The model of a system with several machines may also be simplified further by neglecting the line and load resistances.

2.3 Structure preserving model for a multiple-machine system

In many cases the classical model for the generator does not have the sufficient complexity to describe the dynamics of the machine. This is for example the case when the aim is to study the impact of PSS on a power grid. In such a case, a model like the Structure Preserving Model (SPM) can be applied. This model includes the dynamics governing the internal EMF of the machine. It also allows the loads in the power system to be modeled as general voltage dependent loads with characteristics differing from the pure impedance type. The load at each node is then given by its active and reactive power components

$$P_L = P_{L0}\left(\frac{U_L}{U_{L0}}\right)^{mp} \tag{2.18}$$

$$Q_L = Q_{L0}\left(\frac{U_L}{U_{L0}}\right)^{mq} \tag{2.19}$$

with P_{L0}/Q_{L0} and U_{L0} as the nominal active/reactive power and voltage, U_L the actual node voltage and the exponents mp and mq which are individually specified for each node. The transmission lines are assumed to be lossless in this model which gives the admittance matrix for the system defined by

$$\bar{Y}_{kl} = Y_{kl} = G_{kl} + jB_{kl} = jB_{kl}. \tag{2.20}$$

Note that the loads are not included in this admittance matrix.

Now, assume that the system has n generators and a total of N nodes. The loads may be distributed in any of these nodes. The voltage at each

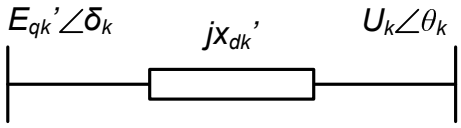

Figure 2.3: Synchronous generator model circuit.

node is given by $U_k\angle\theta_k$. The voltage at the generator internal bus is given by $E'_{qk}\angle\delta_k$ and the circuit model for the generator is depicted in Fig. 2.3. Here, the reactance of the k:th generator transformer should be included in x'_{dk}.

The dynamics of the k:th generator is then for $k = 1...n$ given by

$$\dot{\delta}_k = \omega_k \tag{2.21}$$

$$\dot{\omega}_k = \tfrac{1}{M_k}\left(P'_{mk} - \tfrac{E'_{qk}U_k}{x'_{dk}}\sin(\delta_k - \theta_k)\right) \tag{2.22}$$

$$\dot{E}'_{qk} = \tfrac{1}{T'_{dok}}\left(E_{fk} - \tfrac{x_{dk}}{x'_{dk}}E'_{qk} + \tfrac{x_{dk}-x'_{dk}}{x'_{dk}}U_k\cos(\delta_k - \theta_k)\right), \tag{2.23}$$

introducing the synchronous machine variables M_k=$2H_k/\omega_0$, T'_{do} is the d-axis transient open-circuit time constant, E_{fk} is an EMF proportional to the field voltage and x_{dk} is the machine stationary reactance with the k:th transformer reactance included [3].

It can also be shown that [4] the active and reactive power injected into node k in the power system can for $k = 1...n$ be expressed as

$$P_k = \sum_{l=1}^{N} B_{kl}U_kU_l\sin(\theta_k - \theta_l) + \tfrac{E'_{qk}U_k\sin(\theta_k-\delta_k)}{x'_{dk}} \tag{2.24}$$

$$Q_k = -\sum_{l=1}^{N} B_{kl}U_kU_l\cos(\theta_k - \theta_l) + \tfrac{U_k^2-E'_{qk}U_k\cos(\theta_k-\delta_k)}{x'_{dk}}. \tag{2.25}$$

For $k = n + 1...N$ the expressions become

$$P_k = \sum_{l=1}^{N} B_{kl}U_kU_l\sin(\theta_k - \theta_l) \tag{2.26}$$

$$Q_k = -\sum_{l=1}^{N} B_{kl}U_kU_l\cos(\theta_k - \theta_l). \tag{2.27}$$

Let the active and reactive loads at node k be defined as P_{Lk} and Q_{Lk}. For energy conservation, the following must hold for all nodes $k = 1...N$

$$P_k + P_{Lk} = 0 \tag{2.28}$$

$$Q_k + Q_{Lk} = 0. \tag{2.29}$$

Define

$$x = [\delta_1,...,\delta_n,\omega_1,...,\omega_n,E'_{q1},...,E'_{qn}]^T \tag{2.30}$$

$$y = [\theta_1,...,\theta_N,U_1,...,U_N]^T. \tag{2.31}$$

Now, equations 2.21, 2.22, 2.23, 2.28 and 2.29 form a system of equations which can be written

$$\dot{x} = f(x,y) \tag{2.32}$$

$$0 = g(x,y). \tag{2.33}$$

Equations 2.32 and 2.33 form a set of differential-algebraic equations which describe the dynamics of the system. These are most conveniently solved numerically to determine the behavior of the system after a disturbance. To analyze Equations 2.32 and 2.33 analytically, a linearization is commonly used in the same manner as for the classical model in the last section. Calculation of the eigenvalues and eigenvectors of the resulting Jacobian may aid in the design of PSS and controllers for supplementary power oscillation damping devices like for example the TCSC.

2.4 The dynamics of the power system

The eigenvalues of the Jacobian derived from the linearization of the chosen system model indicate the different frequencies present in the solution of the linearized system equations. For a stable power system, all eigenvalues of the state matrix must lie in the left half plane. If one of the modes has a positive real part, the system will exhibit small-signal instability and continuous operation of the system will not be possible.

Any change in the power system variables, like load changes, line disconnections or fault situations results in a system which is not in steady state. In such a case, oscillations will be initiated in the system. These oscillations will be observable in all system variables. Every oscillation frequency however, is not observable to the same extent in all system variables. From the linearized system equations, the observability of each frequency mode in each of the system variables can be calculated [3].

Generally, the modes in the solution corresponding to the eigenvalues which have the largest real parts (hence the lowest damping) are the so-called electro-mechanical oscillations of the system. These are modes which are connected to the oscillation of the voltage phase angles and rotational speed of the different machines in the system. An imbalance in the power flow in the system leads to power oscillations between the synchronous machines in the system. These modes can be classified in local modes which are associated with machines in one power system area with frequencies in the range of 0.7-2.0 Hz and inter-area oscillation modes with frequencies in the range of 0.1-0.7 Hz. The local modes are almost always present in a power system while the inter-area modes are especially seen in systems where one power system area is connected to another by long transmission lines.

2.5 Stability of the power system

Obviously, power systems need to be operated in a way which minimizes the risk of interruptions of the power flow from generating units to end consumers of power. Another goal is to minimize the losses which arise from the transmission of power. It is not possible to optimize both the system losses and the stability of the system at the same time. This means that the operation of a power grid can be described as a constrained optimization problem. The threats to power system stability can be divided into the different categories below:

2.5.1 Frequency instability

The total generated active power and the active power load in the power system must at all times be kept equal. If this criterion is not met, the electrical frequency of the system will start to change. If there is excess load, rotational energy is extracted from the synchronous machines, slowing down the electrical frequency and if the generation is larger then the load, the excess energy will accelerate the machines, causing the electrical frequency to increase. To avoid frequency instability, there are several different systems which are designed to keep the load and generation of the power system equal. These are usually characterized as *primary control*, *secondary control* and *tertiary control*. *Primary control* is automatic and achieved by applying dedicated frequency controllers to a number of generating units in the system. These work to increase the generation of the unit if the grid frequency decreases and decrease the generation if the frequency increases. This regulation is usually applied to water power plants where the power can be changed rapidly by changing the water flow through the turbines. *Secondary control* is used when a larger disturbance is present, which makes the primary controllers saturate at their upper or lower limits. Here the power reference values provided to generating units in the system by the TSO are changed to counteract the disturbance and restore the frequency to the nominal value. *Tertiary control* is an automatic response which is initiated if the system frequency is significantly reduced from the nominal value. This happens when the generating units are incapable of further increases in power generation. The action constitutes of shedding parts of the load in the system. This is a dreaded situation which the TSO:s try to avoid at all costs. Frequency instability is not treated at any length in this thesis and this concludes the brief review of the subject.

2.5.2 Transient instability

Transient instability may occur in a power grid between one synchronous machine and the rest of the grid or between two grid areas. This form of instability typically results when the power flow between the single machine and the rest of the grid or between the two separate grid areas cannot be

maintained due to a fault on one of the interconnecting lines. During the time of the fault, there is usually very little power transfer on the interconnecting lines which alters the power balance in the system. The sending end machine or machines are then accelerated since a surplus of power is generated in the sending end and the receiving end machine or machines are decelerated since a power shortage arises. If the fault is not cleared fast enough, the difference in electrical frequency between the two systems may cause the voltage angle difference to increase above 180 degrees and the systems will fall out of phase, eventually causing blackouts in the system. Commonly, the equal-area criterion [2] is used to determine whether a particular system is stable or not when subject to a certain fault. For each fault, a critical clearing time can be specified which determines the maximum duration time of the fault that can be allowed before clearance for the system to remain transiently stable. Transient instability is generally seen in systems with weak interconnections with high series reactance. It may be improved by installing series compensation on weak inter-ties or by installation of FACTS devices in the system. In this thesis, a simple control method to improve transient instability by means of a Controlled Series Compensator (CSC) or a Dynamic Power Flow Controller (DPFC) is proposed.

2.5.3 Voltage instability

Voltage instability typically occurs when the generators in the power system cannot provide enough reactive power in order to give a sufficiently high voltage at all nodes in the system. The problem commonly arises as a result of one or several faults which are cleared by disconnecting lines or generators in the system. It is not uncommon that voltage instability is a slow process which is affected by tap-changer operations in the grid and the dynamics of the voltage regulators of the generating units. Automatically controlled tap-changers which are installed to keep the voltage within predefined levels in distribution grids are necessary, but they are generally deteriorating the voltage stability of the power grid. When a strained situation occurs, the tap-changers operate to increase the voltage in the distribution network. This in turn often increases the load in the system even more due to the voltage dependence of the loads resulting in a system which is even more strained.

Voltage instability is not treated in this thesis, but it is recognized that it may be improved by operating series connected FACTS devices like the TCSC or the DPFC appropriately when the instability is detected. To improve the voltage stability more effectively, shunt connected FACTS devices which can inject reactive power at suitable nodes in the power system can be used.

2.5.4 Small-signal instability

So called small-signal instability arises when one or more of the eigenvalues of the power grid system matrix are found in the right half plane. This means that the damping of one or several modes of oscillation is negative and that the system is likely to be unstable in the particular mode of operation. Such a situation is rarely found in undisturbed power systems, but it may arise when the system is severely strained by high power transfers and line disconnections due to faults. To improve the damping of power oscillations, PSS are commonly applied to the Automatic Voltage Regulators (AVR) of the generators in the system. This method is effective but in some cases some modes may still be unstable during high loading conditions even if PSS are applied and properly tuned. In these cases it is possible to add supplementary damping to the system by installation of FACTS devices at suitable locations in the system. Series connected devices like the Thyristor Controlled Series Capacitor (TCSC), Thyristor Switched Series Capacitor (TSSC), and the Dynamic Power Flow Controller (DPFC) are among the most suitable for the damping of power oscillation but also shunt connected devices like the SVC (Static Var Compensator) can be used. In this thesis an adaptive controller for power oscillation damping using series devices like the TCSC, TSSC, and DPFC is proposed.

3 FACTS devices and their control

The definition of a Flexible AC Transmission System (FACTS) is according to the IEEE:

"Alternating current transmission systems incorporating power electronics-based and other static controllers to enhance controllability and increase power transfer capability."

The definition of a FACTS controller is, according to the IEEE:

"A power electronics-based system or other static equipment that provide control of one or more AC transmission system parameters."

In this chapter, a brief review of the principles behind the most common FACTS topologies is given. Special attention is given to the devices which are closest related to the DPFC discussed in this thesis work, namely the PST and the TCSC/TSSC. For these devices, an additional discussion on the recent research on control aspects is carried out.

3.1 Power electronic converters

Generally, FACTS devices are based on power electronics. They include switchable devices like the Gate-Turn Off thyristor (GTO) and Insulated Gate Bipolar Transistor (IGBT) but also passive devices like capacitors and inductors. The details on power electronics are omitted in this thesis but the interested reader may refer to [5] for further information.

Many of the FACTS devices that are currently used are based on converters. These may be either a Voltage-Source Converter (VSC), where the voltage feeding the converter is kept almost constant by means of a large capacitor, or a current-source converter, where instead the feeding current is kept unchanged using a large inductor.

The principal function of the voltage-source converter is to convert the constant DC voltage on one side of the converter to an AC voltage on the other side by switching the power electronic devices in a controlled manner. Using appropriate converter technology it is possible to vary the AC output voltage in phase as well as in magnitude. If the storage capacity of the DC capacitor is small and no external supply to the DC side exists, the converter cannot supply active power to the AC grid any substantial amount of time and the device is restricted to interchange reactive power with the AC grid. The function of the current-source converter is to present the DC current to the AC side as an AC current by appropriate switching of the power electronic devices. This current is variable in phase and amplitude.

The details of the converter types will not be discussed here since this topic is not considered to be within the scope of this thesis. A more thorough discussion of this topic is found in [5].

3.2 Shunt-connected FACTS devices

The primary task of shunt-connected FACTS devices is usually to provide voltage support in the power grid. However, they may also be used to improve the transient stability in a power grid and to damp power oscillations even though series connected devices often are a more effective choice for these tasks.

Some of the most important shunt-connected FACTS devices are shown in Fig. 3.1. In Fig. 3.1 (a), the Static Synchronous Compensator (STATCOM) is depicted. In this configuration, a VSC is used to balance the reactive power need of the grid by automatically controlling the VSC output voltage magnitude. STATCOM can also be used as an active filter to reduce

harmonics in the grid. In Fig. 3.1 (b), a STATCOM with energy storage is shown. It can provide active power support in addition to improving the reactive power balance in the system, see [6] and [7].

A collection of different Static Var Compensators (SVC) are shown in Fig. 3.1 (c)-(d) and (f)-(g). This group of devices work by inserting a variable reactive load in shunt with the power line, thereby improving the reactive power balance. In Fig. 3.1 (c), a Thyristor Switched Capacitor (TSC) is seen. This device consists of a high voltage capacitor which is connected to the grid by high power thyristor units. To avoid excessive currents, the switchings of the thyristors are determined according to a point-of-wave approach which switches the thyristors when the voltage across the capacitor reaches its lowest value during the fundamental frequency cycle. The TSC represents a single capacitive admittance which may be connected to the power grid. In order to achieve step-wise control of the admittance, several TSC elements can be connected in parallel. Fig. 3.1 (d) may represent both a Thyristor Switched Reactor (TSR) and a Thyristor Controlled Reactor (TCR). The TSR is a shunt reactor which is either fully connected or disconnected to the grid. To achieve step-wise control of the reactive power consumption, several TSR units may be connected at the same node. In contrast to the TSR, the TCR works with a firing angle control of the thyristor valves to control the effective shunt reactance of one reactor.

Fig. 3.1 (f) and (g) show mechanically switched shunt reactances which may also be used in the power system in coordination with the other shunt devices to form a Static Var System (SVS). Finally, Fig. 3.1 (e) shows a Thyristor Controlled Braking Resistor (TCBR) which can be used to aid power system stability by minimizing acceleration of generating units during a disturbance. With this device, firing angle control is optional.

3.3 Series-connected FACTS devices

Series connected FACTS devices are commonly used for power flow control, power oscillation damping, and transient stability improvement. They

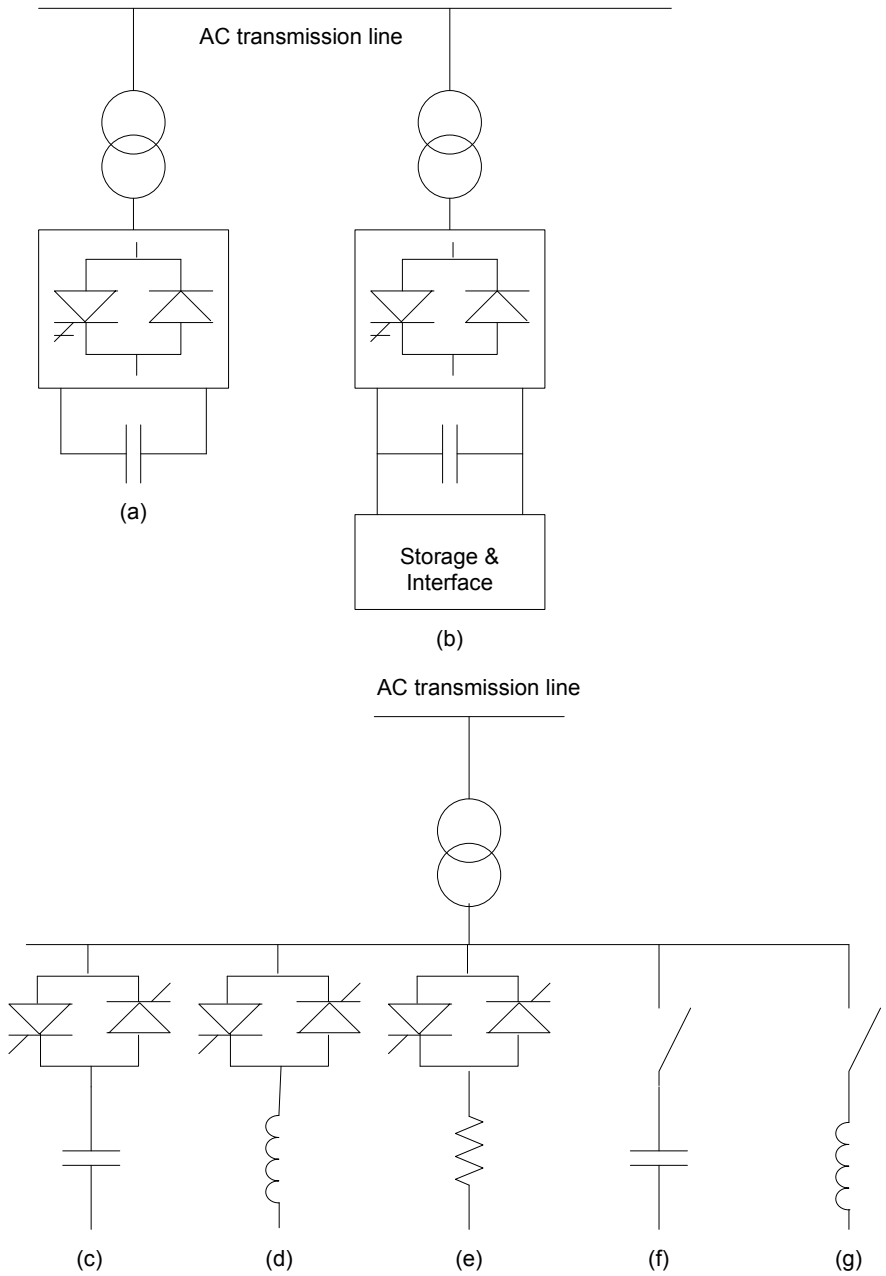

Figure 3.1: Different shunt-connected FACTS devices: (a) Static Synchronous Compensator (STATCOM), (b) STATCOM with energy storage, (c) Thyristor Switched Capacitor (TSC), (d) Thyristor Switched Reactor (TSR) or Thyristor Controlled Reactor (TCR), (e) Thyristor Controller Braking Resistor (TCBR), (f)-(g) Mecanically switched reactances.

may also be used to improve voltage stability even though shunt-connected FACTS are usually more effective in this respect.

Some of the key series-connected FACTS devices are shown in Fig. 3.2. In Fig. 3.2 (a), a Static Synchronous Series Compensator is shown (SSSC). This device is capable of injecting a variable voltage in quadrature with the line current. In this way, the active and reactive power flow on the line can be changed. Fig. 3.2 (b) shows a SSSC with energy storage. This device can inject a voltage of variable magnitude and angle in series with the line during a transient period of time and a voltage in quadrature with the line current with no limit on the duration. The energy storage extends the working region of the SSSC which is especially useful in a disturbance situation.

In Fig. 3.2 (c), the Thyristor Controlled Series Capacitor (TCSC) is shown. The picture may also be used to illustrate the Thyristor Switched Series Capacitor (TSSC), even if this device often consists of several units of the same type connected in series. The TCSC device acts as a variable series capacitor in the grid when the firing angle of the thyristor valves is changed. It consists basically of a TCR which is connected in parallel to a series capacitor. The TSSC is in contrast to the TCSC not operated with firing angle control and is therefore either connected or diconnected to the grid. Here a step-wise variable line impedance can be achieved if several thyristor controlled units are connected in series. The functional properties of the TCSC and the TSSC are discussed in more detail in Section 3.5.2.

Finally, in Fig. 3.2 (d), the Thyristor Controlled Series Reactor (TCSR) or Thyristor Switched Series Reactor is shown. This device may be controlled with firing angle control (TCSR) or with fixed angle control (TSSR) analogously with the TCSC and TSSC. This device may change its impedance in the region between the impedance of the reactor in parallel to the TCR and that of the two reactors in the circuit connected in parallel.

In this thesis, the denotation Controllable Series Compensators (CSC) is used to describe the devices TCSC, TSSC, TCSR and TSSR as a group. A lot of work is devoted to control of CSC in this thesis and a review of the current research in this field is given in section 3.5.2.

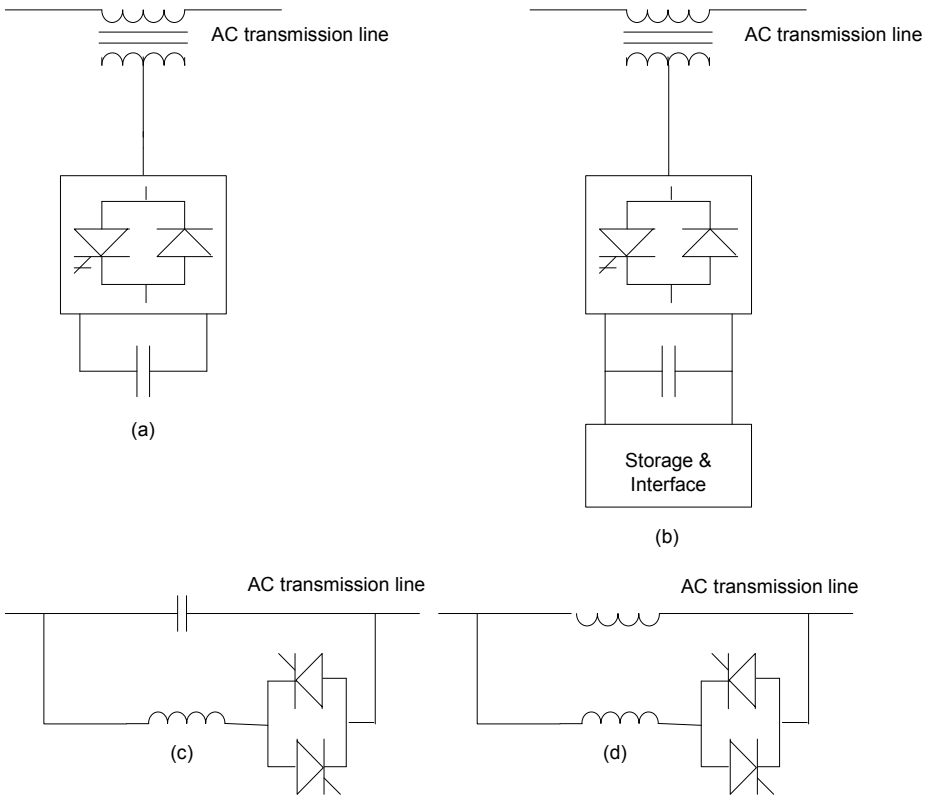

Figure 3.2: Different series-connected FACTS devices: (a) Static Synchronous Series Compensator (SSSC), (b) SSSC with energy storage, (c) Thyristor Controlled Series Capacitor (TCSC) or Thyristor Switched Series Capacitor (TSSC), (d) Thyristor Controlled Series Reactor (TCSR) or Thyristor Switched Series Reactor (TSSR.)

3.4 Combined shunt- and series-connected FACTS devices

Combinations of shunt- and series-connected FACTS technology provide additional functionality to the FACTS device. The most known device of this type is the Phase-Shifting Transformer (PST), which is widely used throughout the world. The topology is based on one shunt transformer - the exciting unit, and one series transformer - the boost unit. The exciter unit is equipped with a tap-changer which is used to change the phase angle shift of the device. By inserting a series voltage in quadrature with the line voltage, the device is capable of changing the voltage phase angle difference across a line, leading to a change in the power flow on the line. While the phase-shifting transformer is traditionally based on mechanical switches for tap-changing, faster devices, based on thyristor controlled tap-changers have been proposed. Fig. 3.3 (a) shows a Thyristor Controlled Phase-Shifting Transformer (TCPST). In the traditional version of the PST, the thyristor valves in the figure are exchanged for mechanical switches. Most installations of PST:s around the world are based on mechanical switches making it a slow device with a response time in the range of 10 s for one step of the tap-changer. In this work, the main assumption has therefore been that the PST is a slow device which cannot be operated during the first time period following a major disturbance.

A device which has recieved a lot of interest recently is the Unified Power Flow Controller (UPFC), see Fig. 3.3 (b). This device is a combination between a STATCOM unit and an SSSC unit. The active power to support the series unit (SSSC) is obtained from the line itself via the shunt unit (STATCOM). By means of this device, reactive and active power on a line can be controlled independently. Also, the device is capable of controlling the line voltage. With this functionality, the UPFC is known as a complete FACTS controller. However, due to its complexity and cost of installation it has not yet been installed in any great numbers around the world.

The main topic of this thesis is the Dynamic Power Flow Controller (DPFC)[8], which can be said to provide a low cost alternative to the UPFC.

The DPFC, drawn in Fig. 3.3 (c) is a combination of one traditional PST and a TSSC/TSSR, which provides a set of thyristor controlled reactance steps connected in series with the line. A Mechanically switched Shunt Capacitor (MSC) is optional in the DPFC configuration, depending on the system reactive power requirements. In this thesis, a DPFC without an MSC has been considered.

The DPFC configuration has a much faster dynamic performance than a traditional PST and it is capable of rapidly controlling the active and reactive power transmitted through a line. The main advantages of the DPFC in relation to a common PST are:

(1) **The speed of the power flow control of the DPFC is much higher than that of the PST.** This means that the DPFC can be used for power oscillation damping and transient stability improvement in the power system. Due to its limited speed of control, a PST is usually operated with preventive control, that is, with a preset tap changer position which does not change during or immediately after a fault. This tap setting needs to satisfy the stability criteria of all N-1 contingency situations and it is usually not the optimal setting if the transmission losses of the system are considered. The DPFC may in contrast to this be operated with corrective control, where the tap setting giving the lowest power system losses at all times is used. In case of a contingency, the power flows in the system can be rapidly altered using the TSSC/TSSR to comply with the (N-1) requirements.

(2) **The DPFC allows for reactive power support and control of the reactive power flow of the line.** This feature can be used for improvement of system voltage stability/recovery. For example, it can be used to give fast voltage support in an overload situation by engaging full capacitive compensation of the TSSC. In some networks, the reactive power consumption of a regular PST is unacceptable. By using a DPFC instead, the TSSC can be used to compensate for the tap-dependent series inductance of the PST, keeping the total series reactance of the device close to zero.

With these features, the DPFC can be used for power flow control, power oscillation damping, transient stability improvement, and voltage stability improvement. *The focus of this work so far has been to develop strategies*

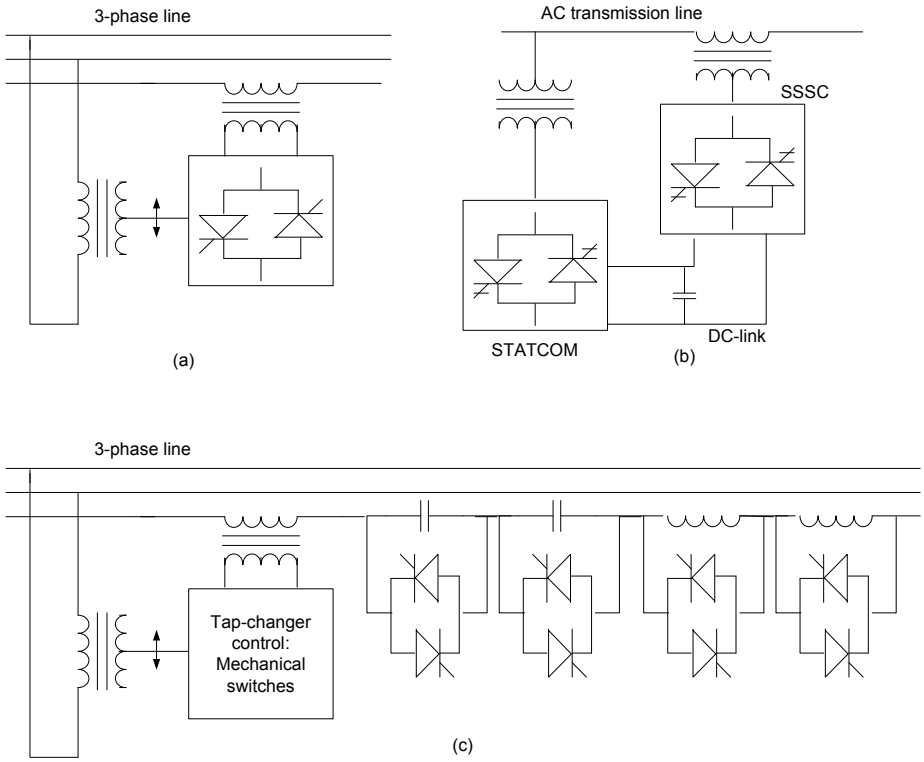

Figure 3.3: Combined series- and shunt-connected FACTS devices: (a) Thyristor Controlled Phase-Shifting Transformer (TCPST), (b) Unified Power Flow Controller (UPFC), (c) Dynamic Power Flow Controller (DPFC), drawn with no MSC. Only the equipment for one phase is shown for each device.

for the first three tasks, where the voltage stability issues have been left as future work.

3.5 Previous work on control issues for PST and TCSC/TSSC

Since the control of a DPFC involves coordination of the control of a phase-shifting transformer and a controllable series reactance it is meaningful to

take a look at the current field of research on the control of PST and TCSC/TSSC devices. Since the mechanically switched PST is a slow device which is not capable of any fast control moves following a grid contingency, most of the work in this thesis has been devoted to the control of the TSSC part of the DPFC. Some of the work is considering the effect of a series connected PST while most of the thesis concentrates on adaptive control of a single controlled series reactance in the grid like the TCSC or TSSC. A massive amount of research has been done on the control of TCSC in particular during the last 10-15 years while only a small amount of research has been reported on automatic control of PST:s. In the following section, the function of the PST and TCSC/TSSC is described in a more detailed manner and a brief review on the current research on automatic control of these devices is given.

3.5.1 Phase-shifting transformers

Basic functionality of the PST

The PST is a device that is used for power flow control in order to relieve congestions and minimize power losses in grids around the world. There are many different topologies for the PST. Functionally, one of the most important distinctions is between the asymmetrical and the symmetrical PST. This refers to the capability of the PST to inject a voltage directly in quadrature with the line voltage resulting in an alteration in the voltage magnitude (asymmetrical) or that of a voltage injection capability which alters the line voltage angle with no change in the line voltage magnitude (symmetrical). This may be accomplished with either a single-core or a two-core design. The topology of a two-core asymmetric design PST is shown in Fig. 3.4 and a two-core symmetric design is shown in Fig. 3.5. The design of the so called "quadrature booster" PST in Fig. 3.4 clearly illustrates the principle behind phase shifters. Here a the voltage of each phase is fed to a shunt transformer which is tap controlled. The voltage difference between the voltages on the secondary sides of the shunt transformers corresponding to the first phase and the one corresponding to the second phase is then a voltage in quadrature with the voltage of the third phase. This voltage difference is added in

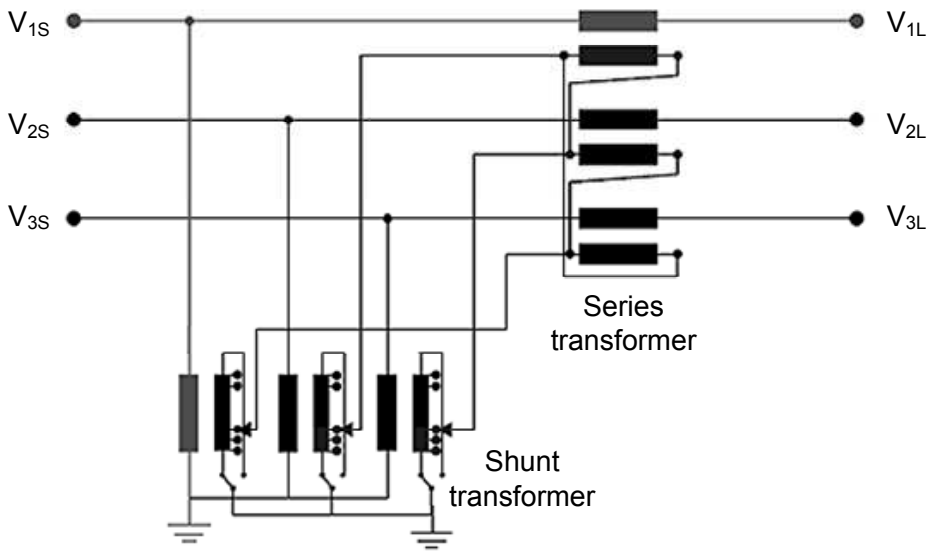

Figure 3.4: Two-core asymmetric design phase-shifting transformer (picture from ABB).

series with the third phase by means of a series transformer. The result is a voltage phase and magnitude shift of the third phase according to Fig. 3.6 (c). The same principle is used for all three phases to finalize the design of the PST.

In Fig. 3.6 (a), the general phase shifts in all three phases accomplished by an ideal (symmetric) PST is shown. In Fig. 3.6 (b) and (c) the voltage phasors of one phase before and after the PST are shown for an ideal symmetric and an ideal asymmetric PST topology. Note that the asymmetric design alters the voltage magnitude, whereas a symmetric design does not.

In order to get a more accurate description of the PST electrical characteristics, the internal series impedance of the PST must be taken into account. This value will be dependent on the selected tap of the shunt transformer. In Fig. 3.7 (a), the PST is schematically depicted including the PST impedance Z_T=R_T+jX_T. In Fig. 3.7 (b), the voltage phasors of one phase on both sides of the PST are shown as well as the voltage phasor at an imaginary point excluding the impedance of the device. This is done both when the PST supplies an advance and a retardation to the voltage phase angle.

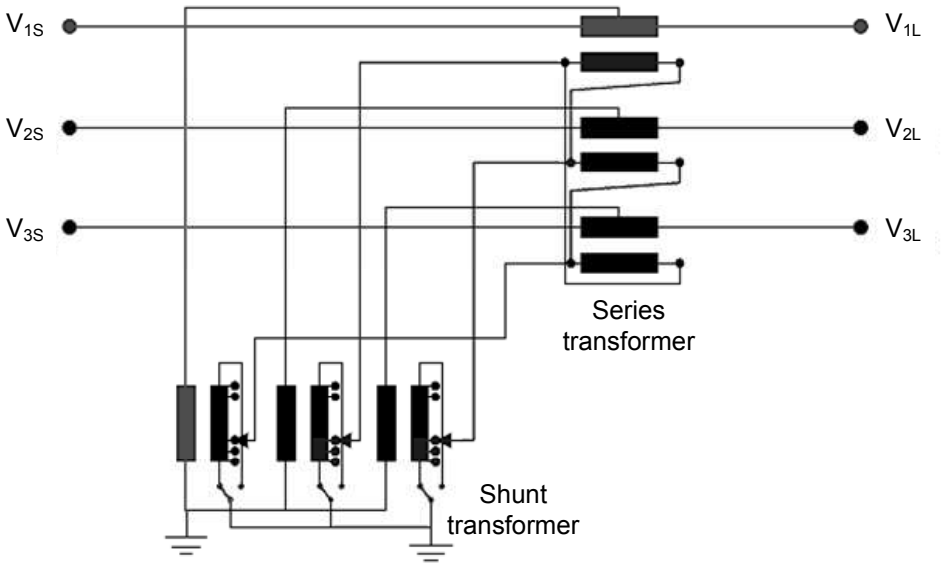

Figure 3.5: Two-core symmetric design phase-shifting transformer (picture from ABB).

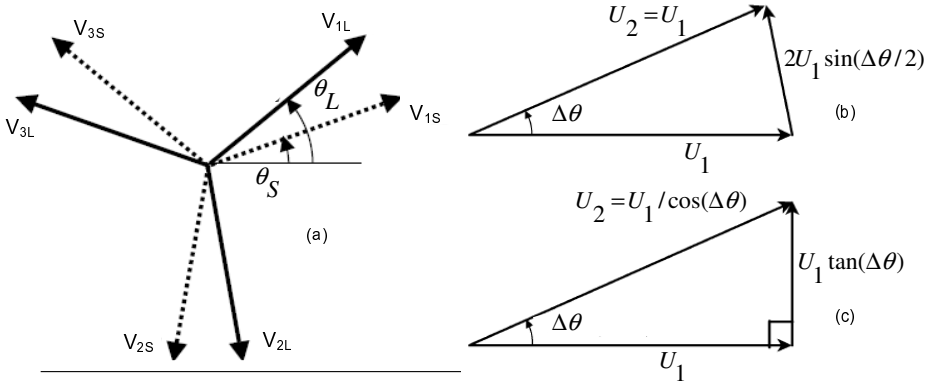

Figure 3.6: Principal voltage shifts for different PST topologies: (a) Phase shifts of a symmetric PST - all phases, (b) Phase shift of a symmetric PST - one phase shown, (c) Phase shift of an asymmetric PST "Quadbooster"- one phase shown (pictures from ABB).

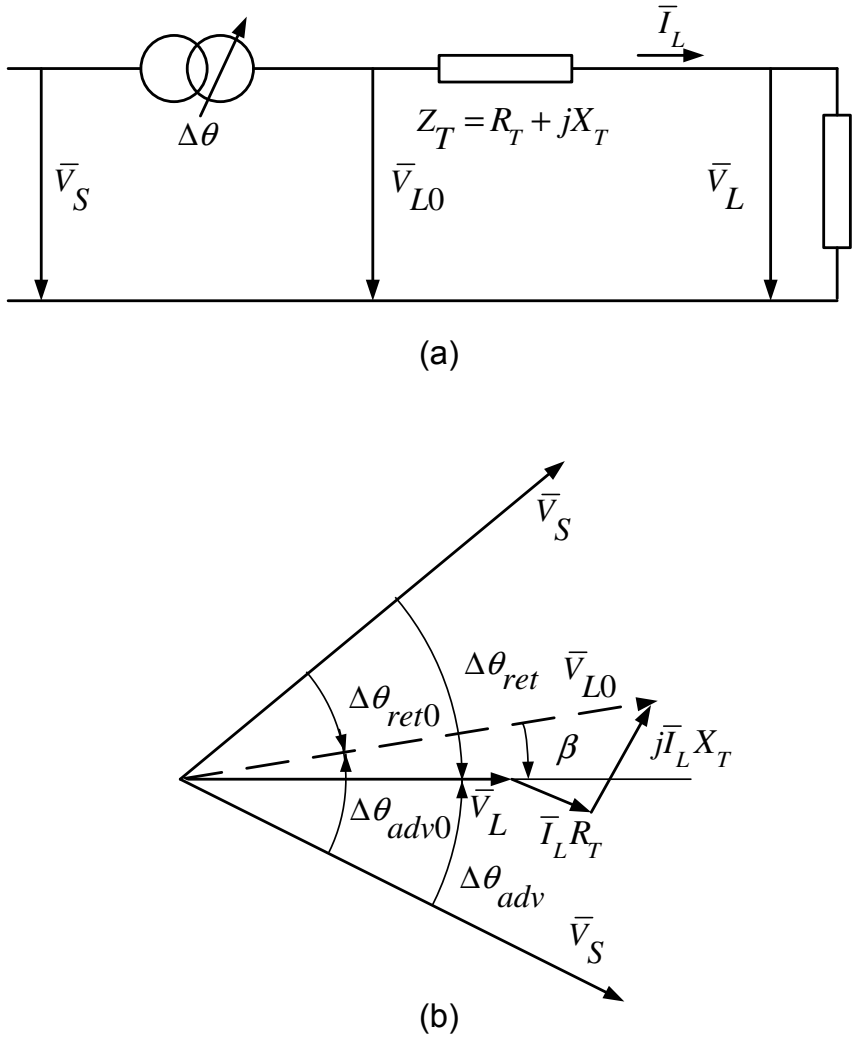

Figure 3.7: (a) Principal schematic of a PST with denotations, (b) Phasor diagram of the advancing and retarding angles including the influence of the PST series impedance shown for one phase.

In the case of an advancing phase angle, the PST ideally gives a phase angle shift of $\Delta\theta_{adv0}$. However, the current passing through the device gives a phase retardation of β yielding a total phase advancement of $\Delta\theta_{adv}$=$\Delta\theta_{adv0}$-β. In the case with a retarding phase angle, the PST gives a phase shift of $\Delta\theta_{ret0}$ ideally and the current passing through the device impedance adds another angle β to the total phase shift $\Delta\theta_{ret}$=$\Delta\theta_{ret0}$+β. The value and sign of the angle β can be calculated with the knowledge of the values of the device impedance, current and the load power factor.

The series impedance of a PST is dependent on the tap settings of the tap changers used in the particular topology. Generally, it increases from its value at zero phase shift both when the angle is advanced and when it is retarded with the same behavior in both directions. An estimate for a two-core asymmetric PST is that the series impedance starts at zero phase shift at the value of the short circuit impedance of the series transformer and increases with increasing tap (in both directions) to a peak value when the phase angle shift is at its maximum (in both the positive and the negative direction) which is roughly twice the initial value at zero phase shift.

The phase-shifting capability of installed (ABB) PST:s range from ± 10 degrees to about ± 70 degrees depending on power grid requirements with voltage ratings in the range of 100 kV to 400 kV and power ratings between 100 MVA and 1600 MVA.

Control of phase-shifting transformers

The control of a PST is usually operated manually by the TSO in the particular power grid where the device is placed. The impact on the line power flows of a certain change in phase angle at a particular PST is dependent on the grid parameters. This dependence is subject to change if the grid topology changes for example as a result of a disturbance in the grid. A steady-state model for the dependence of the line power flows on the phase angle shift of a PST situated somewhere in a power system is given in [9].

Using this model, the active power P_{ij} through a line with a PST and the power P_{pq} through another line in the same system can be written:

$$P_{ij} = P_{ij}^0 + \Delta\theta_{ij}\xi_{\Delta\theta}^{ij} \tag{3.1}$$

$$P_{pq} = P_{pq}^0 + \Delta\theta_{ij}\xi_{\Delta\theta}^{pq}. \tag{3.2}$$

Here, the phase shift angle of the PST is given as $\Delta\theta_{ij}$ and the Phase Shifter Distribution Factors (PSDF) given by ξ can be calculated with the knowledge of the admittance matrix of the grid as

$$\xi_{\Delta\theta}^{ij} = \frac{\partial P_{ij}}{\partial\Delta\theta} = y_{ij}(1 + y_{ij}(2c_{ij} - c_{ii} - c_{jj})) \tag{3.3}$$

$$\xi_{\Delta\theta}^{pq} = \frac{\partial P_{pq}}{\partial\Delta\theta} = y_{pq}y_{ij}(c_{pj} - c_{pi} + c_{qi} - c_{qj}) \tag{3.4}$$

with y_{ij} and c_{ij} denoting the element at row i and column j in the admittance matrix and the inverse admittance matrix respectively.

Recently, attention has been given to the issue of coordinated control of PST:s. In interconnected grids with multiple phase shifters, it is a complicated task to determine how the PST:s should be controlled in order to optimize the grid losses and security margins. One automatic control method for coordinated control of multiple PST:s based on the steady-state load flow model described above is given in [9]. The controller successfully uses the Linear Least Squares method to calculate the optimal settings for multiple PST:s in the Dutch and Belgian power grids, achieving a previously known loading target of the cross border flows. It is noted, however, that it is essential that the admittance matrix is updated when a topology changing disturbance occurs since the PSDF may change significantly in such an event, causing the controller to fail.

Another automatic control approach [10], focusing on the different objectives that may arise for different TSO:s in an interconnected power system, uses game theory to develop a control scheme for control of multiple phase shifters. The proposed solution is the Nash equilibrium of a sequence of optimizations performed by the various TSO:s, each of them taking into account the other TSO:s' control settings as well as operating constraints relative to the whole system.

3.5.2 Thyristor Controlled - and Thyristor Switched Series Capacitors

Basic functionality of TCSC and TSSC

The work in this thesis on TCSC and TSSC concerns the outer loop of control which determines which series reactance value that should be selected at a particular instant. There is also an inner loop of control for each device which determines the firing angle of the thyristor valves. This loop determines how to switch the thyristors in order to achieve the reactance value for the device selected by the outer loop. Even if this control loop is not taken into account in this work it is briefly reviewed here for completeness.

The TCSC and the TSSC can topologically be seen as the same device, that is a series capacitor which is connected in parallel with a thyristor switched reactor. However, in the TSSC case, the reactor inductance is generally chosen to be very small whereas the inductive reactance in the TCSC case is usually in the range of 5-20 % of the capacitor reactance. The TSSC usually consists of several thyristor switched units in series as is seen in Fig. 3.8 (a) whereas the TCSC is more commonly used as a single phase-angle controlled unit as in Fig. 3.8 (b) even if series connected installations exist.

The operation of the thyristors in the two different devices is also quite different:

In the TSSC, the thyristors are always turned on at instants with zero(minimum) capacitor voltage to minimize the surge current through the switches. The thyristors are then naturally turned off as the current through the devices passes through zero. This mode of operation yields a device where the capacitors in the circuit is either fully connected in series with the line or fully disconnected, avoiding any introduction of harmonics in the power grid. With a scheme of several switched capacitive units, the TSSC can control the degree of series compensation of the line in steps depending on the chosen values for the different capacitive units. It should be noted, however, that the demand for zero-voltage turn on of the thyristor valves

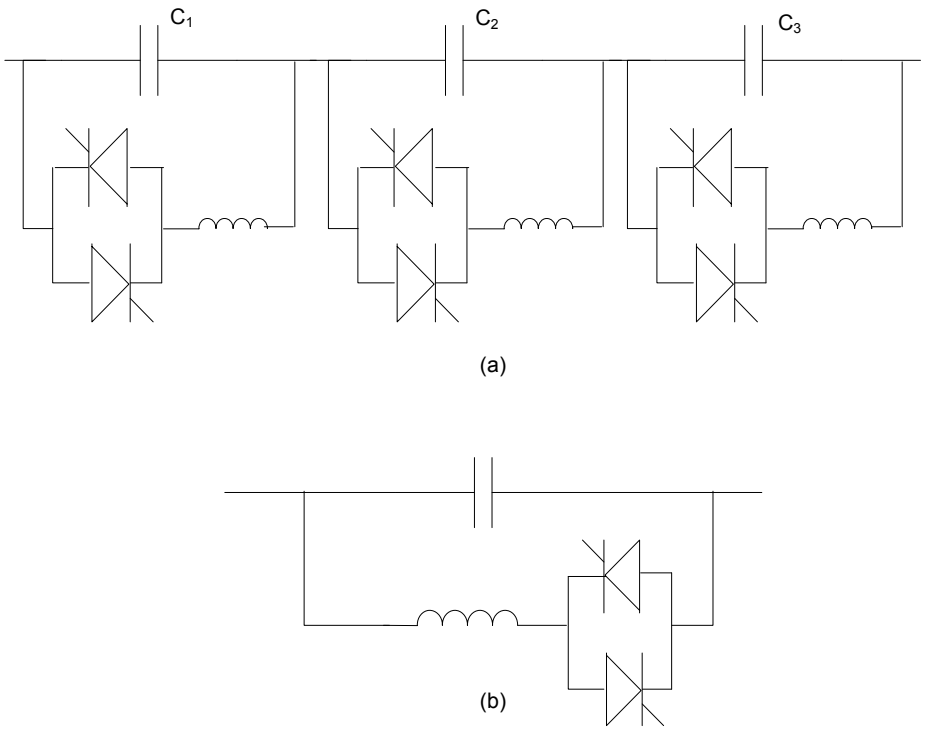

Figure 3.8: (a) Principal schematic of a TSSC with three different capacitor units, (b) Principal schematic of a TCSC.

introduces a delay of up to one full cycle for bypassing series capacitors in the circuit. This delay limits the speed of control of the TSSC.

The TCSC is, on the other hand, operated by changing the conduction time of the thyristor valve by controlling the fire angle. Using this strategy, the actual fundamental frequency reactance of the device may be changed in a continuous manner. The variable reactive impedance of the device can be written as

$$X_{TCSC}(\alpha) = \frac{X_C X_L(\alpha)}{X_L(\alpha) + X_C} \tag{3.5}$$

with $X_L(\alpha)$ as the fundamental frequency reactance of the TCR branch which is variable with the firing angle and X_C being the fixed reactance of the capacitor (which is a negative number). $X_L(\alpha)$ is variable in the region $X_{L0} \leq X_L(\alpha) \leq \infty$ with X_{L0} denoting the reactance of the TCR branch

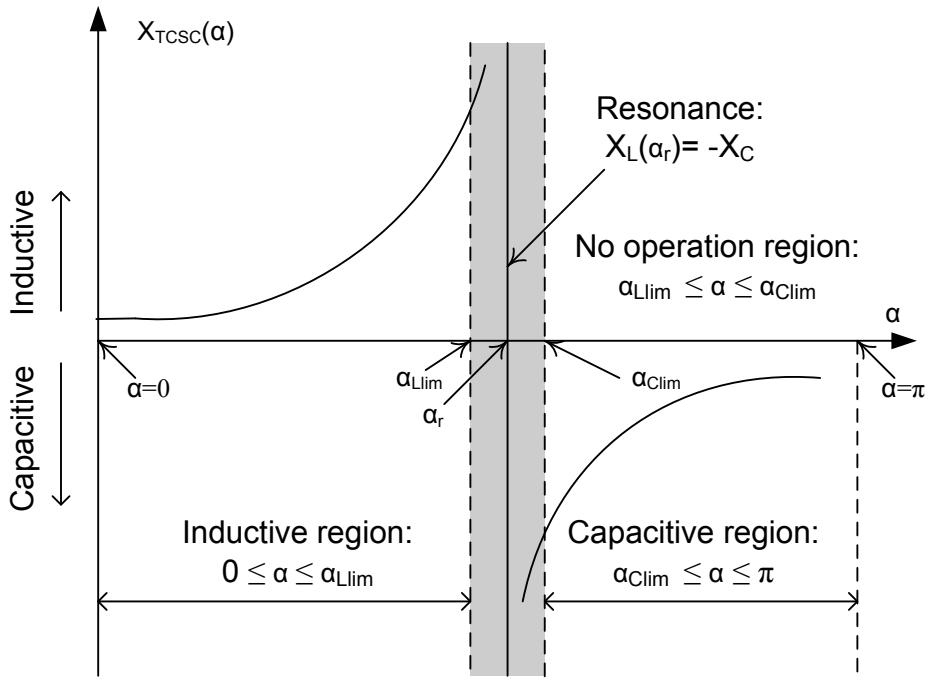

Figure 3.9: TCSC reactance versus thyristor turn on delay angle.

with the thyristors fully conducting. The delay angle α is defined as the delay angle for the thyristor valve turn on measured from the zero crossing of the capacitor voltage. From Eq. 3.5 it can be seen that parallel resonance occurs when $X_L(\alpha) = -X_C$ which leads to a TCSC impedance which is theoretically infinite. To avoid the resonance region, TCSC operation is inhibited in a region $\alpha_{Llim} \leq \alpha \leq \alpha_{Clim}$ around the resonance angle α_r. The operation region of the TCSC is illustrated in Fig. 3.9.

The static model of the TCSC presented above provides some insight into the function of the device. To understand the dynamic properties of the device a more detailed study is required. Since this thesis does not focus on these issues, this part is omitted. A more elaborate discussion on the TCSC properties can be found in [5].

Control of TCSC and TSSC

There has been a lot of research in the field of control of controlled series compensation. Most of the work has been done on the outer loop of control of the devices, that is, assuming that the device acts as a fast controllable reactance connected in series with one transmission line in the grid. The focus of most research in the field has been to use controllable series compensators to damp inter-area oscillations and to improve the transient stability of the power system. The proposed approaches include traditional pole placement techniques, robust control, adaptive control, and non-linear control.

The work on switched series compensators dates back to 1966 with E. W. Kimbarks classic paper on stability improvement [11] where he shows the benefit of switched series compensation for improvement of transient stability in power systems. He also shows that it is possible to significantly reduce any subsequent power oscillations after a disturbance in a power system by switching in a suitable series capacitor at a suitable location at the time of the fault. More work on bang-bang control of switched capacitors was done in the 1970:s where optimal control laws for damping of power oscillations in a one machine - infinite bus system in minimum time with a small number of capacitor switchings were developed [12] [13]. These control laws were based on a Hamiltonian approach where the power system characteristics are known after the disturbance and the voltage phase angle at the generator is known to the controller. Other approaches to time-optimal control of switched series capacitors for transient stability improvement and oscillation damping were proposed in the late 1990:s with the works of D. N. Kosterev et. al. [14] and J. Chang et. al. [15]. These authors use an energy function approach together with numerical phase plane analysis to determine the switching instants for the time optimal controller which stabilizes the system by means of a small number of switching events. Both authors also move on to design a suboptimal control scheme which is more robust and better suited for stabilization of complex power systems.

All of the above mentioned schemes aim at time-optimal control of any transients following a fault, that is both transient stability improvement and oscillation damping. In most recent works, however, it is common to use

two controllers, one for transient stability improvement and one for power oscillation damping. The transient stability controller is usually a controller which utilizes an open-loop preprogrammed response to severe disturbances. The damping controller is usually a closed loop controller designed using control theory of some kind.

With the invent of the continuously controllable TCSC in the late 1980:s, more conventional methods to design especially damping controllers became available. The residue method, which is a well known approach for design of PSS controllers, was used to design a damping controller for the TCSC in [16]. Since most power systems are complex, and the design of a controller based on a full system model is time-consuming and demanding computationally, a power system reduction technique was proposed for damping controller design of CSC in [17]. Here a complex power system with an unstable inter-area oscillation mode is reduced in order by a factor of ten based on the singular values of the Gramians of the power system model after which a damping controller is designed based on an LQR (Linear Quadratic Regulator) approach. Another, less computation intense reduction technique based on Modal equivalents in [18] showed promising results when applying reduction techniques to the huge Brazilian power system. Here, the original system has over 1600 state variables which were reduced to 22 and 34 respectively. These reduced models were then used to design TCSC damping controllers to damp the north-south inter-area oscillation mode in the system with good results. This paper shows that relatively low order models based on a relatively small amount of system data (dominant eigenvalues and their residues) may be effective in the design of damping controllers, significantly reducing the effort in the controller design.

A controller based on robust control theory and in particular the H_∞ controller design technique was proposed in [19]. The controller was here realistically implemented in hardware and tested in a real-time system emulating the grid using a computer. The controller objective was to damp three different modes of power oscillation by means of one installed TCSC unit in a model of the New England - New York power system. The study showed good damping performance in a wide range of operating conditions and disturbances in real-time simulations of the power grid.

Some research on adaptive controllers for power oscillation damping by means of TCSC has been done recently. In [20], the authors investigate an approach which uses a number of predefined linearized models of the system corresponding to different topologies that may arise due to faulted lines or other changes in the grid characteristics such as changes in load characteristics or major changes in the power flow levels of critical lines. These models are put in a model bank and the controller then uses the actual system response to determine the linear combination of the possible configurations which best describes the current system. This approach is denoted Multiple-Model Adaptive Controller (MMAC) and it uses a probabilistic method to determine the weights of the predefined models in the system model guess which most accurately describes the current system. For each predefined model, a TCSC controller is initially tuned by conventional loop shaping techniques and the resulting adaptive controller is then formed by continuously summing up the responses of the different controllers weighted by the probability of the corresponding models and normalizing the result. The controller was shown to perform well when tested in digital simulation of a four-machine system of the type described in [21], which is a standard system to study inter-area oscillations. Another approach to adaptive control of TCSC for damping of power oscillations was demonstrated in [22]. Here the system identification is done by considering the system to be Auto-Regressive with external input (ARX-model). The parameters of this model are then estimated by means of a Kalman filter using the response in the TCSC line power to the changes in line reactance inserted by the TCSC to determine the system parameters. The controller design is continuously updated by pole placement in the estimated closed loop system. The function of the TCSC controller was tested in simulation of the New England system with the aim to damp out one critically damped oscillation mode with promising results. Another adaptive damping approach which was used in an installation of a TCSC in Brazil was described in [23]. Here a gain-scheduling technique based on a phasor estimation of the power oscillation characteristics was used to create the control signal to the TCSC. The scheme is currently used for damping of the critical oscillation mode on the North-South interconnection in Brazil since 1999.

While most of the recent research on controllable series compensators was devoted to damping control, some work was also done on transient stability control. This includes the work presented in [24], where a discrete control scheme was developed based on an energy function approach and [25] which is an application study of a TCSC installation in Montana, U. S.. In this paper, Phasor Measurement Units (PMUs) are used to give a picture of the disturbances in the phase plane and the transient scheme is triggered if the $\delta - \omega$ curve trajectory leaves a predefined transiently stable region. The scheme then inserts series compensation which is a function of the voltage phase angle deviation between the grid areas which are separated as a result of the disturbance. Another interesting contribution to the research on transient stability improvement is provided in [26]. Here a discrete scheme for transient control of shunt FACTS devices is developed based on the equal-area criterion. This scheme may also be extended for use with series connected FACTS devices like the TCSC.

A summary of the recent research on TCSC control can be found in [27].

4 System identification

In order to design a controller using conventional control theory a system model is required. This includes an assumption for the model structure and additional information about the current values of the model parameters. Power systems are very complex systems with a structure which is changing with time and parameters that are also subject to changes in different time scales. Load changes may change the grid characteristics both very rapidly but also in a more controlled slower fashion. Faults in the power grid may change the grid characteristics both in the very fast time-scale, where short-circuits may cause systems to lose synchronism and in the slow time scale, when voltage instabilities may occur due to interactions between the AVR of the generators and the dynamics of tap-changers in the grid. This scenario poses a great challenge to control engineers trying to design control systems for grid connected devices.

In the previous chapter we have seen different approaches to this problem. Conventional linearized control loop shaping approaches may be straightforward to apply and can work very well in a number of operating conditions. However, if the grid topology changes or if the operating conditions are far from the assumed ones, these approaches may fail. Robust control theory offers an alternative where the possible deviations from the initial system are classified as disturbances and an optimal controller may be designed taking these deviations into account. The disadvantages of these methods are that detailed knowledge of the system is required and that it may be hard to classify the possible disturbances in the manner which the methods require. Another option for designing controllers in this system is adaptive control. There are many approaches which can be used here, but they all have in common that the system parameters are explicitly of implicitly estimated during a control event in order to optimize the controller performance. So

far, the robust control and adaptive control methods have not been widely used in the power industry for control of FACTS devices. This may be due to their relative complexity when compared to traditional loop-shaping methods and the demands of reliability in the business. A utility may prefer a simple sub-optimal solution with well-known stability characteristics over a less documented method which improves performance to the cost of a more complex implementation.

In this thesis, adaptive control methods for CSC and DPFC are proposed. Two different generic system models are used for the control design. One which may be used for any controlled series compensation device and one which takes into account the phase shift introduced by the PST in the DPFC configuration. The control methods for a pure CSC device may be seen as an intermediate step towards the design of a controller for the full DPFC device. Examples of CSC devices are the Thyristor Controlled Series Capacitor (TCSC) and the Thyristor Switched Series Capacitor (TSSC).

The system models that are used in this thesis are very simple. The goal of the work has been to design a controller with as few parameters as possible in order to simplify the implementation and to facilitate the understanding of the controller performance.

4.1 System model for control of CSC

4.1.1 Power flow control by means of CSC

The goal for the work presented in this thesis is to design a controller for power oscillation damping (POD), power flow control, and transient stability improvement. Initially, the focus will be on the tasks of oscillation damping and power flow control. First, it is instructive to qualitatively investigate the nature of power flow control by means of CSC. For a short transmission line, neglecting the line resistances, the power transmitted on a transmission line of reactance X can be expressed using Eq. 2.26:

$$P = \frac{U_1 U_2 \sin(\theta_1 - \theta_2)}{X}. \tag{4.1}$$

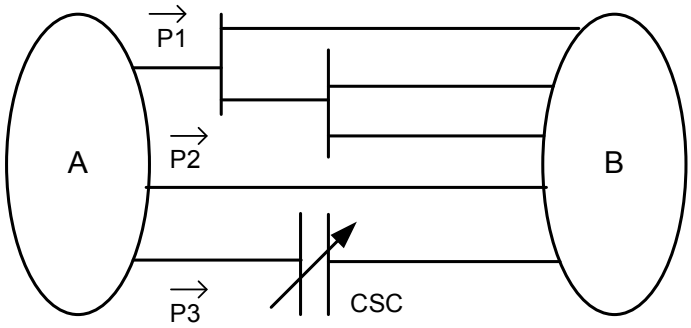

Figure 4.1: Simplified schematic diagram of two power grid areas with interconnecting lines and a controllable series compensator.

Here the voltage magnitudes on each side of the line are given as U_1 and U_2 and the voltage phase angles are given as θ_1 and θ_2. Equation 4.1 is a key relation for power flow control and it will be used in different forms in the following.

In Fig. 4.1, two interconnected power systems with a controlled series compensator on one of the tie-lines is shown. In a system of this type, the total active power flow on the interconnecting lines is determined by the total amount of active power generation in the two areas A and B and the total amount of active power load in each of the areas. In a functioning power system, the amount of generated power must equal the amount of consumed power in order to keep the electrical frequency of the system constant. This task is performed by the automatic frequency control described in Chapter 2. Assuming a system which is balanced with respect to generation and load, the total power transmitted over the inter-tie between areas A and B in Fig. 4.1 will be constant $P_{tot0} = P_1 + P_2 + P_3$ in a steady-state situation. Now, consider what happens if the CSC in the figure changes its series reactance. This will change the total reactance of the transmission lines connecting A and B, altering the characteristics of the system. This disturbance will change the power flow steady-state solution of the system equations and an oscillation of the generator electrical phase angles will be initiated in the system. This oscillation will persist until a new steady-state is reached. It is important to realize that this new steady-state of the system will correspond to the same total active power P_{tot0} as before the change in

compensation being transmitted between the areas (neglecting the voltage dependence of the loads in the grid). However, since the relative impedances of the interconnecting tie lines in the system now are different from the initial state, the distribution of the power among the different ties will have changed. If a capacitive reactance step is inserted by the CSC, the average power flow on the CSC line will be higher than before and the power flow on the other ties will be reduced. On the contrary, if an inductive reactance step is inserted by the CSC, the average power flow on the CSC line will be lower than before and the power flow on the other tie-lines will be increased. These relationships may be expected from Eq. 4.1 but since the voltage phase angles at the line ends also change due to the change in compensation level, a mathematical derivation is necessary to determine the effect of controlled series compensation on the steady-state line power.

4.1.2 System model

This section will focus on the system model which is used for the controller design. Initially, a number of general assumptions on the characteristics of the power system are established:

- *The power system is assumed to consist of mainly two grid areas which are prone to inter-area power oscillations of one dominating frequency.* This assumption is based on the fact that many power systems which require supplementary power oscillation damping are of this type.

- *The generators in the system are assumed to provide the grid with voltages which are well controlled in magnitude.* This is according to the classical modeling approach for synchronous machines. If PSS are used, the dynamics of these are seen as a contribution to the general damping of the inter-area mode and these dynamics are not modeled explicitly.

- *The loads in the system are assumed to be voltage-independent static loads.* The voltage characteristics of loads in a power system influences the damping of power oscillations in the system. In the models, this

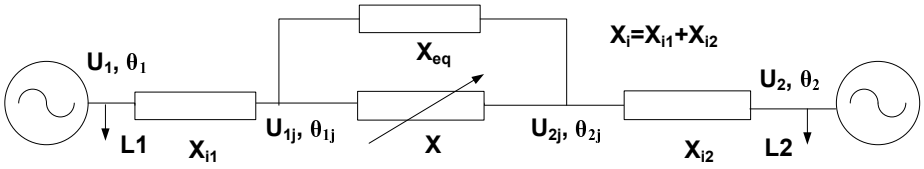

Figure 4.2: Generic system model for control of CSC.

influence on the mode damping is considered as a part of the general damping of the inter-area mode.

With these assumptions in mind, a very simple way to describe a power system of this type is according to Fig. 4.2. Here, each of the power system areas (1 and 2) is represented by a synchronous machine modeled by the classical model. The transmission line where the CSC is installed is represented by a variable inductive reactance X whereas the grid reactances are reduced to one parallel reactance X_{eq} and one series reactance X_i. X_i is the sum of the series reactances X_{i1} and X_{i2} corresponding to each of the grid areas.

It should be stressed that variables denoted by $X_{subscript}$ in the following generally refer to reactances which are given with a positive sign if the reactance is inductive and by a negative sign if the reactance is capacitive. This means for example that the reactance of the CSC device, X_{CSC} is negative if the device inserts a capacitive reactance in series with the line and that the maximum capacitive reactance of the CSC, denoted by X_{CSCmin}, is a negative number.

The system in Fig. 4.2 will exhibit one mode of electro-mechanical oscillation when it is subject to a disturbance. It is assumed that the angular frequency of this mode is ω_{osc} (or f_{osc} expressed in Hz) and that the damping exponent of the mode is σ. This means that the inter-area power oscillation in this system can be described by an equation of the form $P_{osc}(t) = Ce^{\sigma t}sin(\omega_{osc}t)$. The loads in the system are represented by two loads $L1$ and $L2$ which are assumed to be constant active power voltage-independent loads connected close to each machine representation.

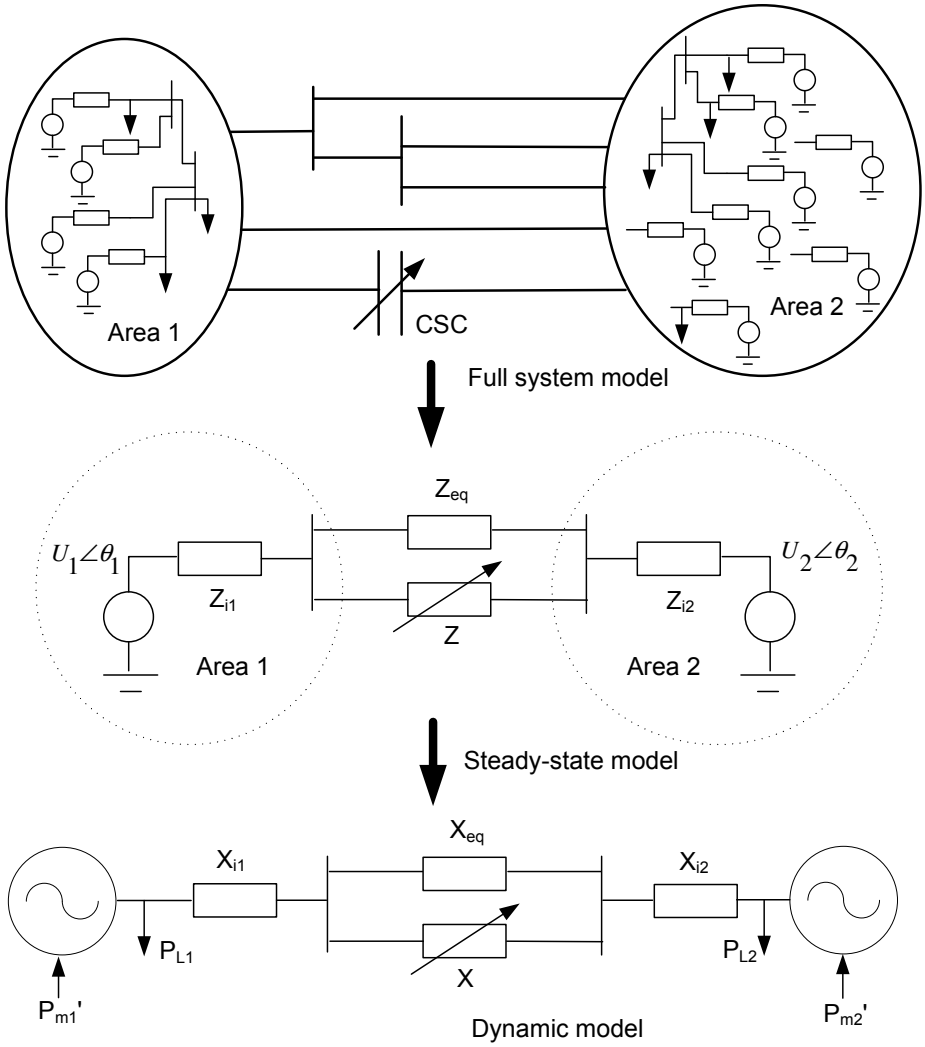

Figure 4.3: Motivation for the choice of CSC system model.

An attempt to motivate the choice of system model is made in Fig. 4.3. In the upper part of the figure, a power system consisting of two grid areas that are weakly interconnected is shown. In the middle of the figure, this system has been reduced to a steady-state model where the grid areas are represented by the voltage phasors $U_1\angle\theta_1$ and $U_2\angle\theta_2$ behind the short-circuit impedances Z_{i1} and Z_{i2}. The interconnecting lines are represented by the impedances Z and Z_{eq}. In order to extend this model to a dynamic representation of the grid, it is assumed that local modes of oscillation are neglected in each of the grid areas. This makes it possible to represent each grid area as a single synchronous machine model with the aggregated moment of inertia of all synchronous machines in the grid area. The resistances in the system are also neglected and all lines in the model are represented by their reactance values. We introduce the total mechanical power which is generated at the turbines in each area as P'_{m1} and P'_{m2} for the grid areas 1 and 2 respectively. The total load in each area is represented by the constant loads P_{L1} and P_{L2}.

The system model was first described in Paper 1 together with an outline of estimation routines and a verification study on the prediction capability of the model for larger power systems.

4.1.3 Theory

The parameters in the system model must be estimated for each system and system topology in order to base a controller on the model. To perform this basic estimation, the dynamics of the system model must be investigated. In order to proceed, it is important to know which parameters that are measured and available to the controller in real-time. Since the goal is to develop a controller based on locally measured quantities, the focus should be on these parameters. A natural start is to investigate how changes in the inserted series reactance at the FACTS device affect the active power transmitted on the FACTS line. Once an expression for the step response in the line power has been derived, this can be used to estimate the grid parameters in the system model from actual measurements at the CSC location.

Assume that the power system can be described by the model in Fig. 4.2. First, the change in the average CSC line power resulting from a step change in the CSC reactance is derived.

The total instantaneous power transmitted across the inter-tie may be expressed as

$$P_{tot} = \frac{U_{1j}U_{2j}\sin(\theta_{1j} - \theta_{2j})(X_{eq} + X)}{X_{eq}X}, \tag{4.2}$$

with denotations from Fig. 4.2. The instantaneous power on the CSC line is then given by

$$P_X = \frac{U_{1j}U_{2j}\sin(\theta_{1j} - \theta_{2j})}{X}. \tag{4.3}$$

Combination of these two equations yields

$$P_X = \frac{X_{eq}}{X_{eq} + X}P_{tot}. \tag{4.4}$$

Equation 4.4 is also valid for the average values of the power (averaged over a full oscillation cycle) on the line during a power oscillation and the total power. This means that the average power on the CSC line can be expressed as

$$P_{Xstat} = \frac{X_{eq}}{X_{eq} + X_0}P_{tot0}, \tag{4.5}$$

with X_0 as the constant reactance of the CSC line. P_{tot0}, the average transmitted power between the areas (measured over a full oscillation cycle), is assumed to be constant for any change in the reactance X according to the discussion in Section 4.1.1.

Equation 4.5 also applies to the transmitted power after a step in reactance such that $X{=}X_0{+}\Delta X$. Accordingly, the average line power after the step can be expressed as

$$P'_{Xstat} = \frac{X_{eq}}{X_{eq} + X_0 + \Delta X}P_{tot0}. \tag{4.6}$$

Dividing Eq. 4.6 by Eq. 4.5 yields

$$P'_{Xstat}(X) = P_{Xstat}\left(\frac{X_{eq} + X_0}{X_{eq} + X_0 + \Delta X}\right). \tag{4.7}$$

This expression shows the dependence of the average line power on the line compensation level in the reduced system of Fig. 4.2. Equation 4.7 can be used to estimate X_{eq} from measurements in a system which fulfils the general assumptions of Section 4.1.2.

In order to estimate the other grid parameter X_i it is necessary to derive equations for the dynamic response in the line power as a result of a step in the line compensation. This derivation is given in detail in Paper 1 while a brief summary of the calculations is given below.

The dynamics of a synchronous machine connected to an infinite bus can be expressed as in Eq. 2.1:

$$\frac{d^2\theta}{dt^2} = \frac{\omega_0}{2H}(P'_m - P'_e). \tag{4.8}$$

Here the electrical angle of the machine is denoted θ, P'_e is the power transmitted from the generator to the grid and P'_m is the mechanical power delivered to the generator from the turbine(s). H is the constant of inertia of the generator and ω_0 is the electrical angular frequency of the power grid.

In a system of the type described in Fig. 4.2, the active power delivered to the grid from the resulting generator model of area 1 can be written as $P'_{e1} = P_{L1} + P_{e1}$ where P_{L1} is the total load in area 1 and P_{e1} is the power transmitted from area 1 to area 2 which can be expressed as

$$P_{e1} = \frac{U_1 U_2 \sin(\theta_1 - \theta_2)}{X_{tot}}, \tag{4.9}$$

where

$$X_{tot} = X_i + \frac{X X_{eq}}{X + X_{eq}}. \tag{4.10}$$

The variable X_{tot} defined in Eq. 4.10 will for simplicity be referred to as the "total reactance between grid areas" in the following. In steady-state, P'_{e1} must equal the total mechanical power generated in grid area 1, P'_{m1}. Equations 4.9 and 4.10, together with the equations describing the generator model of area 2 can be combined to describe the dynamics of the system model in Fig. 4.2. If the resulting system equations are linearized around

the stationary stable difference in the voltage phase angles of the grid areas, θ_{stat}, the system equations can be written:

$$\frac{d^2\Delta\theta_1}{dt^2} = \frac{\omega_0}{2H_1} P_{e\max}\cos(\theta_{stat})(\Delta\theta_2 - \Delta\theta_1) \tag{4.11}$$

$$\frac{d^2\Delta\theta_2}{dt^2} = \frac{\omega_0}{2H_2} P_{e\max}\cos(\theta_{stat})(\Delta\theta_1 - \Delta\theta_2), \tag{4.12}$$

where

$$P_{e\max} = \frac{U_1 U_2}{X_{tot}}. \tag{4.13}$$

Here, subscripts 1 and 2 refer to the respective generators in the system model with $\Delta\theta_1$ and $\Delta\theta_2$ denoting the respective voltage phase angle differences from the point of linearization. Since the average value of the total power transmitted between the grid areas, P_{tot0} is assumed to be constant, a changed total reactance X_{tot} will lead to a change in the phase angle difference between grid areas in steady-state, θ_{stat} dictated by Eq. 4.9. Thus, the change in line reactance inserted by the CSC can be seen as a sudden change in θ_{stat} from $\theta_{stat} = \theta_{1stat} - \theta_{2stat}$ to $\theta'_{stat} = \theta'_{1stat} - \theta'_{2stat}$, and the resulting oscillation will be of the type illustrated in Fig. 4.4.

Since an oscillation in voltage phase angles corresponds to a power oscillation, the change in series compensation leads to a change in the CSC line power which can be divided into two parts. The first is given by Eq. 4.7 and corresponds to the stationary change in power on the line and the second is an oscillatory term. The derivation of the oscillatory term is performed in Paper 1 and the derivation is omitted here. The dynamics of the ideal step response at $t = t_0$ when the system is initially at rest can be expressed:

$$P_X(t) = P_{Xstat} \quad t < t_0 \tag{4.14}$$

$$P_X(t) = P'_{Xstat}\Big(1 + \tfrac{X_{tot} - X'_{tot}}{X'_{tot}} e^{\sigma(t-t_0)}\cos(\omega'_{osc}(t-t_0))\Big) \quad t \geq t_0 \tag{4.15}$$

where

$$P'_{Xstat} = P_{Xstat}\frac{X + X_{eq}}{X' + X_{eq}} \tag{4.16}$$

and

$$\omega'_{osc} = \sqrt{\frac{U_1 U_2\cos(\theta'_{stat})\omega_0}{2X'_{tot}}(\frac{1}{H_1} + \frac{1}{H_2})}. \tag{4.17}$$

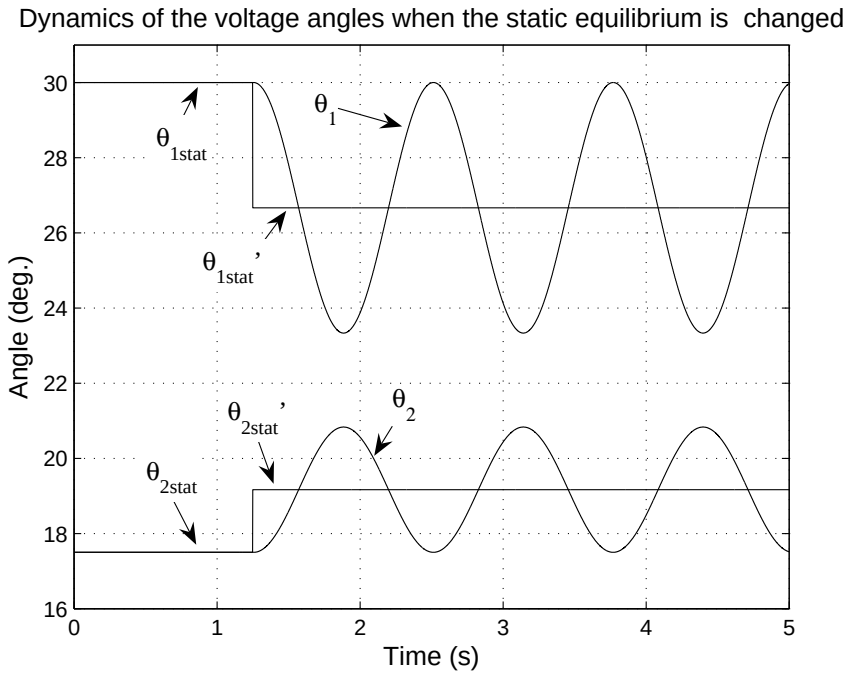

Figure 4.4: Typical dynamic behavior of generator rotor angles in response to a changed steady-state angle difference resulting from a change in the CSC reactance in the system model.

Here, P_{Xstat} is the initial constant power on the line before the step, $P_{Xstat'}$ is the average active power on the line after the step, X is the CSC line reactance initially and X' is the CSC line reactance after the step. X_{tot} is the total line reactance between the areas according to Eq. 4.10 and X'_{tot} is the total reactance after the step change in compensation. It can be seen that Eq. 4.15 includes one change in the stationary value and one oscillatory term. This equation can be used to estimate the parameters of the system model using measurements of a step response at the CSC line power if the power system is at steady-state initially.

Before proceeding, it is necessary to discuss the situation when the system is not at steady-state when a reactance change is applied. This is the normal case for parameter estimation during an oscillation damping event. To begin with, note that Eq. 4.7 is valid even if the system is not at rest initially since

it shows the dependence of the average values of CSC line power to a changed line reactance. In order to find out more about the dynamic properties of a system which is in oscillation it is instructive to set $t = t_0$ in Eq. 4.15 and derive the expression for the power on the line directly after a step in the line reactance for a system at rest initially. Using Eq. 4.16, an expression for the instantaneous power on the line right after the reactance change, P'_X can then be derived. This yields

$$P'_X = P_{Xstat} \frac{X + X_{eq}}{X' + X_{eq}} \frac{X_{tot}}{X'_{tot}}. \tag{4.18}$$

It can be shown that the same relation holds for a system which is not at steady-state initially. Regardless of the system state, the following holds:

The total power transmitted between the areas before and after the reactance change can be expressed by Eq. 4.9. Since it is assumed that the voltages at the machines are well controlled, the voltage magnitudes in Eq. 4.9 are equal both before and after the disturbance. The phase angles of the voltages at the reduced model machines are governed by inertia and these will change very little during the change in reactance, which we assume to be very fast (a few tens of milliseconds). Hence, the voltage phase angles before and after the reactance change can also be assumed to be equal.

It should be noted that the assumption of constant generator voltage magnitudes when a reactance step is executed will introduce model errors. Since the dynamics of the instantaneous changes in line power are very fast, the dynamics of the generator exciters will influence the step response in the line power. However, judging from time-domain simulations of the four-machine test system, the effect appears to be quite small. The generator terminal voltage magnitude changes resulting from steps in the CSC reactance are generally less than 1 % in the simulations.

Expressing the total transmitted power by Eq. 4.9 immediately before and immediately after the change in reactance and eliminating voltage angles and voltage magnitudes yields

$$P'_{tot} X'_{tot} = P_{tot} X_{tot}. \tag{4.19}$$

Here, the instantaneous values of the total power transmitted between the grid areas before and after the step are given as P_{tot} and P'_{tot} respectively

and the total reactance between the grid areas is given as X_{tot} initially and X'_{tot} after the reactance change. Expressing the power transmitted on the the CSC line by Eq. 4.4 gives

$$P'_X \frac{X' + X_{eq}}{X_{eq}} X'_{tot} = P_X \frac{X + X_{eq}}{X_{eq}} X_{tot}. \tag{4.20}$$

Here, P_X and P'_X denote the instantaneous values of the power on the CSC line before and after the step while X and X' denote the initial and final values of the CSC line reactance. Rearranging yields

$$P'_X = P_X \frac{X + X_{eq}}{X' + X_{eq}} \frac{X_{tot}}{X'_{tot}} \tag{4.21}$$

which is the same as Eq. 4.18.

The key results of the above derivation are the two relations, Eq. 4.7 and Eq. 4.21, that are valid even if the system is not at steady state when the reactance change occurs. It is important to note that no linearization has been used in deriving these two expressions. The relations can be used to estimate the parameters X_i and X_{eq} which will be shown in the following sections.

4.1.4 Parameter estimation

The parameters in the system model which are explicitly used in the proposed controller are X_i, X_{eq}, σ and ω_{osc}. The estimation routines are based on a Recursive Least Squares (RLS) estimator with a dedicated PI controller for frequency correction. This procedure provides an estimate of the CSC line power oscillation amplitude, phase and the frequency of oscillation ω_{osc}. This information is essential for the function of the damping controller as well as for the interpretation of the step responses used in the parameter estimation of X_i and X_{eq}.

A conventional way to estimate the parameters of the system in Fig. 4.2 would be to initially linearize the system equations and work out the transfer function from the input variable X denoting the CSC line reactance to the output variable P_X denoting the CSC line power. Then, a least-squares

approach could be used to estimate the grid parameters from the step responses in the output variable. However, considering the non-linearity of the system, this technique would not be optimal when the system is operated far from the point of linearization. In order to find a more suitable estimation technique it is instructive to review the equations for the dynamic and static step responses of the system Eq. 4.7 and Eq. 4.21.

$$P'_{Xstat}(X) = P_{Xstat}\left(\frac{X_{eq}+X}{X_{eq}+X'}\right). \tag{4.22}$$

$$P'_X = P_X \frac{X+X_{eq}}{X'+X_{eq}} \frac{X_{tot}}{X'_{tot}} \tag{4.23}$$

Now, discretize the system in time, denoting each time step with a number $k = 1, 2, ..., N$. Let $y_1(k)$ denote the average power (during a full power oscillation cycle) passing through the CSC line following the k:th time-step and $y_2(k)$ denote the instantaneous power measured initially at each time step. Additionally, let the input signal X be denoted by $u(k)$. Then the estimators for $y_1(k+1)$ and $y_2(k+1)$ at time instant k can be written as

$$\hat{y}_1(k+1) = y_1(k)\left(\frac{X_{eq}+u(k)}{X_{eq}+u(k+1)}\right) \tag{4.24}$$

and

$$\hat{y}_2(k+1) = y_2(k)\frac{(X_i+X_{eq})u(k)+X_iX_{eq}}{(X_i+X_{eq})u(k+1)+X_iX_{eq}}, \tag{4.25}$$

where Eq. 4.10 has been used in the second equation. A standard least squares approach estimation of X_i and X_{eq} from known values of the system responses $y_1(k)$ and $y_2(k)$ to changes in the control signal $u(k)$ would be to minimize the least squares loss function

$$V(N,X_i,X_{eq}) = \frac{1}{2}\sum_{k=1}^{N}\left((y_1(k)-\hat{y}_1(k))^2+(y_2(k)-\hat{y}_2(k))^2\right). \tag{4.26}$$

It can be seen that both relations Eq. 4.24 and Eq. 4.25 are non-linear and to apply standard RLS-estimation to estimate the parameters would require linearizations where some system information would be lost. Since the proposed oscillation damping controller may work with large discrete

changes in the series reactance in a wide range of operating conditions, this type of approximations are not optimal. Non-linear optimization, which presents another more accurate way to solve the problem is considered to be too time-consuming at this stage of the project, but it should be considered as a future improvement to the controller.

In order to find a reasonably accurate, approximate solution to the problem, an alternative method is used here. For each known step response, it is assumed that the model of the power system equals the real system. The system parameters can then be calculated using the non-linear relations Eq. 4.22 and Eq. 4.23. The parameter values obtained for each time-step are then recursively averaged to form the actual estimates of the parameters in real-time. If the actual parameter estimates for each time step are denoted $X_i(k)$ and $X_{eq}(k)$ and the results from each of the individual estimations of parameters are known as $\hat{X}_i(k)$ and $\hat{X}_{eq}(k)$ then

$$X_{eq}(k+1) = \frac{\gamma X_{eq}(k) + \hat{X}_{eq}(k+1)}{\gamma + 1} \tag{4.27}$$

$$X_i(k+1) = \frac{\gamma X_i(k) + \hat{X}_i(k+1)}{\gamma + 1} \tag{4.28}$$

are defined as the weighted averages of the old estimates and the most recent estimates of the parameters. Here, γ is a factor which weights the influence of old estimations when the actual parameter estimates are derived. The parameter γ may range from 0 for a system which completely trusts the most recent estimation to ∞ for a system which does not trust the most recent estimation at all. In the implementation of the controllers assuming a measurement noise of 1 %, a suitable value for γ was found to be $\gamma = 1$.

The used estimation method optimizes the parameters for every individual step response in a non-linear fashion and averages the obtained estimates in contrast to non-linear optimization which would find the optimal parameters considering all the available step responses data and solve the full optimization problem.

The procedure of obtaining the individual estimates $\hat{X}_i(k)$ and $\hat{X}_{eq}(k)$ from one known step response is discussed in Section 4.1.6 and Section 4.1.7.

Finally, it should be mentioned that the damping parameter σ is not estimated at all so far in the project. This parameter is considered to be hard to estimate since the controller requires the parameters to be estimated within the span of half an oscillation cycle. In the controller implementation, the parameter is set to $\sigma = 0$ in order to assume a system with poor damping of the critical model.

4.1.5 Estimation of the power oscillation mode characteristics

In the controller, a Recursive Least Squares (RLS) algorithm is used to estimate the oscillation mode characteristics from the measured CSC power data. The RLS routine used in the controller resolves the measured CSC power data in real time into an average part and an oscillating component. The latter component is represented as a rotating phasor. From the phasor, the amplitude, phase, and frequency of the oscillation can be obtained. The procedure utilizes an initial oscillation frequency which is selected based on knowledge about the power system gained by simulation or from practical experience. When a power oscillation is present, the actual oscillation frequency is estimated using a PI controller to minimize the frequency difference between the estimated and the measured power oscillation data. The RLS formulation used here is found in [28], where the details of the derivation are presented. In this work, the method is briefly summarized.

Assuming that the power oscillation frequency is known as ω_{osc}, the argument of a rotating coordinate system can be established as

$$\theta = \omega_{osc} t. \tag{4.29}$$

Now, assume that the line power data measured at the FACTS device can be expressed as a function of time:

$$p(t) = P_{av} + \mathrm{Re}(\Delta \bar{P} e^{j\omega_{osc} t}) + v(t), \tag{4.30}$$

where P_{av} is the average value of the line power and the oscillative part of the line power is given by $Re(\Delta \bar{P} e^{j\omega_{osc} t})$. Here, the complex phasor is given by

$$\Delta \bar{P} = \Delta P_D(t) + j \Delta P_Q(t), \tag{4.31}$$

and $v(t)$ denotes the process noise which includes the characteristics of the process which are not modeled. With $y(t) = p(t)$, the expression becomes

$$y(t) = P_{av} + \Delta P_D(t)cos\theta(t) - \Delta P_Q(t)sin\theta(t) + v(t). \tag{4.32}$$

The algorithm which estimates the model parameters $\hat{p}(\theta)$ from the noisy observations $y(t)$ by the method of least squares can be expressed as

$$\frac{d\hat{p}(\theta)}{d\theta} = K_C(\theta)\left[y(\theta) - h(\theta)\hat{p}(\theta)\right] \tag{4.33}$$

where

$$\hat{p}(\theta) = \begin{bmatrix} P_{av} \\ \Delta P_D \\ \Delta P_Q \end{bmatrix} \tag{4.34}$$

$$h(\theta) = \begin{bmatrix} 1 & \cos\theta & -\sin\theta \end{bmatrix} \tag{4.35}$$

$$K_C(\theta) = \begin{bmatrix} \kappa_{av} \\ \kappa_{ph}\cos(\theta+\mu) \\ -\kappa_{ph}\cos(\theta+\mu) \end{bmatrix} \tag{4.36}$$

with the constants

$$\kappa_{av} = \xi_F(1+\xi_F^2), \quad \kappa_{ph} = \xi_F\sqrt{\xi_F^4 + 5\xi_F^2 + 4} \tag{4.37}$$

$$\mu = \arctan\left[\frac{3\xi_F}{2-\xi_F^2}\right], \quad \xi_F = \frac{\omega_{CO}}{\omega_{osc}}. \tag{4.38}$$

Here ω_{CO} is the cut off frequency of the algorithm which can be interpreted as the bandwidth of the changes which can be detected by the RLS. The frequency of oscillation ω_{osc} is initialized at an expected value of the oscillation frequency and is then, once an oscillation is detected by the algorithm, adapted by a PI controller which attempts to keep the difference in phase angle of the rotating coordinate system and the phase angle of the phasor $\Delta\bar{P}$ estimated by the RLS constant.

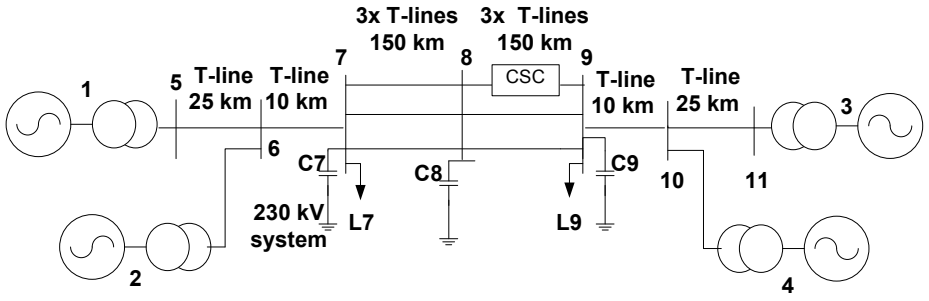

Figure 4.5: Four-machine power system inspired by P. Kundur.

4.1.6 Estimation of the parameter X_{eq}

The parameter X_{eq} has an intuitive interpretation as the total parallel reactance contribution from the transmission lines which are connected in parallel to the line where the CSC is placed, connecting the two areas. It may be roughly estimated from inspection of a line schematic of the power system with information of the transmission line lengths and electrical characteristics. This type of estimation may function as a reality-check to determine if the parameter value which is estimated from line power measurements is in the expected range.

The estimation of X_{eq} is based on the change in average active line power which is caused by the insertion of a known inductive or capacitive reactance in series with the transmission line. As an example, the simulated step response of the CSC line power in a two-area, four-machine system as in Fig. 4.5 is shown in Fig. 4.6. Using such a measured step response, the parameters X_i and X_{eq} can be estimated.

In the controller, which is time-discrete in nature, an estimation of X_{eq} is performed at every time-step provided that the CSC reactance is changed significantly. The estimation relation can be derived from Eq. 4.22. Thus,

$$\hat{X}_{eq} = \frac{X - \frac{P'_{Xstat}}{P_{Xstat}} X'}{\frac{P'_{Xstat}}{P_{Xstat}} - 1}. \tag{4.39}$$

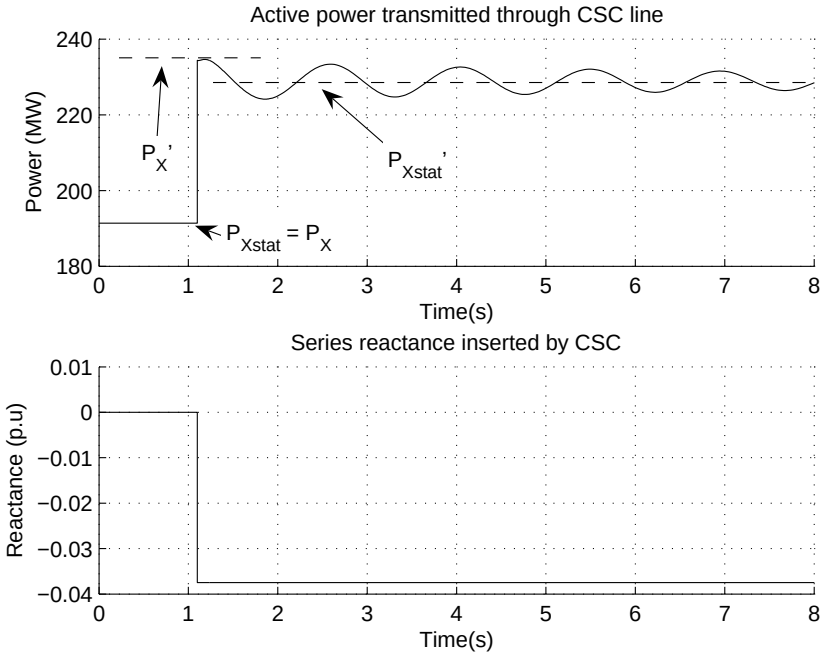

Figure 4.6: Simulated step response of the CSC line power in a two-area system when the CSC reactance is changed at t=1.2 s.

The values of $\hat{X}_{eq}$ calculated from equation Eq. 4.39 should be positive provided that the measured average power values before and after the reactance step are correct. However, if bad data is provided to the estimator, the value may be negative. To improve the controller stability in such cases, the controller is instructed to discard negative X_{eq} estimates in the implementation. Also, to reduce the impact of noise on the estimation process, a minimum change in the average power on the line is required in order to make an estimation.

It be further be noted from Eq. 4.39 that when the ratio P'_{Xstat}/P_{Xstat} approaches one, the estimate grows towards infinity. This is a desired behavior since if this ratio is one, it means that changes in the CSC reactance does not affect the average line power. This in turn must mean that no lines parallel to the CSC line exist and X_{eq} is thus infinite.

4.1.7 Estimation of the parameter X_i

The intuitive interpretation of the parameter X_i is somewhat less clear than the one for X_{eq}. If the connection between the two grid areas in the power system geographically can be viewed as a number of interconnecting lines, these may be seen as corresponding to X_{eq} and X while the line reactances belonging to each of the areas may be seen as included in the parameter X_i. Also the transient reactances of the synchronous machines contribute to this variable. It is hard to estimate this parameter by inspection of the power system, but a rough estimation is possible with the knowledge of the θ_{stat}, the power transmitted between the areas and the values of X and X_{eq} using Eq. 4.9 to calculate X_{tot} and then Eq. 4.10 to derive X_i.

Detailed estimation of X_i is performed using the dynamic step response in the line power to a change in the line reactance. The estimation for a system at rest initially can be done by means of Eq. 4.15 while Eq. 4.23 can be used to estimate the parameter when the system is not at steady-state initially. Since this case is more general, we threat this estimation technique in the following.

Assuming that the parameter X_{eq} has been estimated by means of Eq. 4.39 which is also valid for an oscillating system, the parameter X_i can be derived using Eq. 4.23. The necessary input data for these estimations are the average and instantaneous values of the line power initially and after the reactance step together with the CSC line reactance before and after the change in reactance. In a real-life system, it is necessary to consider the time delay of the CSC device (which may be in the range of 20 ms) when collecting the instantaneous power data for the estimation.

One way to estimate X_i is to note that the change in total reactance between the areas due to the reactance step can be written without knowledge of X_i using Eq. 4.10 as

$$\Delta\hat{X}_{tot} = \frac{X'\hat{X}_{eq}}{X' + \hat{X}_{eq}} - \frac{X\hat{X}_{eq}}{X + \hat{X}_{eq}}. \tag{4.40}$$

Then, by rearranging Eq. 4.23, X_{tot} can be expressed in quantities that are known as

$$\hat{X}_{tot} = \frac{\Delta \hat{X}_{tot}}{\frac{P_X(X+\hat{X}_{eq})}{P'_X(X'+\hat{X}_{eq})} - 1}. \tag{4.41}$$

Finally, by Eq. 4.10

$$\hat{X}_i = \hat{X}_{tot} - \frac{X\hat{X}_{eq}}{X + \hat{X}_{eq}}. \tag{4.42}$$

As in the case of estimation of X_{eq}, bad data may cause large estimation errors in $\hat{X}_i$. For example, Eq. 4.41 goes to infinity for small changes in X and P_X. In the implementation of the controller, no estimation is performed if the step response is too small following a reactance change. Also, a negative estimate of X_i causes the controller to discard the current estimation of both X_i and X_{eq} and to revert to the last valid estimation data.

4.2 System model for control of a DPFC

4.2.1 Power flow control by means of a DPFC

The topology of the DPFC gives two means for controlling the line power. Either, the tap of the PST may be changed, altering the phase angles of the voltages in Eq. 4.1, or the reactance value of the TSSC may be changed in order to change the denominator in Eq. 4.1 to control the line power. Since the PST is a slow device when compared to the TSSC, the tasks that require speed of control like power oscillation damping, transient stability improvement, and voltage stability improvement are performed by the TSSC. The PST is thought to act on a slower time-scale, for instance optimizing the power system losses. When the fast control tasks are considered, the PST is a device contributing with its constant electrical characteristics to the grid environment surrounding the TSSC. This is the basis for construction of the system model for the DPFC control which is aimed at controlling the dynamic TSSC part of the device. The control of the internal PST of the DPFC has not been considered in detail in this thesis. However, the aim of

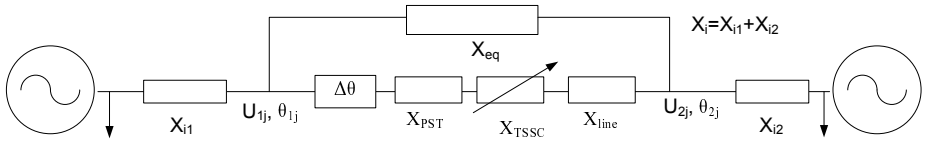

Figure 4.7: Generic system model for control of dynamic part of DPFC.

this controller may for instance be to minimize the overall grid losses and to balance the power flows in the system. These are tasks performed by the TSO at the system level where a large amount of grid data and remote system information must be considered.

4.2.2 System model

The system model for control of the dynamic part of the DPFC is based on the system model developed for control of CSC utilizing the same basic assumptions. A simple model for the PST consisting of a fixed voltage angle shift in series with a tap-dependent series reactance replaces the CSC in the original model yielding a basic model illustrated in Fig. 4.7.

Here, two additional known parameters are introduced, the tap-dependent series reactance of the PST, X_{PST} and the advancing (boost) phase angle shift introduced by the PST, $\Delta\theta$. The series reactance of the uncompensated DPFC line is given as X_{line} and the variable reactance inserted by the dynamic part of the DPFC is denoted X_{TSSC}. The damping of the oscillatory mode is given by the damping exponent σ and the frequency of the mode as ω_{osc} (or f_{osc} expressed in Hz), assuming that the power oscillation can be described by an equation of the form $P_{osc}(t) = Ce^{\sigma t}sin(\omega_{osc}t)$. The unknown grid parameters X_i and X_{eq} remain the same as in the CSC system model. For convenience, the denotation $X = X_{line} + X_{PST} + X_{TSSC}$ is used in the following.

4.2.3 Parameter estimation

The parameter estimation follows the same basic principles as in the model for the CSC. An RLS routine is used to estimate the phase, amplitude, and frequency of the power oscillation as well as the average line power. The damping exponent of the oscillatory mode is not estimated but set to a fixed value $\sigma = 0$. The estimation of the grid parameters X_i and X_{eq} is briefly discussed in the following sections while the detailed calculations are given in Appendix A.

Estimation of the parameter X_{eq}

The X_{eq} parameter can be estimated in a similar way in the DPFC system model as in the CSC system model. By measuring the step response on the DPFC line, the change in average power following a change in the TSSC reactance can be estimated. It can be shown (see Appendix A) that the average power on the DPFC line after a step in series reactance from X to X' is given by

$$P'_{Xstat} = P_{Xstat}\frac{X + X_{eq}\cos(\theta_0 + \Delta\theta)/\cos\theta_0}{X' + X_{eq}\cos(\theta_0 + \Delta\theta)/\cos\theta_0} \tag{4.43}$$

where the average power transmitted on the line is given as P_{Xstat} before the reactance change and P'_{Xstat} after the change in reactance. Here, $\theta = \theta_{1j} - \theta_{2j}$ and its initial average value θ_0 can be calculated from

$$P_{Xstat}(X) = \frac{U_{1j}U_{2j}}{X}\sin(\theta_0 + \Delta\theta_0), \tag{4.44}$$

where it can be assumed that the voltage magnitudes U_{1j} and U_{2j} are constant and equal to the system voltage. Eq. 4.43 is approximately valid assuming that the change in the angle θ as a result of the step is sufficiently small (see Appendix A). Note the large similarity of Eq. 4.43 and Eq. 4.22 valid for the system without PST. Defining

$$X_{eqEff} = X_{eq}\cos(\theta_0 + \Delta\theta)/\cos\theta_0 \tag{4.45}$$

Eq. 4.43 reduces to the expression valid for CSC, Eq. 4.22 with X_{eqEff} replacing X_{eq}. Thus,

$$X_{eqEff} = \frac{X - \frac{P'_{Xstat}}{P_{Xstat}} X'}{\frac{P'_{Xstat}}{P_{Xstat}} - 1} \tag{4.46}$$

can be used together with Eq. 4.45 to find the parameter X_{eq}. If the change in the voltage phase angle difference θ due to the step in line reactance is significant, the average of the phase angle differences calculated by Eq. 4.44 before and after the reactance step, θ_{av} can be used instead of θ_0 in Eq. 4.45. This reduces the errors in the assumptions used in the derivation of the estimation relations. This method is used in the SIMPOW implementation of the estimator.

Estimation of the parameter X_i

If the instantaneous step response in the DPFC line power to a step in the TSSC reactance is derived, the result turns out (see Appendix A) to be the same expression as in the case of the CSC model, that is

$$P'_X = P_X \frac{X + X_{eq}}{X' + X_{eq}} \frac{X_{tot}}{X'_{tot}}. \tag{4.47}$$

Here P_X and P'_X define the DPFC line power immediately before and immediately after a change in the series reactance. X_{tot} and X'_{tot} are defined by Eq. 4.10 with the reactance values before and after the reactance step. Note that X_{tot} is not the total reactance between areas in the DPFC model. Since the PST inserts a fixed voltage phase shift, it is not possible to define a total reactance between areas. X_{tot} is calculated as if there were no phase shift inserted by the PST.

The estimation of X_i in this model may follow the same steps as does the estimation of the parameter in the system model for the CSC by means of Equations 4.40, 4.41, and 4.42.

It is clear from the estimation relations of X_i and X_{eq} that these routines contain elements which are sensitive to modeling and measurement errors.

The calculation of the initial phase angle θ_0 for example involves an inverse sine function which is only defined for arguments less than one and the relation Eq. 4.43 is only approximately valid. Additionally, the risks of bad data and too small step responses are the same as for the estimation in the model for CSC. To robustify the algorithm in the implementation, limits are put on the argument on the arcsine function in the calculation of θ_0. Also, no estimation is performed if the step responses in the average and instantaneous power on the line do not exceed certain limits. As in the case of estimation in the model for the CSC, negative values of the grid parameters due to measurement or modeling errors are always discarded.

5 Principles for control of CSC

In this chapter, we introduce approaches to the different control tasks of the CSC. The system model developed in the preceding chapter is used as the basis for design of the power oscillation damping and power flow controller. The transient improvement mechanism, however, is to a large extent, but not totally, independent of the model.

5.1 Power oscillation damping and fast power flow control

The controller that is described here is a time-discrete non-linear model-predictive controller for power oscillation damping and power flow control. The system parameters are estimated during the controller operation by the methods discussed in the previous chapter, making the control approach adaptive. The principles behind the controller are discussed and verified in Paper 2 and Paper 3. It should be noted, however, that the parameter estimation approach proposed in the thesis is different from the one presented in Paper 3 since the latter was found to produce non-linear equations which were sensitive to numerical instability of the solutions.

5.1.1 Power oscillation damping in one time-step

The motivation for the power oscillation damping approach proposed here originated from the appearance of the step response of the line power when a series reactance is inserted in series with one inter-tie transmission line in a two area system. To discuss this, Fig. 4.6 in the last chapter is revisited.

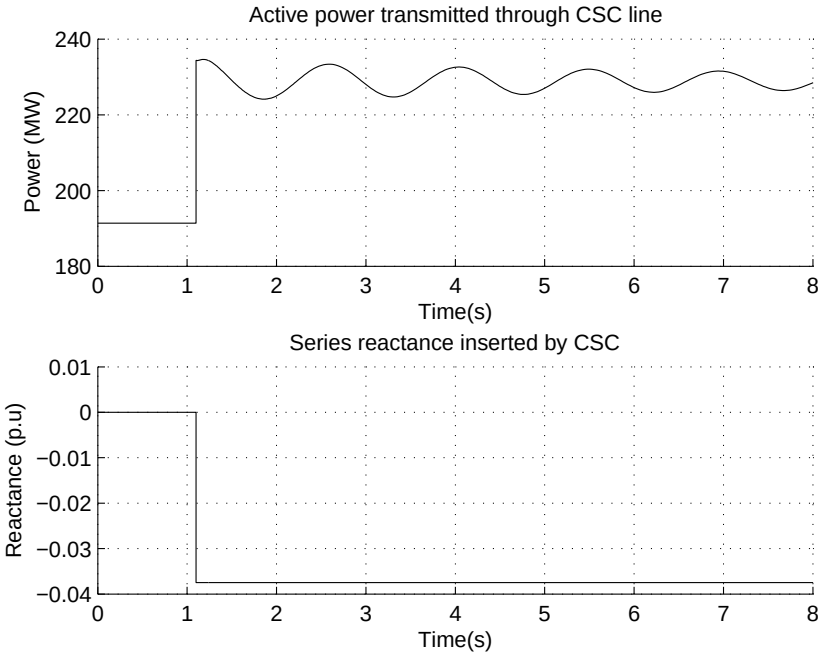

Figure 5.1: Simulated step response of the CSC line power in the two-area system of Fig. 4.5 when the CSC reactance is changed at t=1.2 s.

It can be noted from Fig. 5.1 that a sudden change in the line reactance of the interconnection initiates an oscillation which, of cause has the same oscillation frequency as the inter-area mode which shall be damped. *An interesting thought is then if a step in reactance can be arranged such that the oscillation which is initiated cancels out an already existing oscillation in the system.* From Fig. 5.1 it may be expected that the timing of the step should be such that an increase in the level of series compensation of the line (as in Fig. 5.1) should coincide with a low oscillation peak in order for the initiated oscillation to be exactly in anti-phase with the original oscillation. Similarly, it may be expected that a decrease in the level of series compensation of the line should be chosen to coincide with a high peak in the original oscillation in order to cancel out the oscillation. These thoughts form the basic principles for the oscillation damping controller which is proposed in this thesis.

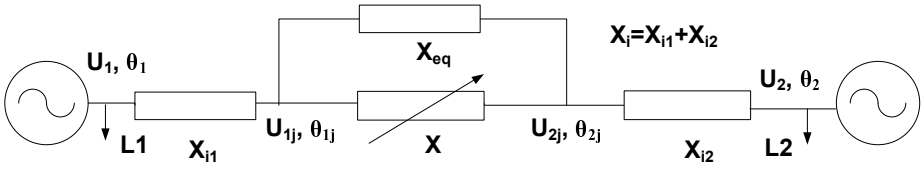

Figure 5.2: Generic system model for control of CSC.

Once a hypothesis on the timing of the reactance step has been established, the next issue is how to determine the magnitude of the step. It does not seem unreasonable to believe that the system model proposed in Chapter 4 can be used to estimate the necessary step magnitude provided that the dynamics of the actual power system can be reasonably accurately predicted by this simple model. The system model is reprinted in Fig. 5.2.

In order achieve the task of determining the reactance change magnitude necessary to cancel out a given oscillation, the system equations of the system model discussed in Chapter 4 are reviewed. The system of differential equations describing the system model for control of CSC can be written as:

$$\frac{d^2\theta_1}{dt^2} = \frac{\omega_0}{2H_1}\left(P_{m1} - \frac{U_1 U_2 \sin(\theta_1 - \theta_2)}{X_{tot}}\right) \tag{5.1}$$

$$\frac{d^2\theta_2}{dt^2} = \frac{\omega_0}{2H_2}\left(P_{m2} - \frac{U_1 U_2 \sin(\theta_2 - \theta_1)}{X_{tot}}\right) \tag{5.2}$$

Here, θ_1 and θ_2 denote the electrical angles of each of the area-equivalent machine models, ω_0 denotes the electrical angular frequency of the system, H_1 and H_2 are the inertia time constants of the reduced machine representations of the grid areas while P_{m1} and P_{m2} denote the excess mechanical power in each area. The excess mechanical power is defined as the power generated in each area which is not consumed by loads in the same area. As before, U_1 and U_2 denote the constant voltage magnitudes at each reduced machine terminal and the total reactance between the areas is denoted X_{tot}.

At the positive and negative peaks of the power oscillation, the difference $\theta_1 - \theta_2$ assumes its highest and lowest values and the time-derivatives of θ_1 and θ_2 are both zero. In order to stabilize the system at one of these instants in time it is necessary to also force the second time-derivative of θ_1 and θ_2 to be zero. If this is done, all higher order derivatives of θ_1 and θ_2 will also be

zero and no oscillations will longer occur in the system. This can be achieved by assuring that the right-hand side of both differential equations is zero. If we assume that the average power transmitted between the two areas is constant during the damping operation, the value of $P_{m1} = -P_{m2} = P_{tot0}$ can be estimated during an on-going oscillation with the knowledge of the grid parameters X and X_{eq} by measuring the average CSC line power P_{Xstat} and using Eq. 4.5 as

$$P_{tot0} = \frac{X_{eq} + X}{X_{eq}} P_{Xstat}. \tag{5.3}$$

Now, in order to force the right-hand side of Eq. 5.2 to zero, assume that the angle difference $\theta_1 - \theta_2$ does not change during the change in reactance and that the voltages at the generators are constant. Then, the product $U_1 U_2 \sin(\theta_1 - \theta_2)$ valid both before and after the reactance step can be calculated in terms of the initial power and reactance values which yields

$$P'_{tot} = \frac{U_1 U_2 \sin(\theta_1 - \theta_2)}{X'_{tot}} = \frac{P_{tot} X_{tot}}{X'_{tot}}. \tag{5.4}$$

Here, the total instantaneous power transmitted between the areas before and after the step is denoted P_{tot} and P'_{tot} respectively, and the total reactance between the areas initially and finally is given as X_{tot} and X'_{tot}. By setting the expression for P'_{tot} equal to P_{tot0}, the ratio of the total reactances before and after the reactance change required in order for the step to cancel the oscillation can be calculated from Eq. 5.4:

$$\frac{X_{tot}}{X'_{tot}} = \frac{P_{tot0}}{P_{tot}}. \tag{5.5}$$

From Eq. 5.5 the required change in the total reactance can be expressed as

$$\Delta X_{tot} = X'_{tot} - X_{tot} = \left(\frac{P_{tot}}{P_{tot0}} - 1 \right) X_{tot} \tag{5.6}$$

and the required change in the initial CSC line reactance X_0 is found by applying Eq. 4.10 to the situation before and after the reactance change, which yields

$$\Delta X = \frac{\Delta X_{tot} (X_0 + X_{eq})^2}{X_{eq}^2 - \Delta X_{tot} X_0 - \Delta X_{tot} X_{eq}}. \tag{5.7}$$

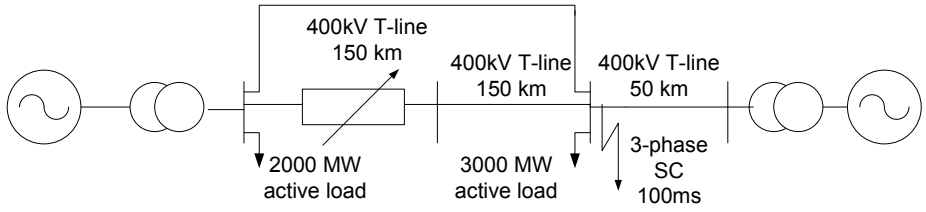

Figure 5.3: Simple test system for time-domain simulation.

To test the derived damping relation, the simple system in Fig. 5.3 is considered.

This system is of the same structure as the system model but it also includes detailed generator models including exciters and governors. The transmission lines are modeled with distributed line parameters. When the system is subject to a 3-phase short circuit which is cleared after 100 ms with no line disconnection and no action of the CSC device indicated by a variable reactance in the figure, a power oscillation is initiated as seen in Fig. 5.4.

Now, consider the case when the grid parameters of the system model have been estimated by measurement of the step response at the CSC device initially and the damping relation of Eq. 5.7 is applied to damp the oscillation at t=3.8 s. The simulation results of the total transmitted power between the machines as well as the power on the two individual transmission lines connected in parallel is shown in Fig. 5.5.

The simulation clearly shows a significant reduction in the power oscillation due to the step in series reactance. This is an encouraging result which indicates that the estimation and damping routines may be applicable in power systems which are described using detailed mathematical models. Note that the application of one reactance step to damp the power oscillation leads to a very large power on the CSC line due to a high degree of compensation. This is clearly not desirable and the technique requires further modification before it can be used as the basis for a real controller. The most straight-forward approach to this is to investigate the possibility of using more than one reactance step to damp an oscillation.

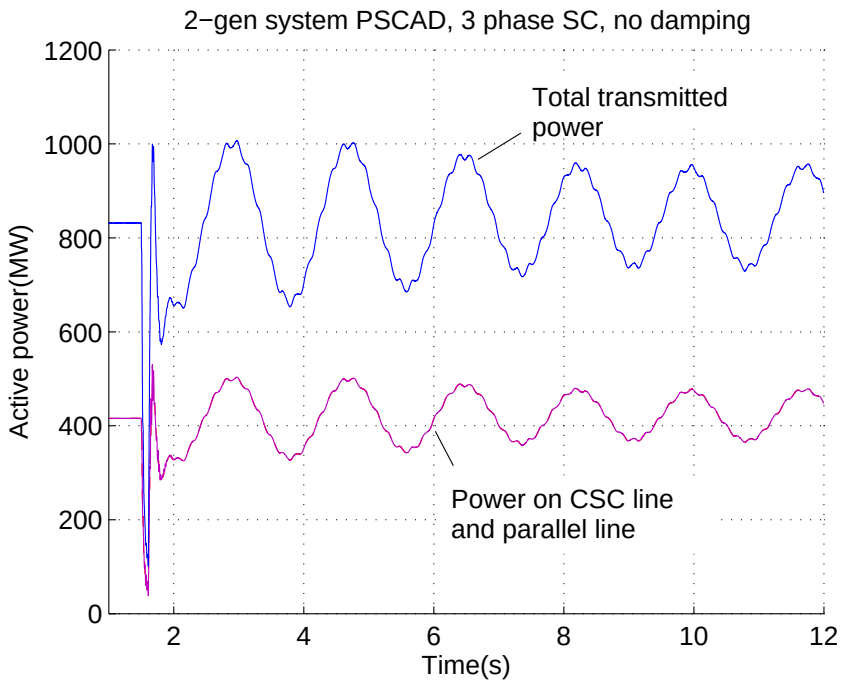

Figure 5.4: Power oscillation in a two-machine system with no damping applied.

5.1.2 Power oscillation damping and power flow control in two time-steps

It has been shown that an oscillation can be ideally damped using only one change in series reactance applied with a suitable timing. Extending the method to use two discrete steps separated in time by half an oscillation cycle gives an additional degree of freedom which can be used to select the final level of compensation of the line. Since the relation between line compensation level and line power is known according to Eq. 4.7, this yields a control method which in the ideal case is able to perform the tasks of power oscillation damping and power flow control using two discrete changes in line reactance separated in time by half an oscillation period.

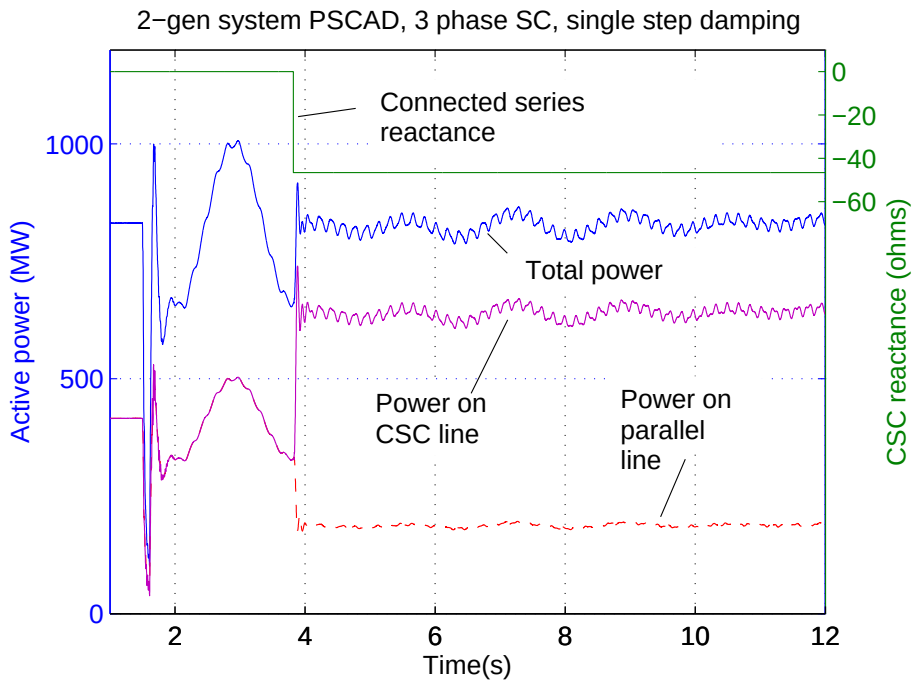

Figure 5.5: Power oscillation in a two-machine system with single step damping applied.

To derive the required reactance steps necessary to achieve these two tasks, it is assumed that the system model is known according to Fig. 4.2. It is also assumed that the the controller is restricted to act only at instants in time coinciding with high or low peaks of the power oscillation. Now it is assumed that the total reactance between grid areas before the first reactance step is X_{tot0}, after the first step X_{tot1}, and after the second step X_{tot2}. The reactance of the CSC line is denoted X_0 initially, X_1 following the first step, and X_2 after the second step. It can be immediately recognized that the final compensation state X_2 can be calculated by means of Eq. 4.7 since it is assumed that the initial average power on the line is known as P_{Xstat} and the desired average power set-point is denoted P_{Xsp}. The expression becomes:

$$P_{Xsp} = P_{Xstat}\left(\frac{X_{eq}+X_0}{X_{eq}+X_2}\right). \tag{5.8}$$

By means of Eq. 4.10, X_{tot2} is then known. To calculate X_{tot1}, denote the instantaneous total power transmitted between the areas before the steps at the point where the controller starts to act as P_{p0}, the total power after the first step as P_{p1}, and the the total power right before the second step as P'_{p1}. The average transmitted total power, which is assumed to be constant during the whole sequence, is denoted P_{tot0} and it is calculated from the CSC line power by means of Eq. 5.3. From Eq. 5.4 it is now found that:

$$P_{p0}X_{tot0} = P_{p1}X_{tot1}. \tag{5.9}$$

The value of the total power right before the second step can be approximated by recognizing that the total power always oscillates around its average value P_{tot0} and that, if it is assumed that the real part of the eigenvalue corresponding to the inter-area mode is σ, the amplitude of the oscillation right after the first reactance will equal the amplitude multiplied by a damping factor $e^{\sigma T_{osc}/2}$, where T_{osc} is the cycle time of the oscillation. Now, the total power right before the second reactance change can be written as

$$P'_{p1} = (P_{tot0} - P_{p1})e^{\sigma T_{osc}/2} + P_{tot0}. \tag{5.10}$$

Here it has been assumed that the power oscillation has the form of a sine function in time. This is an assumption which relies on an assumption of linearity of the system equations. *This is actually the only assumption of linearity which is used in the derivation of the control laws and parameter estimation routines for the adaptive controller.*

Since it is known that the second reactance step must cancel the oscillation completely, the second reactance step must fulfil

$$P'_{p1}X_{tot1} = P_{tot0}X_{tot2} \tag{5.11}$$

and bring the instantaneous total power value to equal the average level P_{tot0}. Combining Eq. 5.9, Eq. 5.10, and Eq. 5.11 now yields

$$\left(\left(P_{tot0} - \frac{P_{p0}X_{tot0}}{X_{tot1}}\right)e^{\sigma T_{osc}/2} + P_{tot0}\right)X_{tot1} = P_{tot0}X_{tot2} \tag{5.12}$$

and the reactance X_{tot1} can be calculated, using Eq. 4.4 to calculate P_{p0} from the measured value of the line power at the peak of the power oscillation

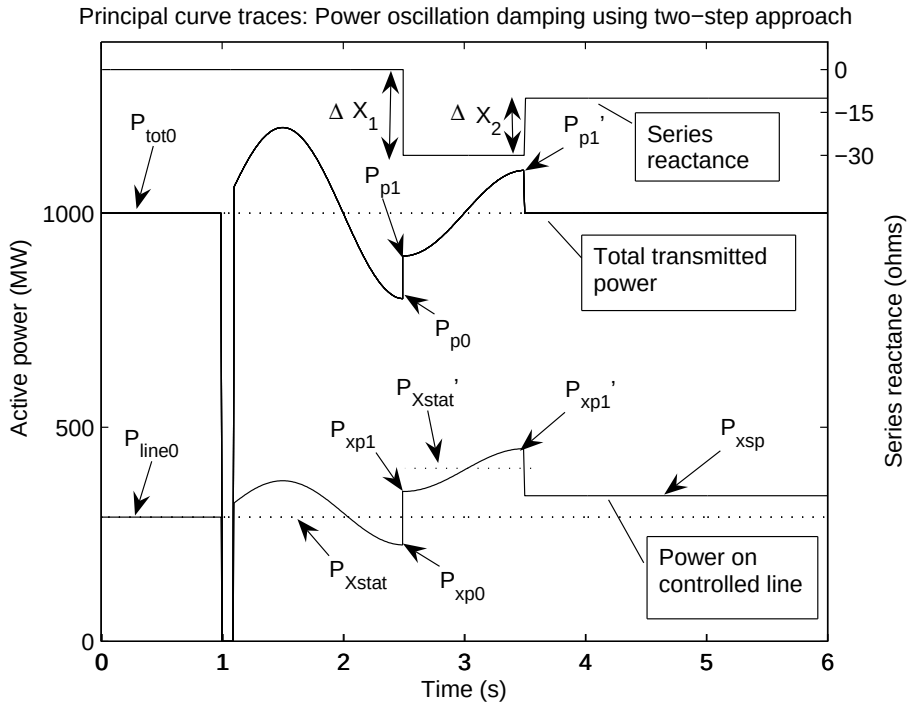

Figure 5.6: Principal function of the two-step damping/power flow control approach.

when the damping sequence is initiated, P_{xp0}. By means of Eq. 4.10 the CSC line reactance X_1 is now known and since X_0 is known initially and X_2 has been calculated, the control law is complete and the necessary reactance changes can be calculated as $\Delta X_1 = X_1 - X_0$ and $\Delta X_2 = X_2 - X_1$. The ideal control process is illustrated in Fig. 5.6.

It should be emphasized that the derived control law is a time-optimal approach based on an idealized system. Naturally, when the control law is used for damping in a more complex system with measurement noise, it will not be perfect. Therefore, in the implementation of the controller, the two step damping process is repeated until the oscillation is completely canceled out.

5.1.3 Combining parameter estimation and power oscillation damping

The control law which was derived in the previous section is based on the assumption that the parameters of the system model are known. In the real case, this is seldom true. The characteristics of the power system may change dramatically as a result of a fault which is cleared by disconnection of some critical lines. Often, such faults initiate power oscillations and if the controller does not utilize remote information, the system parameters will be unknown to the controller. The approach which is proposed in this work uses a controller which utilizes a set of fixed initial values for the parameters. These parameter values are chosen such that they in most system configurations provide suboptimal damping while minimizing the risk of instability. This setting is used at all times when the damping controller is initiated. When the damping controller has started its operation, the step responses in the CSC line power are evaluated and, for each step taken by the controller, the system grid parameters are estimated. The process utilizes equations Eq. 4.39 and Eq. 4.42 to estimate the grid parameters from information of the instantaneous and average step responses in the CSC line power following every reactance change initiated by the controller. Following the denotations from Fig. 5.6, the average power on the CSC line is denoted P_{Xstat} initially and P'_{Xstat} after the first step and the instantaneous values of the line power before the first step P_{xp0} and P_{xp1} after the step are used together with information of the magnitude of the reactance step to estimate the grid parameters. It can be noted that a reliable estimation of the mean power on the CSC line requires some time to stabilize. Since new values of the parameters are not necessary until the decision is made of how the next damping step should be sized, a reasonable approach is to let the estimation of P'_{Xstat} be fast enough to stabilize in about half an oscillation cycle. This gives an estimation process which updates its parameters right before every new reactance step is determined by the controller.

In order to make the estimation process more robust to measurement errors, a weighted average of the estimates is constructed each time a new estimate is availiable as is described in Section 4.1.4.

5.2 Transient Stability Improvement

In a first order approximation, transient stability is governed by the so called equal-area criterion [2]. This is based on plotting the transmitted power between two areas in a graph with power, P versus the voltage phase angle-difference between areas denoted by δ with a horizontal line showing the power which is transmitted in stationary state - the excess mechanical power of the sending area, P_m. The two areas are assumed to be represented by two synchronous machine models with suitable moments of inertia, internal voltage magnitude, and phase. Using this model, the load in each area is assumed to be voltage and frequency independent. The criterion offers a convenient way to calculate the critical clearing time of faults in the system by comparing areas in the $P - \delta$ graph:

The area which is bounded by the the transmitted power $P_{fault}(\delta)$ and P_m when integrating with angle in the accelerating phase during the fault can be expressed as a function of the clearing time of the fault. This area is set equal to the area bounded by the the transmitted power $P_{post}(\delta)$ and P_m integrating during the decelerating phase when the fault has been cleared. The criterion states that these areas are equal when the voltage phase angle difference between the areas reaches its maximum. If the area bounded by $P_{post}(\delta)$ and P_m is less than the area calculated during the accelerating phase, the system is transiently unstable and it will fall out of phase.

The strategy which is proposed in this thesis aims to maximize the transient stability of the system after severe faults, taking into account the thermal overload limit of the CSC line. Before going into the strategy, a few common faults in a power system will be discussed. To this end, it is assumed that the system is of the type which has been described earlier with two grid areas interconnected by a number of transmission lines with a CSC installation on one of these tie-lines.

Case I: A (3 phase) short circuit on one of the interconnecting lines followed by a disconnection of this line. In this case the system will transiently behave in accordance with the principles illustrated in Fig. 5.7.

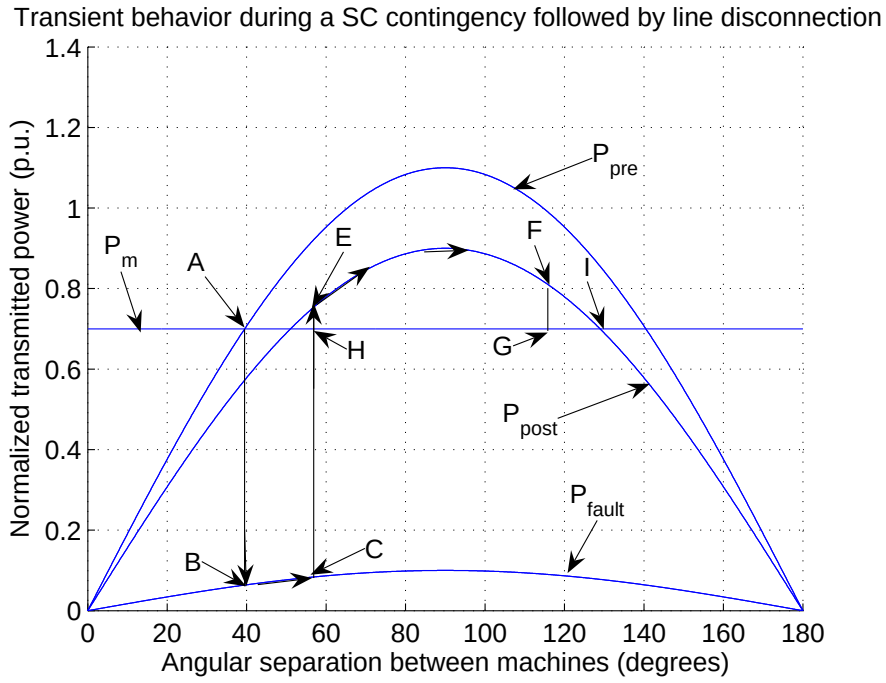

Figure 5.7: Principal transient behavior of the system in the case of a fault leading to line disconnection of one inter-tie line.

The horizontal line P_m in the figure represents the initial power delivered from the sending to the receiving area which equals the excess mechanical power delivered to the generators in the sending area. This power is assumed to be constant during the event. The sinusoidal curves represent the transmitted power over the inter-tie for different values of the tie reactance as a function of the voltage phase angle separation between the areas. Assume that the system starts from a stationary state at A and that the $P - \delta$ relationship is described by $P_{pre}(\delta)$. Then, a severe fault interrupts the transmission and the transmitted power drops to a small value on the curve $P_{fault}(\delta)$ at B. The generators in the sending end are now accelerated with respect to the machines in the receiving end and the angle separation increases. At C, the breakers have isolated the faulted line and the system resumes transmitting power according to $P_{post}(\delta)$. The system will then move with increasing angles along the curve $P_{post}(\delta)$ until it turns back and

the angular separation starts to decrease at F when the areas A-B-C-H and E-F-G-H are equal. In case of a fault with a longer duration, the accelerating area A-B-C-H will be larger and the maximal decelerating area E-F-I-H will be less than A-B-C-H and the system will continue its path with increasing angles passing I, eventually falling out of phase. In this case, it is clear that the transient performance in the first swing can be optimized if the tie reactance is decreased by insertion of series compensation by the CSC at the time of the fault. This action would then raise the $P_{post}(\delta)$ curve and maximize the decelerating area E-F-I-H. Once the system turns back and starts to decrease the angular separation, it is possible to reduce the degree of compensation of the line to reduce the magnitude of the next swing amplitude. This is the start of power oscillation damping, since the system will now oscillate until it settles at a stationary point depending on the final compensation level.

If this type of fault is observed by measurement of the line power on the CSC line, a rapid drop in the transmitted power is first seen followed by a low power transmission level during the fault and a rapid increase in the power when the fault is cleared.

Case II: A fault leading to a load disconnection in the sending area. This type of fault has, in the sense of transient stability, many similarities to a fault leading to a generator disconnection in the receiving area. The case is illustrated in Fig. 5.8.

Assume in this case that the initial system has an excess mechanical power in the sending area which is P_{mPre} and a transmitted power which can be described by $P_{pre}(\delta)$. Then, when the load is reduced in this area, the excess mechanical power increases to P_{mPost}. It should be pointed out that this is not a stable equilibrium power transfer since the total system generation will have to be altered to maintain frequency stability. However, these control actions have a larger time constant and P_{mPost} may be assumed to be constant during the first swing.

At the same time as the load change occurs, the voltage magnitudes at the interconnecting tie line ends will generally change depending on the changed load flow in the system and the voltage dependence of the loads. It is believed

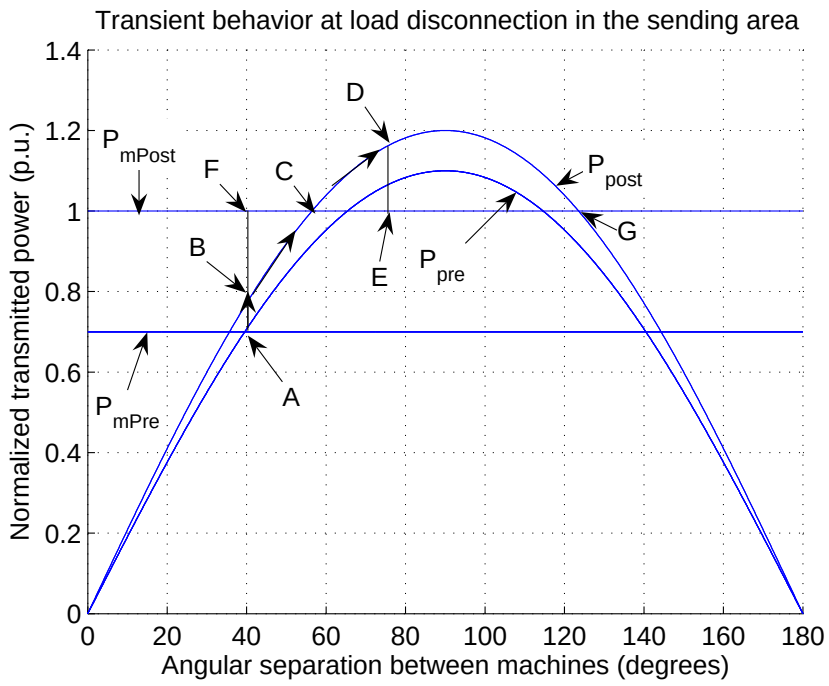

Figure 5.8: Principal transient behavior of the system in the case of a major load loss in the sending area.

that the most common in this case is an increase in the voltage magnitudes at the sending end of the transmission lines, hence we use this case as an example. This initial change in the voltage characteristics can be modeled as a changed voltage for the reduced machine equivalent of the sending end area which gives a post-fault system which transmits power according to the curve $P_{post}(\delta)$. The system will, following the fault, move very rapidly from A to B and then follow the $P_{post}(\delta)$ curve passing C to the turning point at D where the areas B-C-F and C-D-E are equal. In the case of a more severe fault, the system is transiently instable if the area B-C-F is larger than the area bounded by $P_{post}(\delta)$ and P_{mPost}. This area may be enlarged by inserting series compensation at the CSC device as in fault case I.

If this type of fault is viewed by measuring the line power at the CSC device, a rapid change of the line power will be seen followed by a slower increase in the line power when the electrical angles of the machines in

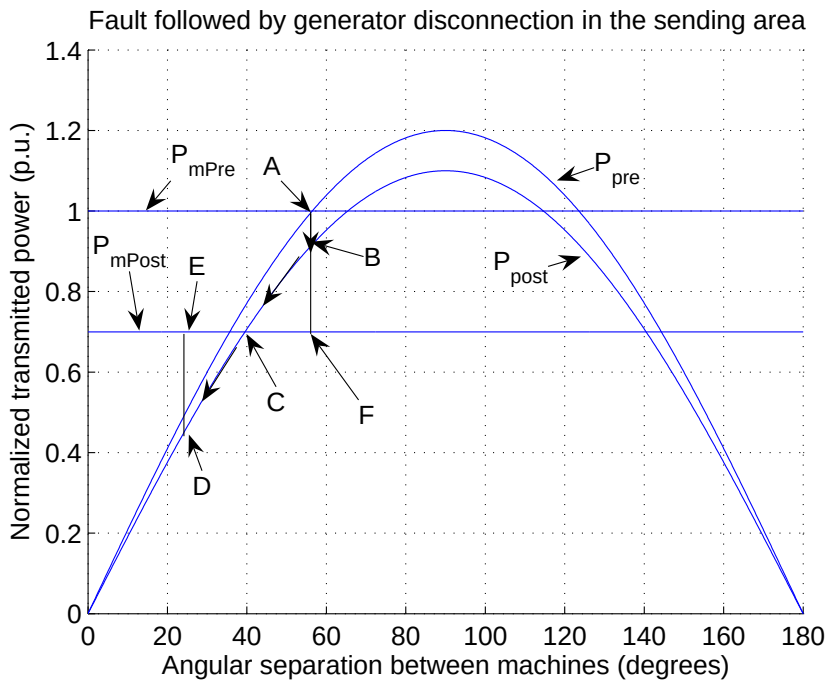

Figure 5.9: Principal transient behavior of the system in the case of a generator disconnection in the sending area.

the system start to change. The initial change in the line power will be either in the positive or in the negative direction depending on the system configuration. It is believed that the line power is most likely to increase initially in a typical case of power system operation.

Case III: A fault leading to a generator disconnection in the sending area. This type of fault is, in the sense of transient stability, similar to a fault leading to a load disconnection in the receiving area. The case is illustrated in Fig. 5.9.

Assume in this case that the initial system has an excess mechanical power in the sending area which is P_{mPre} and a transmitted power which can be described by $P_{pre}(\delta)$. Then, when the generation is reduced in this area, the excess mechanical power decreases to P_{mPost}. As in the previous case, this is not a stable equilibrium power transfer since the total system generation

will have to be altered to maintain frequency stability but it is assumed that the level is constant during the first swing of the generator angles.

Analogously with the argumentation for Case II, the voltage magnitudes at the interconnecting tie line ends will generally change at the instant of the event. This change can be viewed as an alteration of the voltage magnitude of the reduced machine representations and in this example it is assumed that it leads to a lowered $P - \delta$ curve, $P_{post}(\delta)$, which is believed to be the most likely case. In this particular case, the system starts in a stationary state at A. As a result of the fault, the system moves from A to B very rapidly and then on $P_{post}(\delta)$ passing C until it turns at D when the areas B-C-F and C-D-E are equal. In this case, the risk of transient instability is greatly reduced since it is possible for the system to move on the $P_{post}(\delta)$ trajectory also on the the negative δ axis, making the area bounded by this trajectory and P_{mPost} very large. An optimal CSC transient control strategy would in this case initially be to minimize the degree of compensation of the line. Then, if the system passes $\delta = 0$ during the first swing, the degree of compensation should be maximized. When the system starts to swing back, the power oscillation damping strategy should be enabled.

If this type of fault is viewed by measuring the line power at the CSC device, a rapid change of the line power in either direction will be seen followed by a slower decrease in the line power when the electrical angles of the machines in the system start to change. It is believed that the line power is most likely to show a decrease initially in a typical power system operation case.

5.2.1 Proposed transient stability improvement strategy

Based on the above discussion it is clear that fault cases I and II are the ones most sensitive to transient instability. Case I is perhaps the most dangerous case since the accelerating area for the sending area may be very large since the fault generally reduces the transmission to a very low value. Also, the transient capability may in this case be significantly reduced due to a decreased transmission capability resulting from line disconnections. In case

II, the accelerating area may be relatively small but the transient capability can still be reduced significantly due to a higher excess mechanical power in the sending area. Since the nature of a particular fault is difficult to determine in real-time from the CSC device location, it is strongly argued that a method utilizing remote system information should be used to trigger a transient scheme. However, if faults of the type in case I above are considered to be the most threatening to system transient stability, a method using only local signals can be formulated in order to give a controller which is easily implemented in a real power system:

Since the clearance of a fault of type I is seen from the CSC location as a rapid increase in the line power the transient scheme can be initiated when a time-derivative of the line power magnitute exceeding a certain limit C_{lim} is measured at the CSC location during a time exceeding T_{lim}.

This strategy covers all of the faults of type I and likely most of the faults of type II. It may also be triggered in case III faults with adverse effect on the transient stability, however, since this capability is generally very large, this behavior may be tolerated. Due to its simplicity, the strategy may possibly be excessively sensitive and initiate the transient scheme also in cases where a risk of transient instability is not present. However, the triggering method using local signals may still be useful since the implementation effort of this method will be significantly less than that of more elaborate methods based on remote information of the power system. *It should be pointed out that, if the triggering strategy based on locally measured variables is used together with the damping controller proposed in this thesis it is necessary to block the transient controller when the damping controller executes its discrete changes in line reactance.*

The proposed transient switching strategy is illustrated in the following example of a case I fault:

A severe contingency such as a three-phase short circuit in a two-area power system with an interconnection CSC may lead to a case such as the one depicted in Fig. 5.10. Assume that the system starts from a stationary state at A and that the $P - \delta$ relationship is described by $P_{pre}(\delta)$. Then, a severe fault interrupts the transmission and the transmitted power drops to

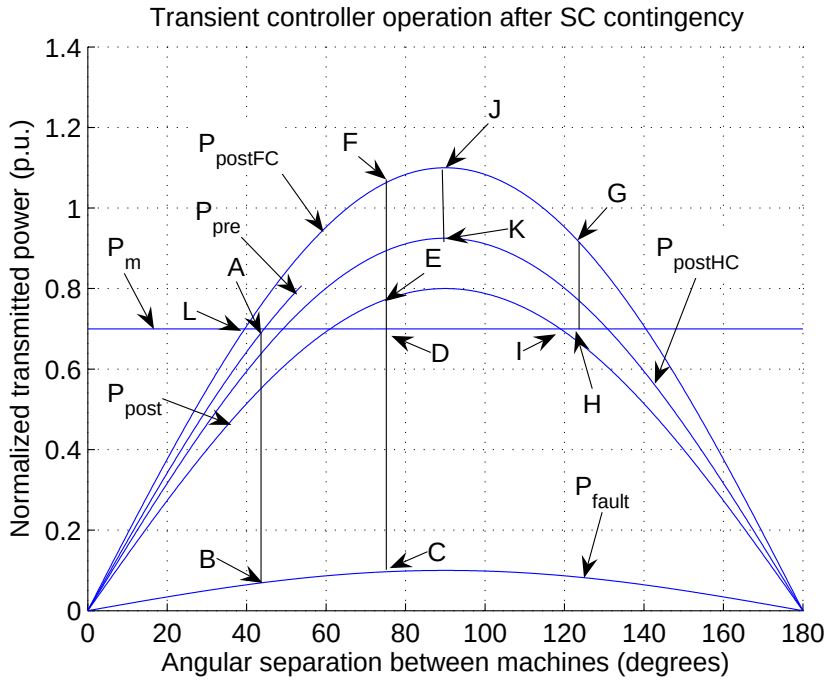

Figure 5.10: Principal function of the transient control strategy.

a small value on the curve $P_{fault}(\delta)$ at B. The generators in the sending end are now accelerated with respect to the machines in the receiving end and the angle separation increases. At C, the breakers have isolated the faulted line and the system resumes transmitting power according to $P_{post}(\delta)$. With no action of the CSC, the system will move along C-D-E and then towards I on $P_{post}(\delta)$. Since the area bounded by D-E-I is smaller than the area A-B-C-D, the system exhibits transient instability and it will fall out of phase. If on the other hand, the CSC is engaged at point C, maximizing the degree of series compensation to the CSC limit X_{CSCmin}, the system will move on the path C-D-E-F-G on $P_{postFC}(\delta)$. and then turn back since the areas A-B-C-D and D-F-G-H are equal. At this point, the system has survived the first-swing and a power oscillation is initiated. It is important to note that the system may still be transiently unstable if the degree of compensation is reduced.

To provide positive damping to the system, the level of compensation should be decreased at some point provided that the system has survived the first swing. This should ideally be done at the turning point G provided that the level of transmitted power after the change in series compensation is larger than the excess mechanical power level P_m in order to avoid instability. To reduce the risk of instability, the proposed controller decreases the level of compensation after turning at G at the point J ($\delta = 90°$) where the transmitted power for all tie reactances is maximized. If the fault case is such that the angle difference never exceeds $\delta = 90°$, the transition is made at the point where δ reaches its maximum value (this case is not illustrated).

The choice of the level of compensation after the change at point J is not trivial. If the level chosen is too low it may push the power curve under the mechanical level P_m resulting in instability. If the level chosen is too high it will provide insufficient damping to the system in the following damping reactance steps. The proposed controller reduces the compensation level at point J to $X_{CSC} = cX_{CSCmin}$ where c is a constant which can be chosen depending on the system characteristics. In the implementation of the controller, $c = 0.5$ has been used. Subsequently, the system follows $P_{postHC}(\delta)$ and the new decelerating area G-J-K-A-H is significantly reduced from the area G-J-F-L-H which would be the case if no change in compensation is applied. This provides positive damping to the system. Since the angle separation between the areas is not available in real-time at the FACTS device location, the time instant for the change in compensation may be determined from measurements of the CSC line current (which is monotonously increasing with angle separation) and estimation the line active power peaks by the RLS routine. This is done by storing the value of the line current on the CSC line at the point where the first peak in line power after the fault is attained. This instant corresponds to $\delta = 90°$ and since the current is monotonously increasing with increased δ, the point J is found when the current passes this level on the back-swing in δ.

The scheme during the first-swing of the generator angles can (after it has been initiated) be concluded in the following compact form:

$$X_{CSC} = X_{CSCmin} \quad (\dot{\delta}_s - \dot{\delta}_r) > 0 \tag{5.13}$$

$$X_{CSC} = X_{CSCmin} \quad (\dot{\delta}_s - \dot{\delta}_r) < 0,\ (\delta_s - \delta_r) > 90^\circ \tag{5.14}$$

$$X_{CSC} = cX_{CSCmin} \quad (\dot{\delta}_s - \dot{\delta}_r) < 0,\ (\delta_s - \delta_r) < 90^\circ,\ c \in [0,1]. \tag{5.15}$$

Here, the electrical angles of the reduced machine equivalents in the sending and receiving area are denoted δ_s and δ_r respectively.

Following the pre-programmed transient control scheme operation in two steps described above, the damping controller is commonly initiated. Even if the system is transiently stable and survives the first swing provided that the pre-programmed scheme is used, the system may still show transient instability if the series compensation level is significantly reduced during one of the subsequent swings. In order to maximize the transient stability during subsequent swings, the controller needs to maintain the maximum possible degree of compensation when the angle separation $\delta_s - \delta_r$ is increasing. To achieve this goal, without exceeding the short-term thermal overload limit of the CSC line, the transient control routine alters the given set-point of the fast power flow control function which is included in the Power Oscillation Damping (POD) controller. The set-point is changed such that the target for the average level of line power (P_{Xsp}) is the short-term thermal overload limit P_{limit} (or the maximum power possible if the overload level cannot be reached). This limit is the active power level on the CSC line which can be allowed for the time it takes for the Transmission System Operator(TSO) to re-dispatch the system to comply with the N-1 criteria of the new conditions (15-30 min).

The strategy of increasing the degree of line compensation during the oscillation damping after a severe fault will help the system to remain transiently stable in the subsequent swings after the first swing provided that the first swing does not give rise to instability by maximizing the decelerating area when $P_{post}(\delta) > P_m$ and $\delta < 90^\circ$. It will also enable the system to operate in cases with high tie reactance ($P_m > P_{post}(\delta)$ for all δ) by increasing the series compensation after the contingency such that a portion of the curve $P_{post}(\delta)$

is pushed above P_m. Additionally, a higher average degree of compensation during the power oscillation damping scheme reduces the risk of the system oscillating in the range where $\delta > 90^\circ$ since the average angle separation during the power oscillation is reduced. This enhances the effectiveness of damping schemes relying on linearization of the system equations, such as the one used in this work.

The proposed transient improvement strategy may be further improved by limiting the operating range of the CSC during the oscillation damping. In this case, a maximum limit of X_{CSC}, X_{CSClim} other than the physical limit of the device would be set when the transient scheme is triggered. This would limit the controller operation to a band $X_{CSCmin} \leq X_{CSC} \leq X_{CSClim}$, ensuring a certain level of compensation of the CSC device during the damping process. This procedure would lower the risk of transient instability during the damping controller operation. However, limiting the operating range of the device decreases the effectiveness of the damping controller which makes the method a trade-off between transient stability improvement and oscillation damping enhancement. Furthermore, an optimal method for limiting the operation region will be dependent on knowledge of the system characteristics and such a method is thus not trivial to design. Nevertheless, the idea is appealing, since such an enhancement of the transient scheme would make the controller more robust which may be required in order to allow a higher power transfer across the inter-tie where the CSC is placed.

Finally, it should be mentioned that, depending on the system configuration, it may be difficult to correctly determine the instant for the second switching in the pre-programmed transient scheme. This is due to the difficulty of accurate estimation of the first peak in the line power oscillation following a major fault. An alternative to the strategy is to omit the second step in the scheme and let the oscillation damping start right away or with a certain delay. This strategy does not take into account the risk for transient instability if a too low compensation level is used when the system angular difference is very large, but it may be used as a backup strategy if the proposed strategy fails.

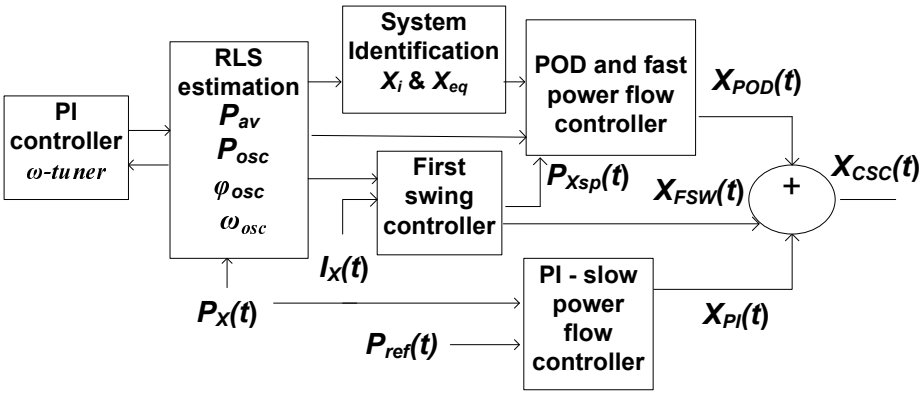

Figure 5.11: Schematic illustration of the full CSC controller.

5.3 The general control approach

Combining the different objectives and principles for controlling CSC discussed in the previous sections, a full controller for CSC may have the structure illustrated in Fig. 5.11. In this figure, the different controllers contribute the terms X_{POD}, X_{FSW}, and X_{PI} to the reactance of the CSC - X_{CSC}. All controllers use the CSC line active power, $P_X(t)$ or estimations of it as input signals. The first swing controller also uses the CSC line RMS current, $I_X(t)$ as an input signal.

The power flow on the line during normal operation conditions is controlled by a slow PI-controller which aims to control the line power to a reference value P_{ref} provided by the TSO. The design of the PI-controller is not discussed in this thesis, but since the speed of this controller is selected to be low, no great difficulties are anticipated in the control design.

In case of an contingency which triggers the transient controller, the fast power flow controller which is included in the power oscillation damping algorithm is used to increase the power flow on the line rapidly to an emergency set-point P_{Xsp}. This action is initiated locally at the CSC device to assure the transient stability of the system until the TSO has had time to analyze the situation and to reschedule the power flows in the system to comply with the new N-1 security constraints. Once this assessment has been done, the

CSC line power can be controlled to the new desired set-point by changing the reference value P_{ref} to the PI-controller. It should be noted that the fast power flow controller included in the POD algorithm is only active as long as the POD controller is in service. This means that once the oscillation amplitude falls below a predefined level, the line power will be completely controlled by the PI-controller. Due to this, it is necessary to increase the value of P_{ref} if the transient controller has been initiated following a contingency to keep the CSC line power at a high level during the rescheduling effort even after that the power oscillations have been damped out.

The power oscillation damping scheme is initiated when the RLS algorithm detects a power oscillation with an amplitude exceeding a certain predefined limit and it is disabled when the power oscillation amplitude falls below the same limit. The controller bases its action on the estimated grid parameters which are supplied by the system identification part and the values of the mean power flow on the line and the power oscillation amplitude and phase provided by the RLS algorithm.

The transient control scheme may be initiated either using remote signals or locally measured quantities as discussed in the preceding section. It consists of an discrete open-loop predefined scheme in two steps and it concludes its operation by providing a changed set-point to the fast power flow controller in order to maintain transient stability during the damping process.

6 Principles for control of the DPFC

In this chapter, the principles for controlling the dynamic TSSC part of the DPFC are discussed. The control is based on the model presented in the system identification part and it aims to achieve the tasks of power flow control, power oscillation damping, and transient instability improvement. The approach is very similar to the methods proposed for the control of CSC.

As it was mentioned in Section 4.2.1, this thesis concentrates on the control of the dynamic part of the DPFC while the PST tap level and thus the stationary power flow on the line is considered to be determined by the TSO by means of loss considerations and grid security optimization. In addition to the power flow control capabilities of the PST, the DPFC can also use the TSSC to control the power flow on the line. The approach in this work is that this capability should be mostly used in emergency cases, when the additional compensation capability is necessary for maintaining system stability. During normal operation, the TSSC operation should be limited to small adjustments in the power flow and if necessary for increasing the control speed of planned power scheduling tasks. The aim of the TSO should be to perform power power flow control tasks primary by changing the tap level of the PST while keeping the TSSC part at zero compensation to reserve this compensation capability for emergency operation.

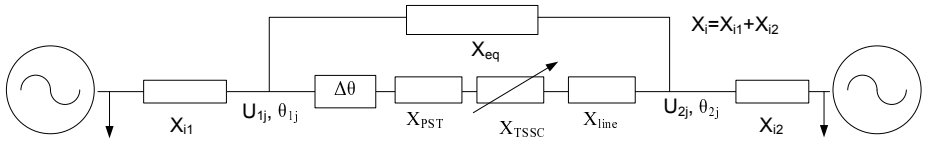

Figure 6.1: Generic system model for control of the DPFC.

6.1 Power oscillation damping and fast power flow control

The principle of power oscillation damping is the same as the the one used for CSC control. The difference is that the system model has to be adapted to include the voltage phase shift introduced by the device PST. By following a similar argumentation as the one used for power oscillation damping in two discrete steps for CSC, a control law including a fast power flow control functionality can be found (see Appendix B). The system model which is used for the DPFC controller given in Chapter 4 is reprinted in Fig. 6.1 for convenience.

Here, the parameters are the tap-dependent resulting series reactance of the PST, X_{PST} and the *advancing* phase angle shift introduced by the PST, $\Delta\theta$. The series reactance of the uncompensated line is given as X_{line} and the variable reactance inserted by the dynamic part of the DPFC is denoted X_{TSSC}. The damping exponent of the oscillatory mode corresponding to the real part of the eigenvalues related to the oscillatory mode is given as σ, the frequency of the mode as ω_{osc}, and the unknown grid parameters X_i and X_{eq} remain the same as in the CSC system model. For convenience, the lumped variable $X = X_{line}+X_{PST}+X_{TSSC}$ is introduced in the following derivation. As for the CSC controller, it is assumed that the damping controller is only allowed to operate at instants in time coinciding with high and low peaks in the power oscillation.

In Appendix B it is shown that the control law which damps a given oscillation in two discrete steps and alters the power flow on the DPFC line to the new set-point P_{Xsp} for a system which can be described by the model in Fig. 6.1 is given by the following expressions:

Assuming that the initial value of X is X_0, the desired value of X after the damping event - X_2 can be calculated from

$$P_{Xsp} = P_{Xstat0}\left(\frac{X_{eqEff} + X_0}{X_{eqEff} + X_2}\right) \tag{6.1}$$

with X_{eqEff} given by Eq. 4.45, P_{Xstat0} denoting the initial average value of the DPFC line power and $\theta = \theta_{1j} - \theta_{2j}$ with its initial value θ_0 defined from Eq. 4.44. Then the value of X following the first step in reactance, X_1 can be calculated as

$$X_1 = \frac{X_{eqEff}(K + A_{p2}) - A_{p1}X_iX_{eq}}{A_{p1}(X_i + X_{eq}) - K - A_{p2}} \tag{6.2}$$

with

$$K = P_{Xsp}X_{tot2}(X_2 + X_{eq}), \tag{6.3}$$

$$A_{p1} = P_{Xstat0}\left(1 + e^{\sigma T_{osc}/2}\right)(X_0 + X_{eqEff}) \tag{6.4}$$

and

$$A_{p2} = P_{Xp0}X_{tot0}(X_0 + X_{eq})e^{\sigma T_{osc}/2}. \tag{6.5}$$

Here, the instantaneous power on the DPFC line right before the first step is denoted P_{Xp0}, the "virtual" total reactance between the grid areas calculated by Eq. 4.10 is denoted by X_{tot0} initially and X_{tot2} following the second reactance step in the sequence while the cycle time of the oscillation is given by T_{osc}. Using these expressions, X_1 can be found and the control law is complete with the necessary reactance changes given by $\Delta X_1 = X_1 - X_0$ and $\Delta X_2 = X_2 - X_1$. Since X_{PST} and X_{line} are constant during the event, ΔX_1 and ΔX_2 are the required steps by the TSSC to damp the oscillation and reach the power flow goal.

Naturally, when the control law is applied in a more complex system with characteristics not completely described by the system model and in the presence of noise, the process will have to be repeated until the power oscillation damping goal is achieved.

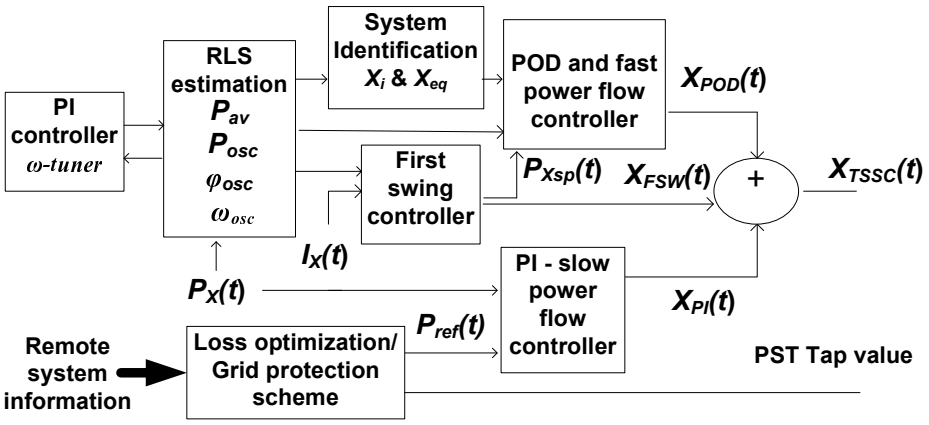

Figure 6.2: Schematic illustration of the full DPFC controller.

6.2 Transient stability improvement

The transient stability scheme developed for CSC is also applicable to the DPFC. For a detailed discussion on this topic, refer to Section 5.2.

6.3 The general control approach

Based on the principles of control described in this chapter, a multi-objective controller for the DPFC can be designed. This controller has a structure according to Fig. 6.2. In this figure, the different controllers contribute with the terms X_{POD}, X_{FSW}, and X_{PI} to the reactance of the TSSC - X_{TSSC}. All controllers use the DPFC line active power, $P_X(t)$ or estimations of it as input signals. The first swing controller also uses the DPFC line RMS current, $I_X(t)$ as an input signal.

This control structure has most properties in common with the multi-objective controller proposed for the CSC in Section 5.3. The power oscillation damping with its fast power flow control functionality and the transient control structure all have the same functions and input signals as in the CSC case. The system identification part provides the estimated parameters to

the controller in the same way as it was done in the CSC controller. The main differences between the controllers lie in the system model, the estimation routines and the damping algorithms. In the overall structure, it is here assumed that the long term reference value for the DPFC line power P_{ref} is provided by the TSO together with the selected value for the PST tap level. In order to select these values, loss optimization targets and grid security constraints must be considered. The optimization of the tap level should in most cases be done in a way such that the PST alone is controlling the long-term stationary power on the line keeping the TSSC compensation close to zero. This is done in order to reserve the TSSC capability for corrective control during contingencies. Since this capability is available for N-1 cases, the PST can be controlled in a more efficient way, optimizing the overall grid losses.

7 Results and discussion

In this chapter, simulation results for the CSC and the DPFC controllers are presented. Digital time-domain simulations were performed in two different test systems including CSC devices in order to determine the controller damping efficiency and the transient controller stability improvement. For the DPFC, simulations were performed in a simple test system in order to determine the feasibility of the damping controller for different settings of the device PST. All simulations were performed using the STRI AB, SIMPOW power simulation software.

7.1 Test systems

7.1.1 Four-machine system

Initially, during testing of the controllers for CSC and DPFC, it is beneficial to use a simple test system which can be easily analyzed. One such system for study of power oscillations was proposed in [21] and a similar one was given in [29]. The system used for this purpose in this thesis is based on the one presented in [29], and it is illustrated in Fig. 7.1. The system used here has the same properties as the system described in [29] except for the following details:

- In the test system, one more transmission line was used to interconnect the two grid areas and the length of all lines in the inter-tie were stretched to 150 km instead of 110 km to give approximately the same total tie line reactance as in the original system. A FACTS device of

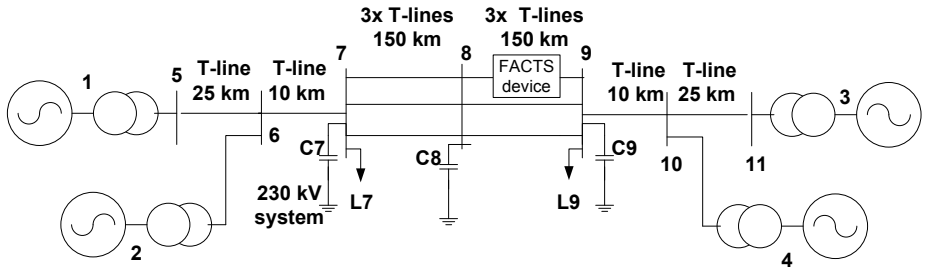

Figure 7.1: Four-machine power system inspired by P. Kundur.

either CSC or DPFC type was installed in series with one transmission line between node 8 and node 9 close to node 8.

- In order to maintain a decent voltage profile across the inter-tie lines, a shunt capacitor was inserted at node 8 in the test system.

- The system was studied in one high and one low power transfer case with the load data (high/low) P_{L7}=967/1367 MW, Q_{L7}=100/200 MVAr, P_{L9}=1967/1367 MW, Q_{L9}=100/200 MVAr and the shunt capacitor data Q_{C7}=-400 MVAr, Q_{C8}=-100 MVAr and Q_{C9}=-400 MVAr.

- In [29] it is assumed that the active components of the loads have constant current characteristics and the reactive components of the loads have constant impedance characteristics. In the test system used in this work, this case is considered together with the case of a system with totally voltage independent loads.

In [29], the influence of different exciter characteristics on the power oscillation modes is investigated. In this thesis, only the case which shows the highest degree of small-signal instability is considered. This is the case with thyristor controlled exciters utilizing high gain.

The test system has two local rotor angle modes of power oscillation with a frequency in the range of 1 Hz with a reasonable damping and one inter-area mode of oscillation with a frequency in the range of 0.5 Hz which is poorly damped. One important goal for the FACTS controllers in this system is to improve the damping of the inter-area mode.

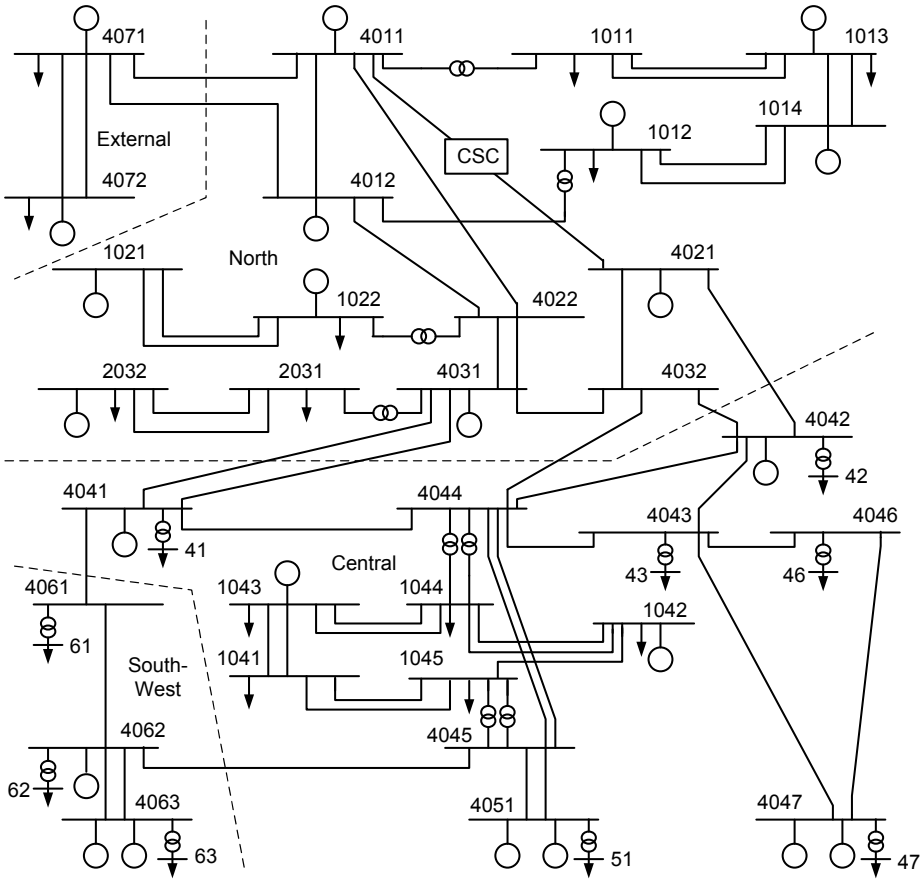

Figure 7.2: 23-machine system by CIGRÉ describing the Nordic power system.

7.1.2 Twenty-three machine system

The twenty-three machine system is the system Nordic 32 from [30] shown in Fig. 7.2.

The system was constructed for transient stability and voltage stability studies in the Scandinavian power system. Although being fictitious the original system has dynamic properties similar to the Swedish and Nordic power system. The system can be divided into four different parts, three of these corresponding to the Swedish areas Southwest, Central, and North

and the fourth corresponding to a foreign part denoted External. There are 19 nodes at the 400 kV voltage level in the system. These are named by four-digit numbers starting with '4'. In a similar way, the two 220 kV buses are denoted with numbers starting with '2' and the eleven sub-transmission 130 kV buses are numbered starting with '1'. The nine pure load buses at 130 kV, denoted by two-digit numbers are connected to the 400 kV power system by means of transformers equipped with tap-changers. The External and Northern regions contain a large number of hydro power generation while the other areas hold thermal power plants. The Southwest and the External areas are essentially self-supporting while the Central region imports half of its power consumption from the Northern area.

The system is in its original form well-damped, mainly because of well tuned PSS units connected to the system generators. A discussion of the original system characteristics is found in [31]. The loads are in the original system modeled using voltage and frequency dependent load models. To challenge the damping controller, all of the PSS used in the system were disconnected and the load characteristics were changed to voltage independent load at nodes 2031 and 2032 and voltage and frequency independent load at nodes 41, 42, 43, 46, and 51. The system was simulated in the normal load case (lf029) and the severe peak load case (lf028) described in [30]. In the peak load case, the system has the three least damped modes: $\sigma_1 = -0.017$, $f_1 = 0.50Hz$; $\sigma_2 = -0.22$, $f_2 = 0.75Hz$; $\sigma_3 = -0.26$, $f_3 = 0.88Hz$ whereas the system in the normal load case has the least damped modes $\sigma_1 = -0.090$, $f_1 = 0.54Hz$; $\sigma_2 = -0.21$, $f_2 = 0.73Hz$; $\sigma_3 = -0.31$, $f_3 = 0.88Hz$. The least damped mode is considered to be the critical one. Geographically, this mode corresponds to the generators in Finland (4071, 4072) swinging towards the rest of the Nordic system. To improve the damping of this mode, improve the transient stability in the system and control the power flows in the system, a CSC device is placed in series with the line 4011-4021 where the observability and controllability of the critical mode is good.

7.2 CSC controller results

7.2.1 Controller implementation

The controller described in Section 5.3 was implemented in the SIMPOW power system simulation software. The implementation was done according to Fig. 5.11 except for the power flow PI-controller which was omitted. The purpose of the studies were to verify the damping controller and transient controller functions during the first 10-20 seconds after a severe fault in the power system. Long-term power flow control by the CSC was not considered in the study. The test systems of [29] and [30] were implemented and the power flow data were verified using reference data before the systems were modified to the versions described in the preceding section. These systems were then configured for a large amount of fault cases and time-domain simulations were performed with and without the CSC controller enabled.

The response time of the TCSC or the TSSC is generally in the range of 20 ms. Since the power oscillations which are subject to damping are of considerably slower dynamics, the dynamics of the CSC have been neglected in this study and the CSC has been assumed to be an ideal variable reactance.

In order to consider the limitations of the control signal and various other aspects, it was necessary to include additional functions to the implementation of the damping controller and parameter estimator described in Chapter 4 and 5. The most important of these are mentioned below along with some remarks on the implementation:

- A limit on the required minimum magnitude of the step response in the line power, both in average and instantaneous terms to trigger a grid parameter estimation was introduced. A suitable limit for the required relative change in the line power was found to be in the range of 1.5-5 %. It is possible to use a lower limit on the change in the line average power used in the estimation of X_{eq} since these values are less sensitive to measurement noise than the instantaneous values used in the estimation of X_i.

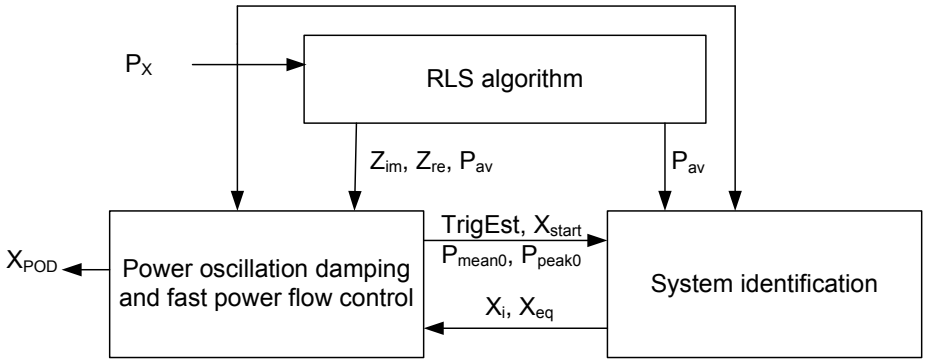

Figure 7.3: Communication between RLS routine, Damping Controller and System Identification unit.

- Since the control signal, the inserted series reactance of the CSC is limited, it is necessary to include limits in the implementation of the damping control law.

- Since there are physical limits for the values that the total reactance in the system model can attain, the controller must contain a structure for handling control law outputs outside the physical limits for the system.

- Due to the high speed demands on the RLS estimation determining the power oscillation amplitude, phase and the average level of power transmitted on the line, the RLS algorithm is reset following every discrete reactance step taken by the damping controller. This improves the accuracy of the estimation and thence the controller performance.

The internal communication between different units in the controller implementation during an oscillation damping sequence is illustrated in Fig. 7.3.

Here, the power flow on the CSC line, $P_X(t)$ is measured and decomposed in its average and oscillative components by the RLS algorithm assuming that the power on the line can be described as

$$p(t) = P_{av}(t) + \mathrm{Re}(\Delta\bar{P}e^{j\omega_{osc}t}) = P_{av}(t) + P_{osc}(t). \tag{7.1}$$

The output from the RLS routine is the real and imaginary parts of the the rotating phasor

$$Z = \Delta\bar{P}e^{j\omega_{osc}t} = Z_{re}(t) + iZ_{im}(t). \tag{7.2}$$

$Z_{re}(t) = P_{osc}(t)$ describes the oscillative part of the line power and $Z_{im}(t)$ is, in a quasi-stationary oscillating state, the same signal phase-shifted by 90 degrees. At the high and low peaks of the power oscillation, $Z_{im}(t)$ will be zero and $Z_{re}(t)$ will attain its maximum value during the oscillation cycle.

To achieve a greater understanding of how the controller implementation is working in order to damp oscillations and perform system identification, it is instructive to view the flow-sheet in Fig. 7.4. This figure illustrates the sequence of communications between the damping controller and the system identification unit. By following this sequence, it can be understood how the different limitations are implemented in the controller and how the two routines work together to form a functioning unit.

The transient improvement controller described in Section 5.2 is dependent on information of the sending and receiving area voltage phase angles and their time-derivative. If this information is not available to the controller, it is necessary to determine the appropriate switching times using measurements of the locally available signals. The method used in this controller implementation utilizes the measured CSC line power and the measured line current as input signals. As described in Section 5.2, the transient controller may be initiated when the measured magnitude of the line power has a time-derivative exceeding a predefined limit during a certain minimum amount of time. The transient controller should inhibit the other controller parts during its operation since transient instability is the most immediate threat to system stability. Since the operation of the damping controller gives rise to high line power time derivatives during its discrete operation, it is necessary to disable the trigger for the transient controller during the execution of the damping and estimation sequences at each time step. The duration of the controller-imposed changes in the line power are well known and the disabling of the transient controller during these short time periods should not have a major impact on the controller reliability.

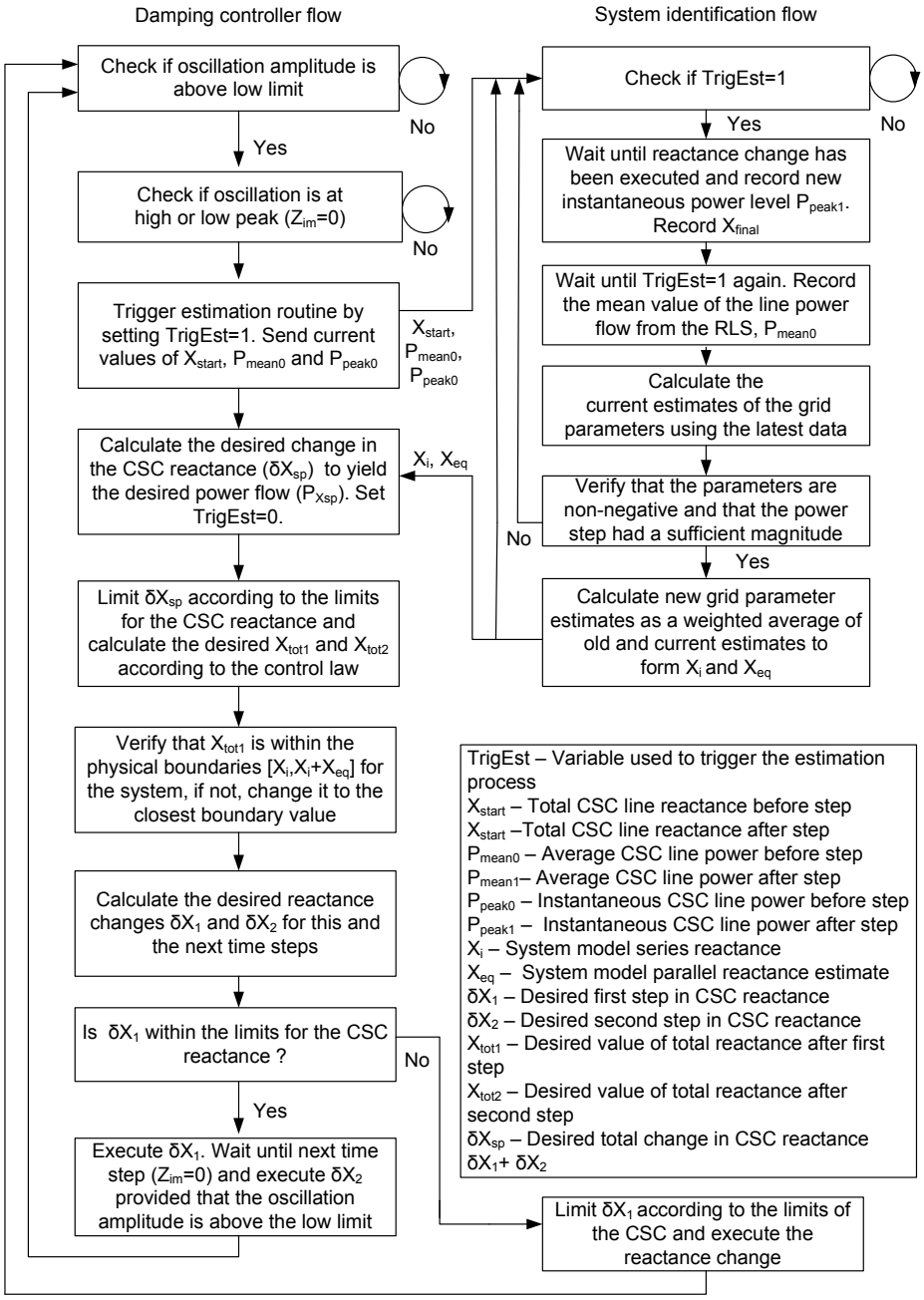

Figure 7.4: Flow-sheet of damping controller and estimation routine actions during the damping process.

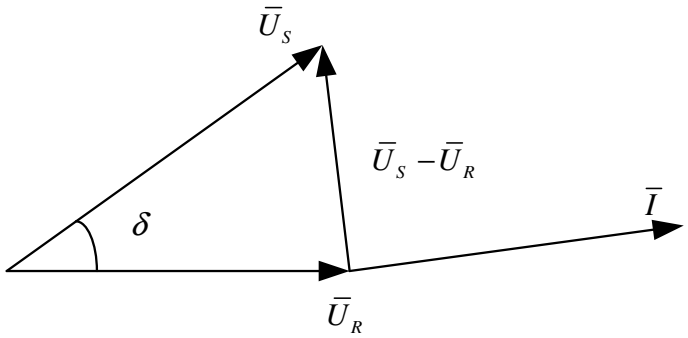

Figure 7.5: Phasor diagram of the sending and receiving end voltages and line current of a transmission line.

Since the sequence of the first swing transient controller only consists of two separate switchings of the CSC, all that remains after the controller has been initiated and the degree of CSC compensation has been set to its maximum is to determine the instant for the second reactance change in the sequence. According to the control law Eq. 5.13 - 5.15, the CSC compensation level should be directly reduced if the angle difference between areas starts to decrease while the angle difference is less than 90°. In the case of higher angle differences, the switching should occur when the angle difference equals 90° and the angle difference is decreasing. To distinguish between these two cases, the controller utilizes the fact that while the power flow between the areas increases with an angle difference up to 90° and then decreases again for higher angles, the current magnitude on the line is monotonously increasing with the angle. That this is the case can be seen by denoting the line current phasor $\bar{I}$, the line reactance X, and the sending and receiving end voltage phasors $\bar{U}_S$ and $\bar{U}_R$. Then,

$$\bar{I} = \frac{\bar{U}_S - \bar{U}_R}{jX}. \tag{7.3}$$

In Fig. 7.5, a phasor diagram for the voltages and currents of one transmission line is drawn.

The magnitude of the line current is proportional to the length of the phasor $\bar{U}_S - \bar{U}_R$. From Fig. 7.5 (and the law of cosine) it can be seen that

the length of this vector is monotonously increasing with δ for angles less than 180°.

From Fig. 5.10 it can be noted that the second change in the series reactance in the transient sequence occurs at a local maximum in the line power. If the angle swing is less than 90°, it will be the first power maximum and if the swing is larger that 90°, it will be the second maximum. The implementation approach to determine the instant for the second reactance change follows from the strategy for the first-swing controller described below:

1. Initiate the first-swing controller when the time-derivative of the line power magnitude exceeds a limit C_{lim} during a time exceeding T_{lim}. Increase the level of compensation of the CSC to its maximum value.

2. When the RLS routine indicates the first maximum in the line power after the fault, record the line current magnitude.

3. Monitor the line current magnitude. When it falls below the value recorded at the first peak in the line power, decrease the level of compensation of the CSC by Eq. 5.15.

4. Conclude the action of the transient controller by changing the setpoint of the fast power flow feature of the damping controller to a value close to the short-term thermal overload level of the CSC line.

Due to the monotonously increasing property of the line current, this strategy will work for angular swings both smaller and larger than 90°. During a small angle swing, the current will immediately start to decline after the first maximum in power and the reactance change will be made at the instant coinciding with the first peak in line power. During a large power swing, the current will continue to increase after the first peak in the power and then start to decline when the angle difference has passed its maximum and hit the recorded current value for the first power peak at 90° angular difference between areas where the reactance change is performed.

7.2.2 Simulation results

Four-machine system

Time-domain simulations were performed in the four-machine system of Fig. 7.1 in order to determine the effectiveness of the damping controller as well as the impact of the controller on the transient stability of the system. Four different contingencies were studied at two different levels of inter-area power transfer, one high line load case with 600 MW transfer and one low load case with 180 MW transfer in steady state. In order to test the CSC controller in a system with a poorly damped inter-area mode, the PSS connected to each generator was set to operate with a reduced gain. The results were described in detail in Paper 4 and they will be summarized here.

The studied contingencies were:

1. A 3-phase short circuit (SC) at node 8 cleared with no line disconnection after 200 ms.

2. A 3-phase SC at node 8 cleared by disconnection of one N8-N9 line in parallel to the CSC after 200 ms.

3. A 3-phase SC at node 8 cleared by disconnecting one of the N7-N8 lines after 200 ms.

4. A disconnection of load at node 7. ΔP=-250 MW ΔQ=-50 MVAr in the high transfer case and ΔP=-250 MW ΔQ=-100 MVAr in the low transfer case.

In order to illustrate the typical behavior of the controller in a fault case, the four-machine system with voltage dependent loads was simulated in contingency nr. 2 above. The short-term thermal overload capability of the CSC line was assumed to be 400 MW and this value was used as the post-contingency set-point of the fast power flow controller. Gaussian pseudo-random noise with a standard deviation of 1 % of the stationary value of the input signal (P_X) was added to the controller input in all simulations in order to simulate measurement noise. From Fig. 7.6 it can be seen that the

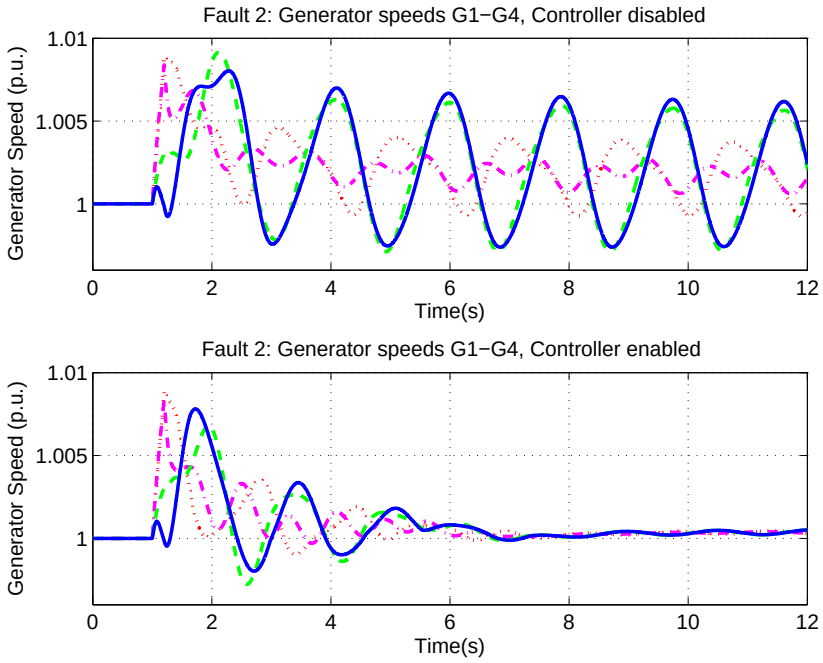

Figure 7.6: Four-machine system with CSC, high load case: Speed of Generators G1-G4 after contingency 2. G1(dotted, orange), G2 (dash-dotted, magenta), G3 (dashed, green) and G4 (solid, blue).

damping of the inter-area mode is greatly improved by the CSC operation. Fig. 7.7 shows the controller action in more detail. The first-swing controller is activated by the high positive time derivative of the line power at fault clearance and performs its two steps at t=1.2 and t=1.7 s. The damping controller is engaged at t=2.3 s. Since the estimation routines are dependent on step response data, the parameters cannot be estimated prior to the first reactance step in a damping sequence. Therefore, a starting guess for the parameters is necessary to determine the initial action of the controller. This starting guess is chosen as the set of parameters which corresponds to the grid (N-1) or even (N-2) configuration case where the product of the controllability and the observability of the inter-area oscillation mode at the CSC location is the largest. This approach leads to a controller which generally

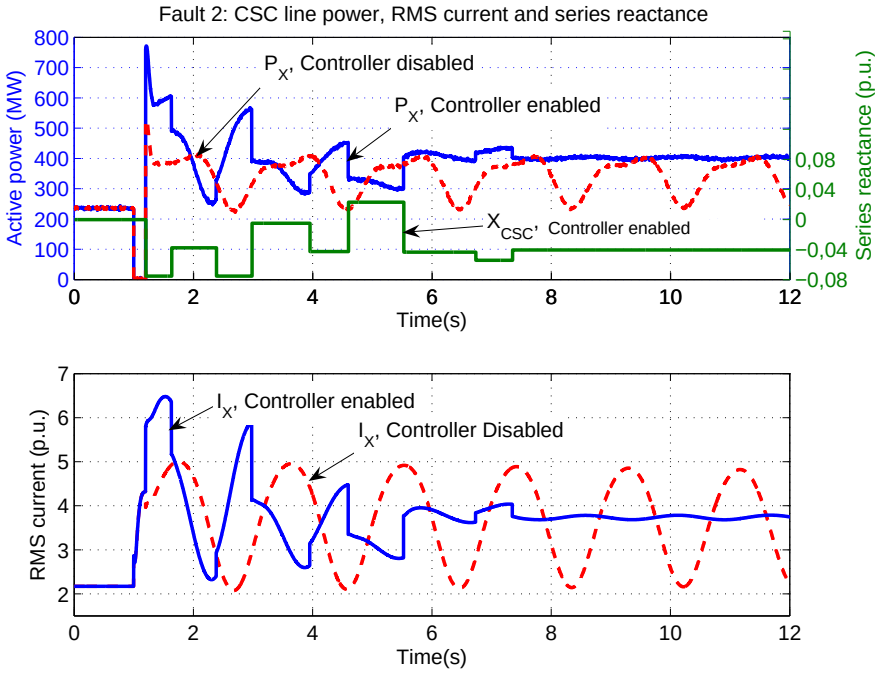

Figure 7.7: Four-machine system with CSC, high load case: Active Power and RMS Current on the CSC line and CSC Reactance after contingency 2.

is sub-optimal initially in order for it to maintain stability in all system configurations. As the system parameters are estimated with better accuracy, the efficiency of the damping controller is increased over time. The damping of the oscillation is completed at t=7.3 s and the power flow on the line is stabilized close to the chosen set-point (400 MW).

Fig. 7.8 shows the evolution of the system identification parameters X_i, X_{eq}, and ω_{osc}. The system exhibits a dominant inter-area mode of oscillation in the range of 0.52-0.75 Hz depending on configuration. The starting guess of ω_{osc} is chosen to be 3.77 rad/s (0.6 Hz). The parameters X_i and X_{eq} are initialized using a conservative approach and they are then updated whenever a reactance step response above the set limit in the active power

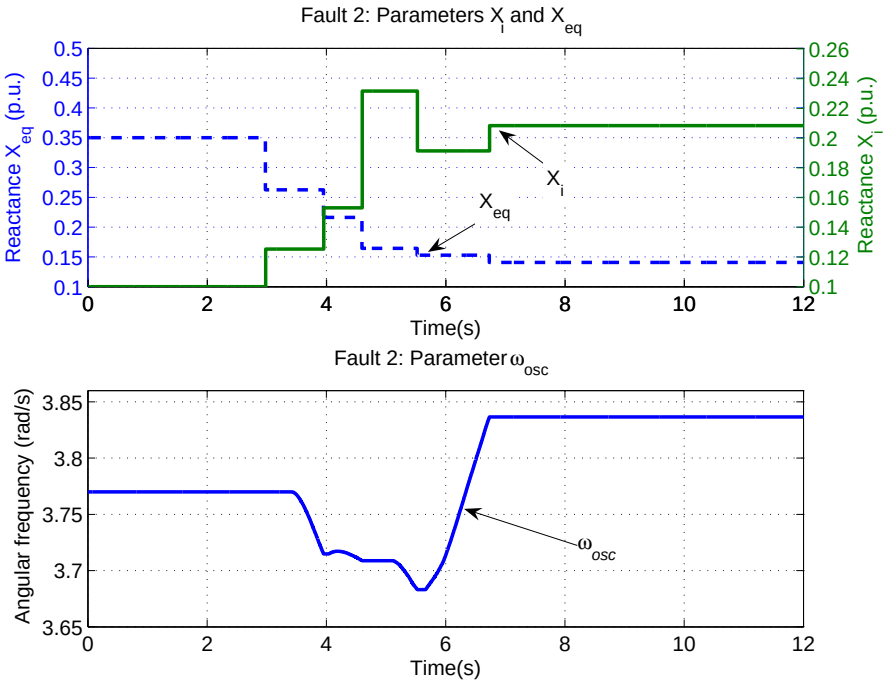

Figure 7.8: Four-machine system with CSC, high load case: Parameters X_i, X_{eq}, and ω_{osc} after contingency 2.

of the CSC line is detected. It can be seen that the parameters stabilize close to X_i=0.21 p.u. and X_{eq}=0.15 p.u. after a few steps in the CSC reactance.

In Fig. 7.9 and Fig. 7.10, the damping exponents (σ) for the critical oscillation mode in the four contingencies and the two different load conditions are shown. This is done both for the case of voltage dependent loads in the system and the case with voltage independent loads. In the figures, the case with no controlled series compensation is denoted by "No Cntrl" and the case when the full CSC controller is enabled is denoted by "Cntrl". The simulations were performed with the first-swing controller and the power flow control feature of the CSC controller activated, leading to a changed line power flow during the damping operation. The values for the damping exponent σ are given as the real part of the eigenvalue of the linearized system matrix corresponding to the critical mode for the system without a

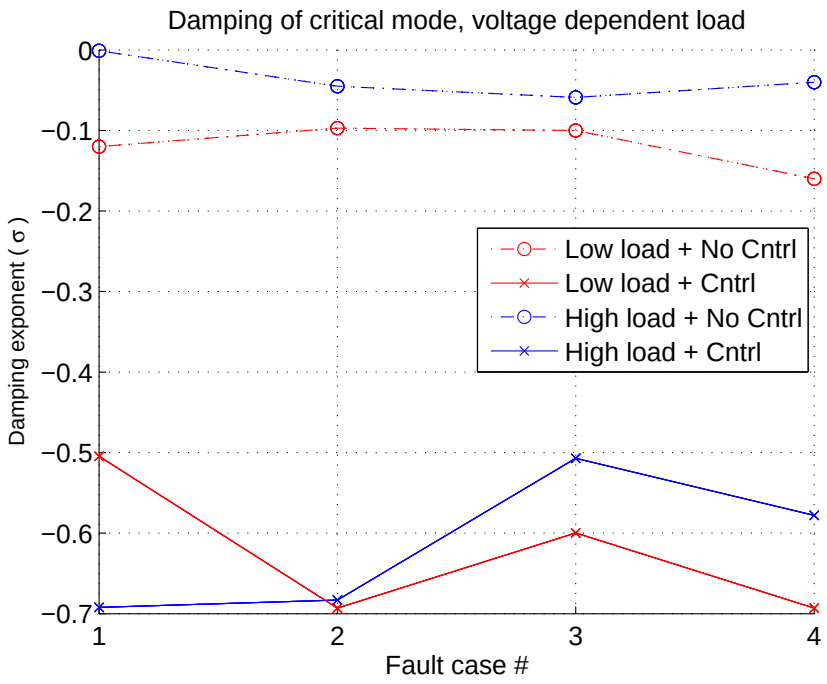

Figure 7.9: Four-machine system with CSC, voltage dependent loads: Damping exponent σ of critical mode for contingencies 1-4.

CSC controller. For the system with CSC controller, σ is calculated from the time-domain simulation results assuming that the total inter-area power oscillation with the critical mode frequency ω_{osc} and maximum oscillation amplitude A can be described by $Ae^{\sigma t}sin(\omega_{osc}t)$ during the time when the CSC controller is active. This interpretation of the damping is used since it is not possible to define a small-signal coefficient in the case of the time-discrete controller since it operates only when oscillations with a certain amplitude are present. Also, the damping exponent will change during the time of the damping and it may theoretically approach negative infinity if the damping should be completed in only one time-step. This method of calculating the damping exponent is used throughout the text.

From Fig. 7.9 and Fig. 7.10 it can be seen that the damping of the oscillations in the original system is least effective for contingency nr. 1 at high load, where the damping of the inter-area mode is close to zero. For the sys-

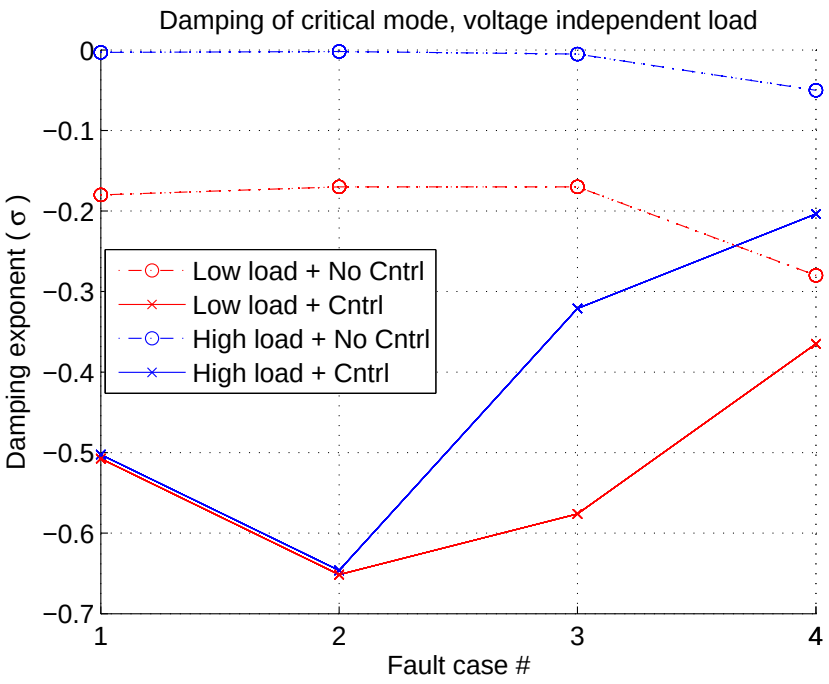

Figure 7.10: Four-machine system with CSC, voltage independent loads: Damping exponent σ of critical mode for contingencies 1-4.

tem with the CSC controller, it can be seen that the damping is significantly improved in all the studied cases. The improvement of the system damping is slightly larger in the system with voltage dependent load.

Fig. 7.11 and Fig. 7.12 show the required time, T_D after the fault until the line power oscillation amplitude has settled below 10 MW (p-p) and the initial maximum power oscillation amplitude (p-p) on the CSC line. T_D for the cases when the controller operates are results from time-domain simulations while the values given for the system when the degree of compensation of the line is zero are approximate and calculated from the small-signal values of σ obtained in an eigenvalue analysis. The maximum line power oscillation was measured with full CSC compensation since this is in most cases the final setting of the CSC following the damping operation due to the high post-contingency power flow set-point.

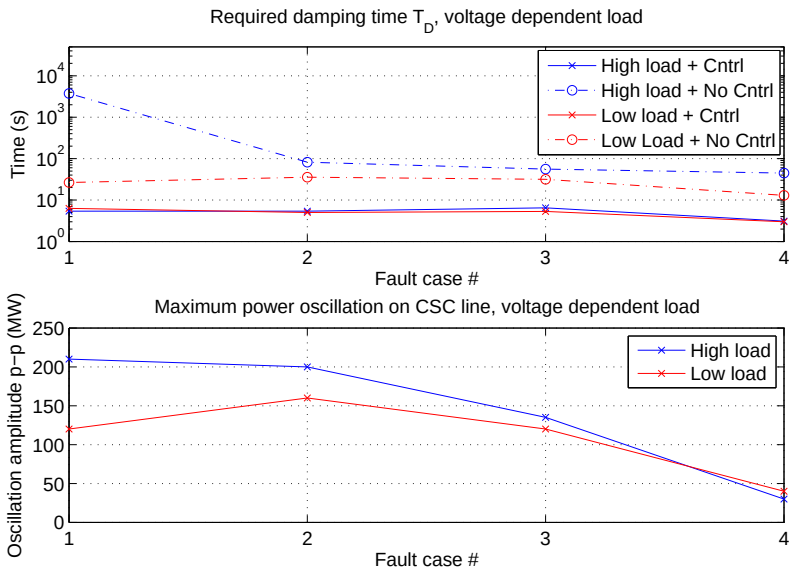

Figure 7.11: Four-machine system with CSC, voltage dependent loads: Required time to damp line power oscillation below 10 MW p-p (T_D) and maximum line power oscillation amplitude for contingencies 1-4.

Fig. 7.11 and Fig. 7.12 give some information on the severity of the faults and the damping effectiveness in the studied contingencies. For the system with voltage dependent loads, contingency nr. 1 in the high load case is the most severe with a very long damping time in the range of 3000 s and a large power oscillation amplitude when the CSC controller is disabled. Also, in the case of voltage independent loads, the original system damping times are generally longer for the high load cases than for the low load cases. Here, the contingencies 1-3 are severe cases with very poor damping initially and damping times longer than 500 s. With the CSC controller enabled, the damping times in the different fault cases are in the range of 5-10 s in all fault cases for both the system with voltage dependent loads and the one with voltage independent loads. It can be concluded that the CSC controller improves the damping of the inter-area mode significantly in the test system and that the obtained values for the required damping times with the CSC controller enabled are acceptable from a system operation point of view.

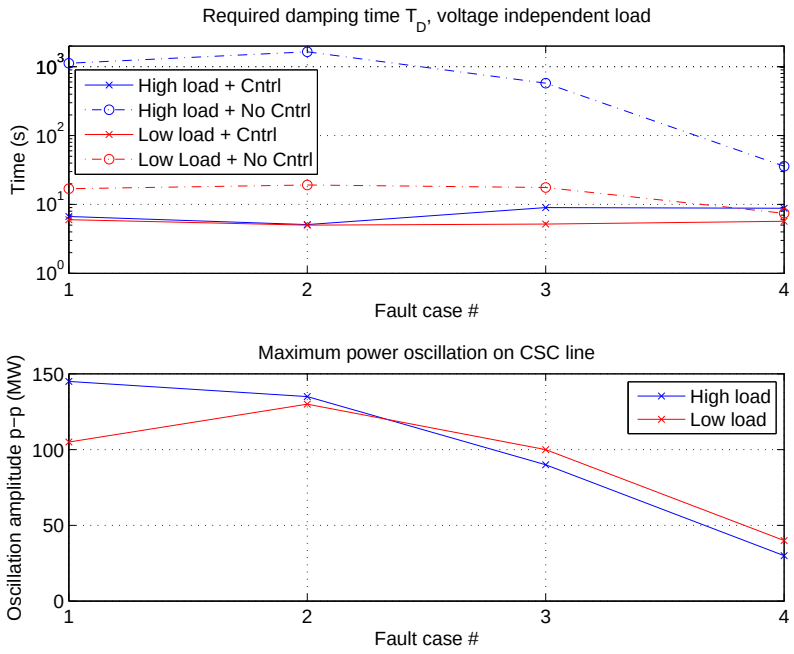

Figure 7.12: Four-machine system with CSC, voltage independent loads: Required time to damp line power oscillation below 10 MW p-p (T_D) and maximum line power oscillation amplitude for contingencies 1-4.

The fast power flow feature of the power flow controller works generally well in the studied cases. The controller was in this implementation optimized for oscillation damping. This means that the controller is disabled when the power oscillation amplitude decreases below a specified level (10 MW p-p in this study). This commonly leads to a remaining difference between the set-point of the fast power flow controller and the actual power flow on the line. The controller could also be optimized for power flow control, where a more accurate power flow control performance would be prioritized on the expense of a slightly less effective power oscillation damping.

The stationary error of the fast power flow controller was in this study usually within ±3% of the set-point value provided that the set-point value was within the operating range of the CSC. In a full controller implementa-

tion, the PI-controller will work to reduce the stationary error in the power flow control to zero. In rare cases, due to modeling errors, the oscillation amplitude was seen to be damped below the specified level already after the first step in a two-step damping event, aborting the second step. This means that the series compensation level after the event will be different from the calculated value and the power flow on the line may not be close to the set-point. The result will, in a full implementation of the controller be that the line power flow will require longer time to reach the set-point since the power flow control will be mainly performed by the slow PI-controller.

In order to investigate the performance of the proposed transient stability controller, additional simulations were made in the four-machine system. It was assumed that the system transfer capacity is limited by the transient stability in the worst case contingency nr. 2. The system was investigated with the CSC in five different configurations:

1. No first swing controller is used. The CSC operates only to damp oscillations.

2. A first swing controller which operates like the one described in this thesis except that the degree of compensation of the line is set to zero when it is reduced from its maximum value. The CSC compensation base level is maintained at zero during the damping event. This approach is similar to the one of [26].

3. The first swing controller proposed in this thesis is used. The controller post contingency power set-point (the CSC line short-term thermal overload limit) is set to 400 MW.

4. The first swing controller proposed in this thesis is used. The controller post contingency power set-point (the CSC line short-term thermal overload limit) is set to 450 MW.

5. The first swing controller proposed in this thesis is used. The controller post contingency power set-point (the CSC line short-term thermal overload limit) is set to 500 MW.

Table 7.1: Maximum total power transfer limit of interconnecting lines in the four-machine system

Case number	Maximum total transfer limit (MW)
1	690
2	720
3	760
4	780
5	820

Repetitive simulations of contingency nr. 2 were performed in order to determine the maximum limit of the transmitted power for which the transient stability and system damping (damping of all oscillations within 10 s) were maintained. To achieve sufficient voltage support in the peak power transfer cases in this study, the total amount of reactive power supplied by the shunt capacitors in the test system was increased by about 40 % from its original value. The results are summarized in Table 7.1. It can be seen that the maximum transfer limit of the tie-lines between the areas is significantly improved by application of the proposed transient controller. The short-term thermal overload limit of the CSC line is seen to be a major determining factor for the total power transfer limit provided that the transient controller described here is used. *It should be noted that the transfer capacity was in all cases limited by unsatisfactory oscillation damping.* This damping performance degradation is due to the fact that the system is in this severe contingency operating in the non-linear range where the voltage phase angle difference between areas exceeds 90 degrees during the oscillation and the assumptions made in the derivation of the damping controller are no longer valid. This problem is likely to affect also other linear damping controllers relying on locally measured signals as controller inputs. The used control approach with a raised degree of compensation during the power oscillation damping improves the damping performance by reducing the average voltage phase angle differences in the system facilitating damping controller action. A higher thermal overload limit of the CSC line makes it possible for the controller to use a higher average compensation level during damping which leads to a better damping performance and thereby a higher power transfer capability by Table 7.1.

Table 7.2

Fault Number	Fault Type	Lines disconnected at clearing
1	3-ph. SC at node 1012	1012-1014
2	3-ph. SC at node 4011	4011-4012
3	3-ph. SC at node 4011	4011-4022
4	3-ph. SC at node 4012	4012-4022
5	3-ph. SC at node 4022	4022-4031
6	3-ph. SC at node 4021	4021-4032
7	3-ph. SC at node 4042	4032-4042
8	3-ph. SC at node 4042	4042-4044
9	3-ph. SC at node 4041	4041-4044
10	3-ph. SC at node 4041	4031-4041
11	3-ph. SC at node 4043	4043-4044
12	3-ph. SC at node 4032	4032-4044
13	3-ph. SC at node 4071	4011-4071
14	3-ph. SC at node 4045	4044-4045
15	Generator trip at node 1012	-
16	3-ph. SC at node 4021	4021-4042
17	3-ph. SC at node 4032	4031-4032
18	Generator trip at node 4051	-

Twenty-three machine system

In order to test the CSC controller in a more realistic power system, the Cigre Nordic 32 system modified according to Section 7.1.2 was used. Here the goal for the CSC controller was to improve the damping of the critical inter-area oscillation mode with an oscillation frequency of approximately 0.5 Hz.

Simulations were carried out in 18 contingencies according to Table 7.2 in two load cases; one peak load case (lf028) and one normal load case (lf029) described in [30]. Simulated pseudo-random noise of 1 % was added to the controller input in order to simulate measurement noise. With the aim to maximize the system stability improvement, the post-contingency set-point

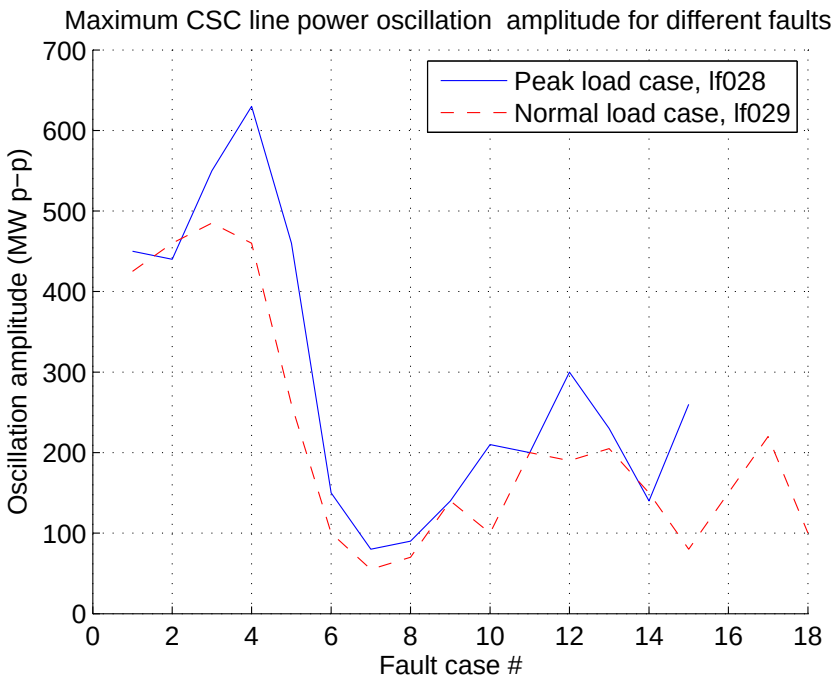

Figure 7.13: Twenty three-machine system with CSC: Maximum CSC line power oscillation amplitude (measured with $X_{CSC} = X_{CSCmin}$)) for different contingencies.

for the line power provided to the fast power flow controller was set to 1300 MW which was assumed to be the short-term thermal overload limit of the 400 kV line where the CSC is placed.

When the series compensation of the line is increased by the controller during the oscillation damping, adjusting the line power to the given set-point, the damping of the critical mode changes. In most cases, the short-term thermal limit of the line cannot be reached and the compensation level ends up at its maximum capacitive value after the damping event. Therefore, the small-signal damping of the critical mode and other results are given both for the case with no compensation of the CSC, with fixed full compensation of the CSC, and with the CSC controller enabled. In Fig. 7.13 the maximum power oscillation amplitude measured at the CSC location after each fault is shown. The simulations were conducted applying $X_{CSC} = X_{CSCmin}$ at

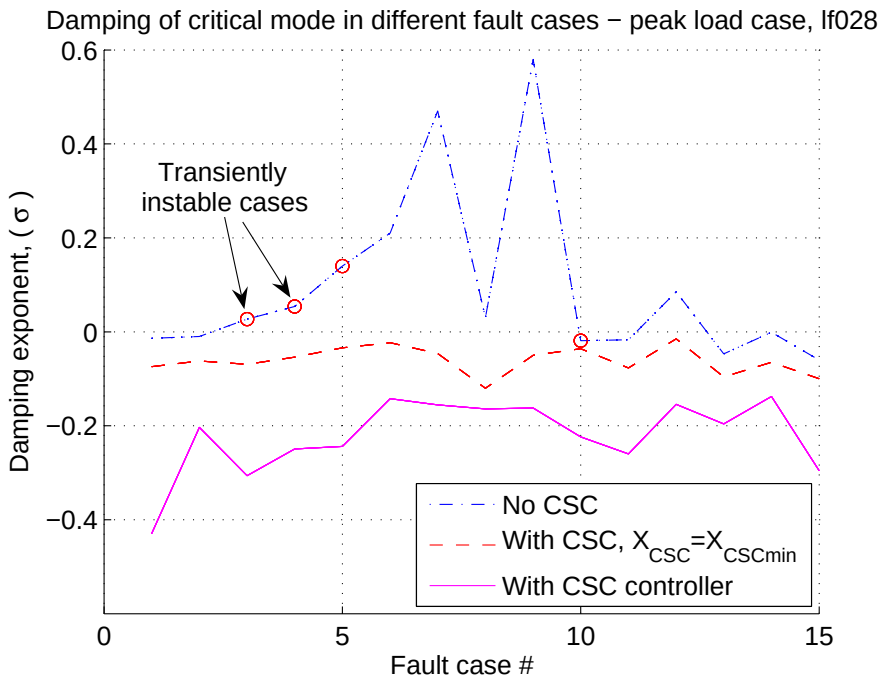

Figure 7.14: Twenty three-machine system with CSC in the peak load case (Lf028): Damping exponent σ of critical mode for contingencies 1-15 for system no CSC, with full compensation of CSC and with CSC controller enabled.

the fault clearance in order to facilitate comparison to the CSC controller results where the transient controller is triggered in all the studied cases. The maximum power oscillation amplitude gives valuable information about the severity of the contingencies. From Fig. 7.13 it can be noted that faults nr 1-5 seem to be the most severe while faults 6-10 are likely to be less severe. Faults 16 and 17 in the peak load case are transiently instable and Fault 18 is transiently stable but it exhibits small-signal instability with a high negative damping. Therefore, it was not possible to reliably determine the maximum oscillation amplitude in these cases.

The simulation results for the small-signal damping of the critical mode are shown for the peak load case (lf028) in Fig. 7.14 and for the normal load case in Fig. 7.15. From Fig. 7.14 it can be noted that faults 3-5 and 10 show

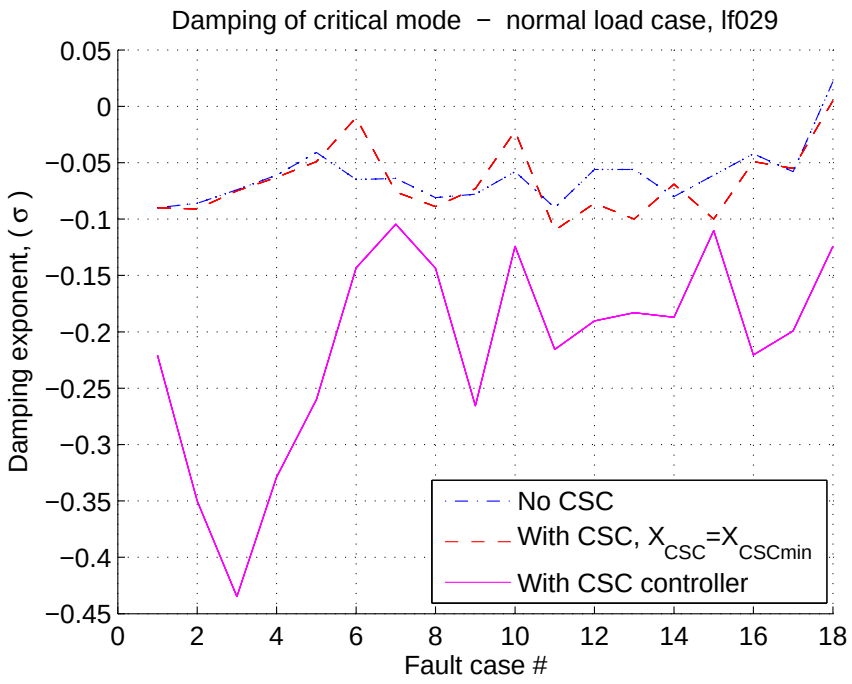

Figure 7.15: Twenty three-machine system with CSC in the normal load case (Lf029): Damping exponent σ of critical mode for contingencies 1-18 for system no CSC, with full compensation of CSC and with CSC controller enabled.

transient instability in the case with no CSC. The cases 16-18 are instable in all cases and are therefore omitted in the figure. Moreover, for the system with the CSC disabled, the damping of the critical mode is negative in most of the fault cases while it in the other cases has a small positive value. The system is transiently stable in fault cases 1-15 both when the transient CSC controller is separately enabled and when the full CSC controller is enabled.

A significant improvement of the critical mode damping in cases 1-15 is seen with the CSC controller enabled. However, it is also important to note from Fig. 7.14 that the damping of the critical mode is in many cases significantly improved just by increasing the line compensation level to a fixed value. Since the controller generally operates with a high average series compensation level, a fair performance evaluation of the damping controller must

compare the damping exponents obtained when the CSC damping controller is active with the values obtained when a fixed high line compensation level is used.

The fault cases 16-18 which were not resolved successfully in the peak load case should be mentioned. Fault 16 is a pure transient instability and it is resolved if the maximum degree of compensation of the CSC is increased to 90 % from the 75 % used in these simulations. Fault 17 is a case where the system operates very close to its limit with voltage angle differences close to 90 degrees in the stationary state. In this particular case, due to modeling errors, the controller chooses a too low degree of compensation at one point during the damping which makes the system transiently unstable. This case can be resolved if a minimum degree of compensation of the CSC during damping is introduced so that the CSC degree of compensation k is limited within a band: $40\% \leq k \leq 75\%$. This, however, reduces the dynamic performance range of the controller. Finally, fault 18 is a case where the damping of the critical mode is negative also with a high compensation level of the CSC. This leads to a case where the discrete damping scheme needs to be reapplied repetitively. Moreover, in this particular case, small step responses of the discrete reactance changes lead to delayed parameter estimation and suboptimal damping performance. The performance can be improved by another choice of the initial values of the parameters X_i and X_{eq} which is not likely to have any adverse effect on the damping in the other fault cases.

In Fig. 7.15, the damping exponent of the critical mode for the system with normal load is shown. It can be seen that in this mode of operation, the system is transiently stable in all the studied cases. In one contingency (fault 18), the system shows small-signal instability with no CSC and with fixed full compensation of the CSC. The damping of the critical mode is significantly improved in all cases and the small-signal instability is resolved with the CSC controller enabled. It can be noted that the damping of the mode does not change significantly from the original values when a fixed full series compensation level is applied by the CSC in this mode of operation.

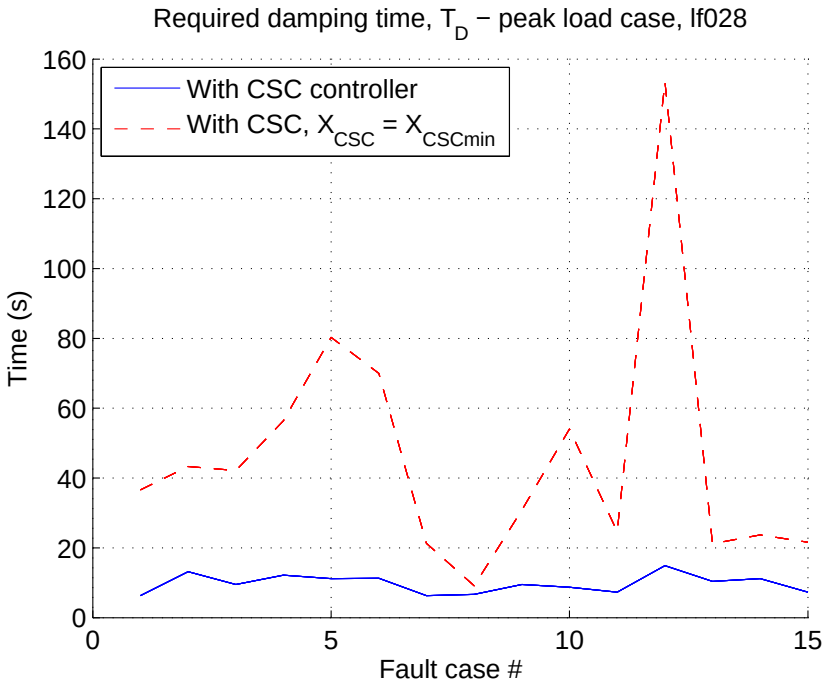

Figure 7.16: Twenty three-machine system with CSC in the peak load case (Lf028): Required time to damp line power oscillation below 30 MW p-p, T_D in contingencies 1-15 for system with full compensation of CSC and with CSC controller enabled.

In Fig. 7.16, the damping time, T_D for each fault in the peak load case is shown as the time after the fault it will take for the power oscillation on the CSC line to be reduced to below 15 MW in amplitude. T_D for the cases when the controller operates are results from time-domain simulations while the values given for the system when the degree of compensation of the line is fixed are approximate and calculated from the small-signal values of σ obtained in an eigenvalue analysis. The damping time of the oscillations is an appropriate parameter to study when judging the effectiveness of the discrete damping controller. In the peak load case, T_D for the studied faults range from 10 to 150 seconds for the case with full series compensation and from 6 to 15 seconds with the CSC controller enabled. *For the original system in the peak load case with no CSC, the mode exhibits small signal instability*

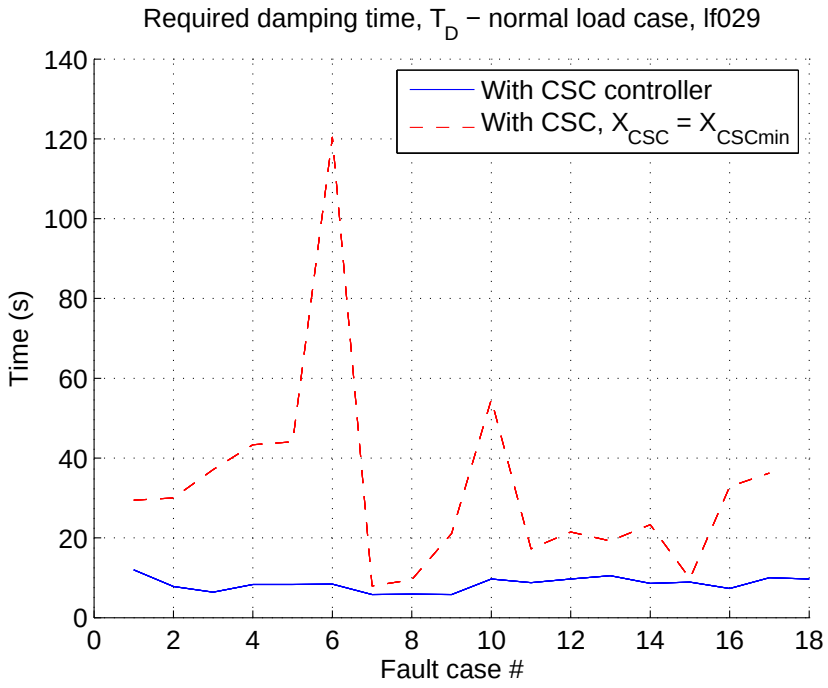

Figure 7.17: Twenty three-machine system with CSC in the normal load case (Lf029): Required time to damp line power oscillation below 30 MW p-p, T_D for contingencies 1-18 for system with full compensation of CSC and with CSC controller enabled. Due to small-signal instability in fault case 18 when the CSC controller is disabled, no value is given for this case

in most cases and the damping times cannot be defined. The damping times for fault cases 1-15 when the CSC controller is enabled are believed to be satisfactory from a system operation point of view.

In Fig. 7.17, the damping times for the critical mode in the normal load case are given. In the system with a fixed high degree of series compensation, the damping times range from 10 to 120 s, while they in the case with the CSC controller enabled range from 6 to 12 seconds. The damping times for the system with no CSC are in this case in the same range as those for the system with a fixed high level of compensation shown in the figure. It can

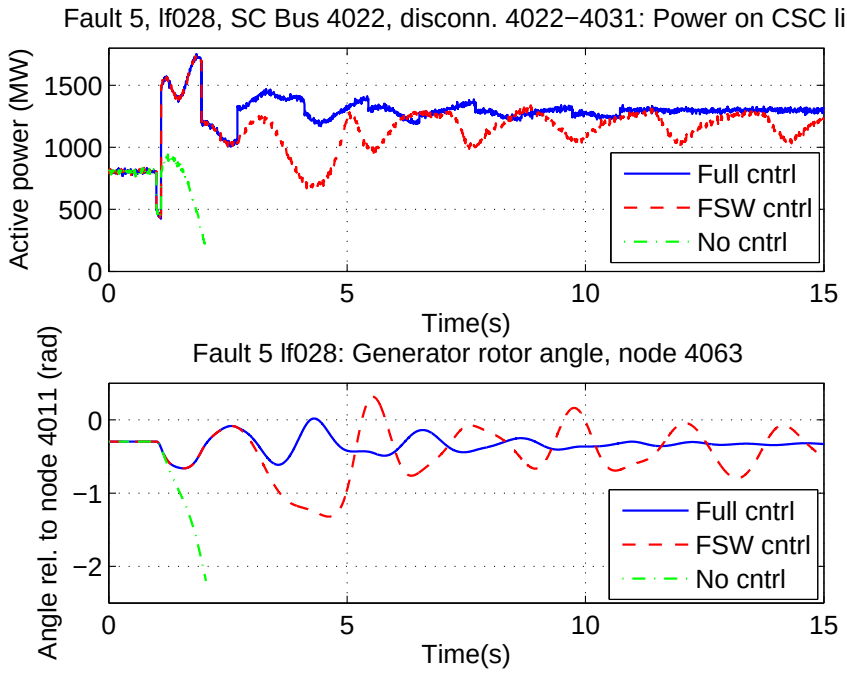

Figure 7.18: Twenty three-machine system with CSC in peak load case (Lf028): Time-domain simulations of Fault 5. Power on CSC line and angle of generator at node 4063 relative to slack node 4011.

be concluded that the CSC controller improves the damping to satisfactory values in all 18 contingencies in this mode of operation.

As an example of the controller behavior in the time-domain, results from the simulations of fault 5 are demonstrated in figures Fig. 7.18, Fig. 7.19 and Fig. 7.20. Fig. 7.18 shows the CSC line power in the peak load case as a function of time for the cases of no controlled series compensation (No cntrl), with a CSC using only the first-swing(transient) controller (FSW cntrl) and for the case of a CSC with the full controller enabled (Full cntrl). Note that the power values are those used as input to the controller, including simulated noise. For the same cases, the figure also shows the rotor angle of the generator at node 4063 located in the far south of the power system relative to the slack node 4011. This generator angle has a high participation

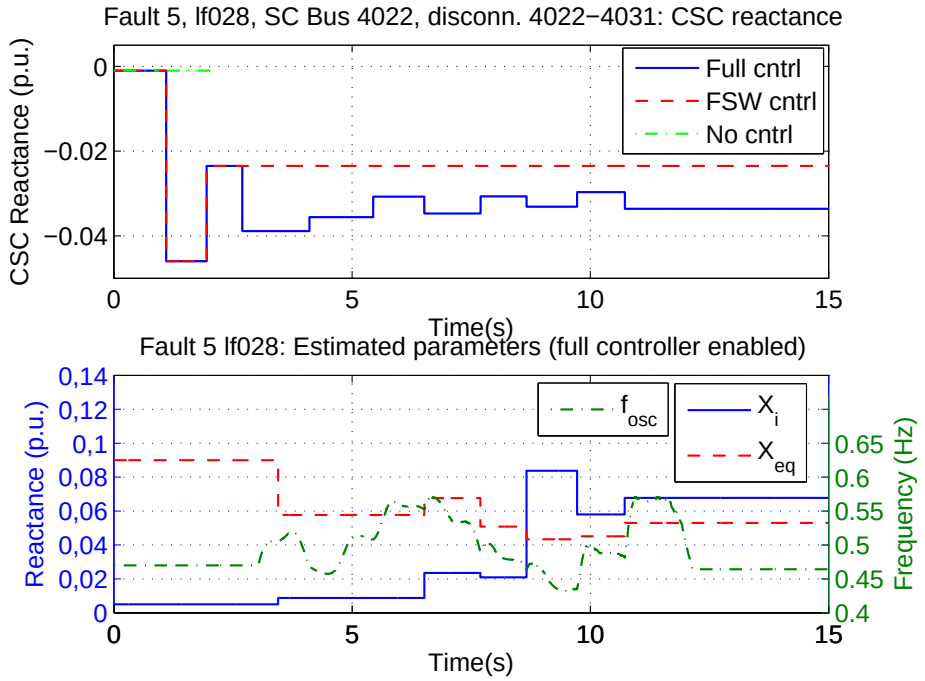

Figure 7.19: Twenty three-machine system with CSC in the peak load case (Lf028): Time-domain simulations of Fault 5. Inserted series reactance of the CSC unit and the estimated reactances X_i, X_{eq}, and the inter-area mode frequency f_{osc}.

factor with respect to the critical mode. It is seen from Fig. 7.18 that the system exhibits transient instability in the uncontrolled case. In the case where only the open loop response of the first-swing controller is enabled, the system remains transiently stable, but the oscillation is poorly damped. Finally, in the fully controlled case, the oscillation is damped at the same time as the power on the line is changed to the set-point 1300 MW. The CSC reactance versus time for the three cases is shown in Fig. 7.19 together with the estimated parameters of the system model.

The system response for the same fault in the normal loading condition (lf029) is plotted in Fig. 7.20. Here it can be noted that the power flow

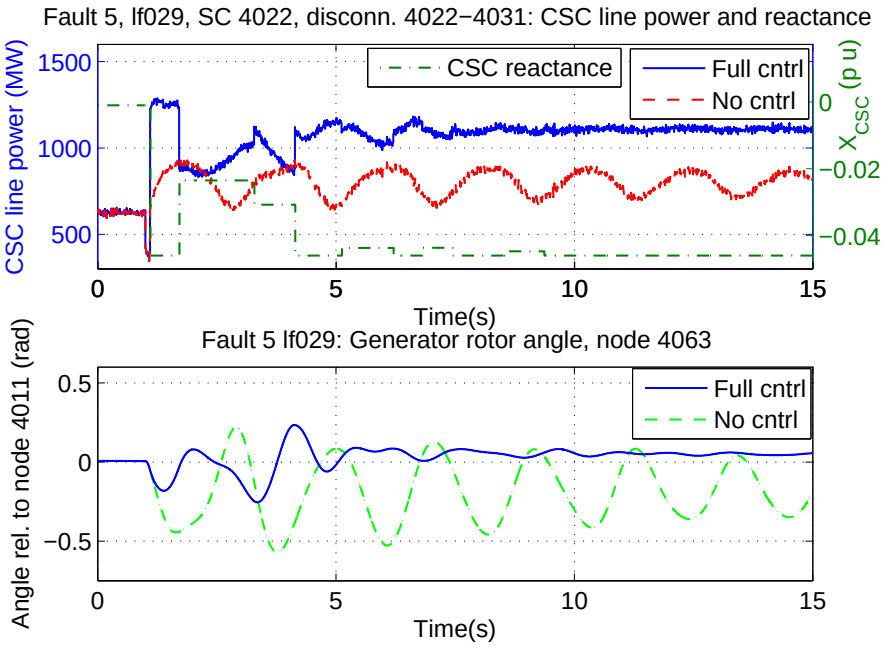

Figure 7.20: Twenty three-machine system with CSC in the normal load case (Lf029): Time-domain simulations of Fault 5. Power on the CSC line and the rotor angle of generator at node 4063 relative to slack node 4011.

set-point of 1300 MW cannot be reached and the CSC reactance settles at maximum capacitive compensation after the damping event.

As in the case of the study of the four-machine system, the fast power flow control feature of the controller shows good performance in this study. In this study, the power flow of the CSC line was generally stabilized within $\pm 2.5\%$ of the set-point value when the power flow was attainable given the limits of the CSC reactance. Also in this case, the controller was optimized for power oscillation damping.

7.3 DPFC controller results

7.3.1 Controller implementation

The controller for DPFC power oscillation damping, fast power flow control, and transient stability improvement was implemented in SIMPOW using the same controller structure as for the CSC controller described above. The PI-controller used for long term power flow control included in Fig. 6.2 was not included in the implementation and the tap setting of the PST was chosen manually before each simulation. The purpose of the studies was to verify the damping controller function during the first 10-20 seconds after a severe fault in the power system for different settings of the PST tap. The differences between the controller implementation for the DPFC and the CSC are mainly due to the different system models. This leads to differences in the estimation routines and the control laws used for damping and fast power flow control. The transient stability improvement control feature is the same in both implementations. Since the DPFC includes a TSSC which only can insert series reactance values according to the values attainable by combination of the switched reactance units in the configuration, the control signal was discretized in the implementation of the DPFC controller. Since the CSC is assumed to be able to insert series reactances which can be chosen arbitrarily within the operating range, such discretization is not necessary in the study of the CSC controller. As in the case of the CSC controller study, the dynamics of the TSSC have been neglected in this study. This can be done since the TSSC dynamics are much faster than the dynamics of the power oscillations subject to damping.

One very interesting fact that was discovered during testing of the DPFC estimator and damping controller is the following:

Given a certain change in the DPFC line reactance and certain step response data, the desired reactance steps, calculated by the controller in order to damp a certain oscillation will be exactly the same regardless of if the controller and estimator are based on the system model for CSC or if the model for DPFC is used.

This means that, assuming that the controller bases its action on previous estimation, it does not matter if the controller takes into account the phase shift of the PST or not. The reactance steps taken by the controller will be the same. However, the estimated parameters X_i and X_{eq} will be different depending of the chosen system model. This is not surprising since the phase angle shift of the PST will be seen as a different line reactance if the CSC system model is used, thereby directly changing the estimated parameters. This leads to that the damping controllers based on the CSC and DPFC system models will behave differently if they base their calculations on the same grid parameters X_i and X_{eq}. This is the case in the beginning of a damping sequence when no prior estimation of the parameters is available and a set of fixed "safe" values of the parameters are used. The controller based on the DPFC system model has then an advantage, since it uses the knowledge of the phase angle shift of the PST which may change during the controller operation together with the fixed initial values of the grid parameters to determine the first step in a damping sequence. The controller based on the CSC model does not take into account changes in the PST setting and makes use of the same initial grid parameters in all operating points. From a damping performance point of view, the usage of the DPFC system model can only be motivated due to this advantage. Once the controller bases its actions totally on previous estimations of the grid parameters, no difference will be seen between the two approaches.

7.3.2 Simulation results

Four-machine system

The four-machine system described in Fig. 7.1 was used to investigate the performance of the DPFC damping controller. An operation example for one particular contingency as well as the details of the study are given in Paper 5. Here, the results of the study are summarized.

In this study, a DPFC with three switched capacitive elements is placed in series with one of the interconnecting lines N8-N9 in the four machine system. The TSSC values were selected on a binary basis resulting in eight

allowed reactance values which are equidistant between zero and the maximum capacitive compensation $X_{TSSCmin}$ (which was chosen to be 2/3 of the inductive reactance of the DPFC line). The available TSSC reactance value closest to the desired reactance value of the controller was chosen at all times during the controller operation.

The PST was implemented as a Quadrature Booster which enables voltage phase angle shifts in the region [-15°, 15°]. In order to test the performance of the damping controller in different operating points, the four machine system was studied in the same four contingencies used for the study of the CSC controller at two different inter-area power transfer levels; a low inter-area transfer of 180 MW, and a high transfer case with 600 MW of transferred power. As in the CSC study, the PSS connected to the generators in the system were chosen to have a low gain to yield a system with a poorly damped inter-area mode. The studied contingencies were:

1. A 3-phase short circuit at node 8 cleared with no line disconnection after 200 ms.

2. A 3-phase short circuit at node 8 cleared by disconnection of one N8-N9 line in parallel to the CSC after 200 ms.

3. A 3-phase short circuit at node 8 cleared by disconnecting one of the N7-N8 lines after 200 ms.

4. A disconnection of load at node 7. ΔP=-250 MW ΔQ=-50 MVAr in the high transfer case and ΔP=-250 MW ΔQ=-100 MVAr in the low transfer case.

The CSC line short-term thermal overload limit was assumed to be in the range of 300-350 MW for the inter-area tie lines in the system. The post-fault contingency set-point for the fast power flow controller was set to 300 MW. The maximum inter-area power oscillation amplitude for each fault case, which is a measure of the severity of the contingencies is plotted in Fig. 7.21. It can be seen that Fault 1 yields the largest power oscillation amplitude with a peak-to-peak amplitude in the range of 400 MW for the high load case and 250 MW for the low-load case. The lowest power oscillation amplitudes are

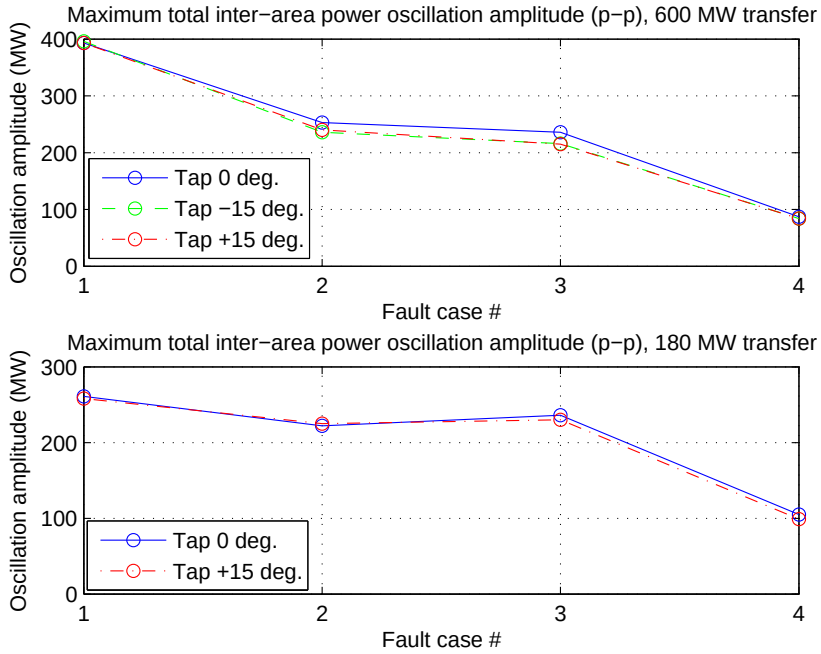

Figure 7.21: Four-machine system with DPFC, voltage dependent loads: Maximum total inter-area power oscillation amplitude with different tap settings of the PST for contingencies 1-4.

observed in Fault 4 with a peak-to-peak amplitude in the range of 100 MW in both cases.

The damping exponents (σ) for the different fault cases at different tap settings are shown in Fig. 7.22. Boosting tap levels, characterized by their advance in voltage phase angle are denoted with positive (+) angles and buck-mode phase shifts are conversely marked as negative (-) angles. No Cntrl. - values are the real part of the linearized system eigenvalues corresponding to the critical mode with the DPFC controller disabled. Cntrl. - values are calculated from time-domain simulations with the DPFC controller enabled by fitting a curve of the form $C * e^{\sigma t}$ (C and σ are constants, t is time) to the total power oscillation envelope. It can be seen that the damping of the system with no TSSC control is quite poor for all contingency situations, especially in the high-transfer case. The least damped os-

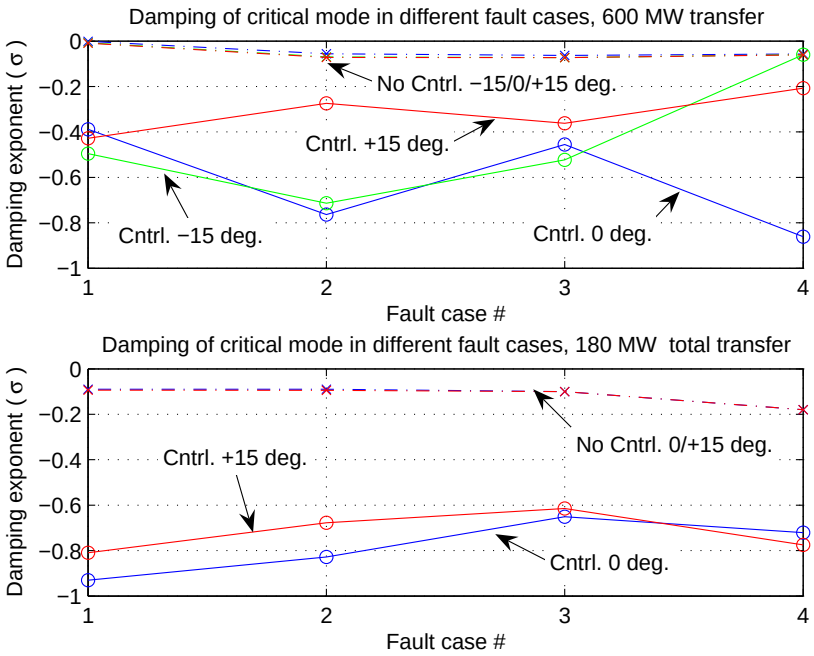

Figure 7.22: Four-machine system with DPFC, voltage dependent loads: Damping exponent σ of the critical mode with different tap settings of the PST for contingencies 1-4.

cillations are seen in Fault 1 where the damping is close to zero. With TSSC damping enabled, the system damping of the inter-area mode is significantly improved.

The damping time T_D, which is the time required after the clearance of each fault until the power oscillation on the DPFC line is damped below 10 MW in amplitude (peak-to-peak) for the two levels of inter-area power transfer and the different tap settings are given in Fig. 7.23 and Fig. 7.24. It can be seen that the damping time, T_D, with the controller enabled is in the range of 2 - 10 s in all cases except for the case with $\Delta\theta = -15°$ in the high-transfer case. This case will be discussed below. With no supplementary damping added, T_D is in the range of 8 - 1300 s in the high-power transfer case and in the range of 9 - 26 s in the low-power transfer case.

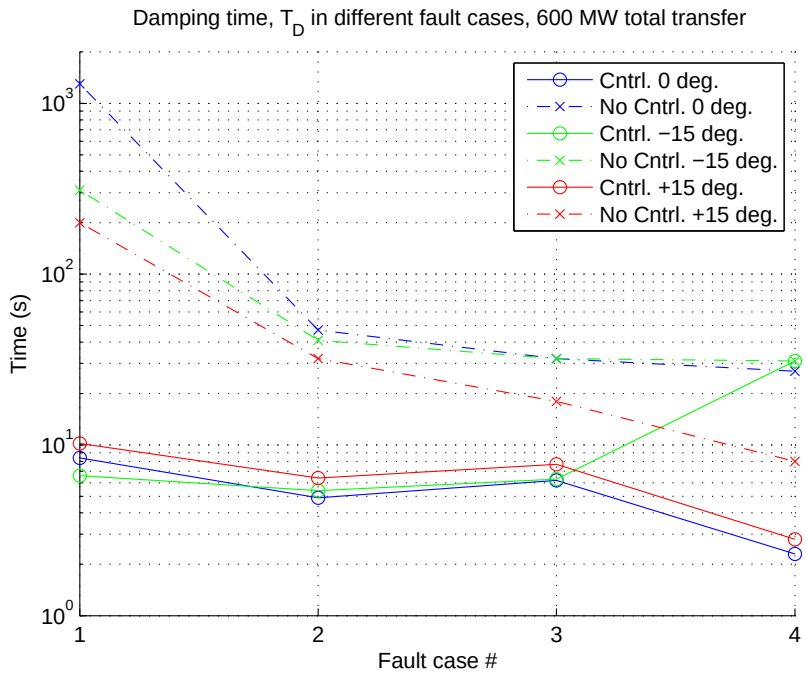

Figure 7.23: Four-machine system with DPFC, voltage dependent loads and total power transfer 600 MW: required time to damp the power oscillation on the line below 10 MW p-p, T_D with different tap settings of the PST for contingencies 1-4.

From the results presented in Figures 7.22, 7.23 and 7.24, two important observations can be made:

- There is a relation between the tap setting of the PST and the damping performance which is most prominent in the high power transfer case. In operating conditions characterized by large boosting (+) phase angles, the damping performance is degraded compared to buck (-) and zero (0) phase angle cases. One reason for this is that the observability of the oscillation mode in the power signal of the DPFC line decreases with increasing boosting phase shift leading to a reduced Signal-To-Noise (SNR) ratio of the controller input signal. Another reason is that the controllability of the mode from the TSSC increases

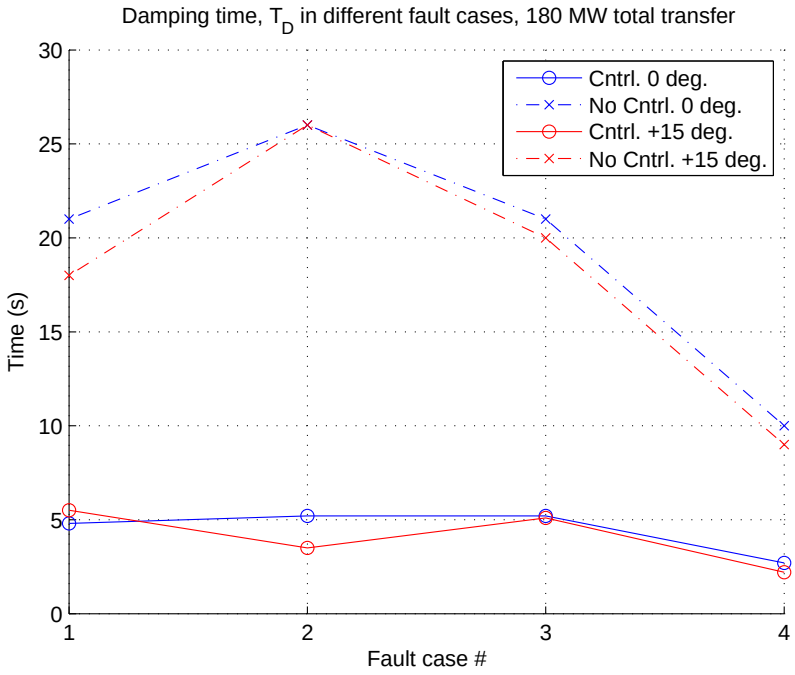

Figure 7.24: Four-machine system with DPFC, voltage dependent loads and total power transfer 180 MW: required time to damp the power oscillation on the DPFC line below 10 MW p-p, T_D with different tap settings of the PST for contingencies 1-4.

with boost angle, amplifying the effect of the control errors introduced by the discretization of the inserted series reactances. A third reason for the degradation is that the assumptions of linearity used in the derivation of the control laws are less accurate at high boosting angles. The degradation issue may affect how the DPFC should be operated regardless of which type of (linear) controller that is used for power oscillation damping. If a certain power oscillation damping performance is required, certain tap/power transfer configurations may not be allowed due to this issue. It should be pointed out that a controller utilizing remote signals for oscillation damping would probably not suffer from this degradation problem.

- In Fault 4 of the high-power transfer case at $\Delta\theta = -15°$, the DPFC does not improve the damping of the system. This is due to the fact that only discrete values of series reactance are available for power oscillation damping. In this fault case, the power oscillation is initially fairly small, and the controller demands changes in reactance which are smaller than the lowest available value given by the discretization. As a result, the controller will not insert any series reactance in the circuit and the damping will not be improved from its initial value.

Another important issue which has its origin in the discretization of the TSSC reactance is that it is important that the first step in a damping sequence, ($\Delta X_{initial}$) is always executed. Due to a low observability of the oscillation mode at the DPFC location, the desired first reactance step in a damping sequence may be smaller than the smallest step available from the group of switched reactances. Thus, $\Delta X_{initial}$ will be zero. Due to this, no estimation of grid parameters will occur and, provided that the power oscillation has an original positive damping, no damping improvement will be seen since no further action of the TSSC will be taken. A conservative setting of the initial grid parameters X_i and X_{eq} does not improve the situation since this will yield a desired first step which is comparably small and likely to be insufficient. One way to improve the controller performance in such cases would be to change the rule for choosing the TSSC reactance such that if the desired first step in a damping sequence is too small to give a change in the TSSC reactance by the "closest value" rule, the smallest reactance step in the right direction should still be executed. This would give the estimation process a chance to change the controller "gain" and improve the damping performance.

As in the case of the study of the CSC controller, the fast power flow control feature of the controller shows good performance in this study. The stationary error of the fast power flow controller was generally seen to be in the range of $\pm 2\% - \pm 3\%$ as in the case of the CSC controller. In one of the studied cases, the amplitude of the power oscillation was reduced below the set disabling limit of 10 MW p-p in the middle of a two-step damping sequence. As discussed for the CSC controller, this yields a larger stationary error of the fast power flow controller which in this case was about 10 %.

As in the case of the CSC controller, the DPFC controller was optimized for power oscillation damping which slightly degrades the power flow controller performance.

8 Conclusions and future work

Controllers for power oscillation damping, power flow control, and transient stability improvement by means of CSC and DPFC have been proposed in this thesis. The damping- and power flow controllers are adaptive and the transient controller is an open-loop scheme. All controllers require very little to be known about the power system where the device is placed as long as the basic system assumption of one dominating power oscillation mode is fulfilled. With these characteristics, the controllers provide an alternative to controllers based on full-scale system models, requiring only a small amount of system information and a short implementation time.

The proposed damping controller performance was studied in simulations of a four-machine test system with one poorly damped inter-area mode of oscillation. The system was studied in four different contingencies at two different inter-area power transfer levels. The damping of the inter-area mode was improved to acceptable levels in all the studied cases when the proposed controllers were used both with the CSC and the DPFC as the controllable device.

In the case of the DPFC controller, a performance degradation of the damping controller was observed at high boosting angles of the PST. This degradation is believed to be due to the changes in controllability and observability of the inter-area mode in the locally measured line power used as input to the controller. This problem is also expected to affect other types of damping controllers for the DPFC using locally measured signals as inputs.

Additionally, the four-machine test system was studied at very high levels of power transfer in order to determine the effectiveness of the proposed transient controller for the CSC. In this study, it was seen that it was possible

to increase the maximum inter-area power transfer by approximately 15 % when the proposed transient controller was used in addition to the damping controller compared to the system with only a damping controller.

The CSC controller performance has also been studied in simulations of a 23-machine system where the aim was to improve the damping of one inter-area power oscillation mode and to improve the transient stability of the system. The system was studied in 18 different contingencies in two different operation points, one with normal load and one with peak load. With the CSC controller disabled, the system exhibited small-signal instability in 9 of the 18 contingencies in the peak-load case. Additionally, the system was transiently unstable in 6 of the 18 studied faults in the peak load case. With the CSC controller, the system was transiently stable and the damping of the inter-area mode was improved to acceptable levels in 15 of the 18 fault cases. In the normal-load case, the system was initially transiently stable, but the damping of the inter-area mode was insufficient in many cases and the system showed small-signal instability in one case. With the CSC controller, the damping of the inter-area mode was improved to acceptable levels in all 18 contingencies.

Possible future work on the proposed controllers includes:

- Study the performance of the DPFC controller in the 23-machine system in a similar way as was done for the CSC controller.

- Investigate if it is possible to improve the DPFC damping controller performance in situations when the observability of the mode is low in the locally measured signals or the total power oscillation has a low magnitude. This may be done by making it mandatory for a first step in a damping sequence to be executed, even if the desired reactance change given by the controller is smaller than half of the smallest possible step magnitude given by the discrete reactance values of the TSSC. In this way, an estimation process could be initiated which may lead to an improved controller performance

- Study if the estimation process may be improved by applying non-linear estimation techniques to the step response data which is collected

during the damping sequence. The estimation process would then directly solve the full estimation problem given all the available data at each time step.

- Study if the quality of the grid parameter estimates can be improved if a linear estimation method of RLS type is used for parameter estimation.

- Investigate the controller performance in the presence of colored noise. This may be noise generated as harmonics by power electronic equipment connected in the power grid.

- Compare the performance of the developed controller and a continuous linear adaptive controller based on the same system model.

References

[1] P. Kundur, *Power System Stability and Control*. McGraw-Hill, 1994.

[2] G. Andersson, *Dynamic Phenomena in Power Systems*. Electric Power Systems, Royal Institute of Technology, Stockholm, Sweden, 2000.

[3] M. Ghandhari, *Dynamic Analysis of Power Systems - part II*. Electric Power Systems, Royal Institute of Technology, Stockholm, Sweden, 2006.

[4] L. Söder, *Statisk analys av Elsystem*. Electric Power Systems, Royal Institute of Technology, Stockholm, Sweden, 2005.

[5] N. G. Hindigorani and L. Gyugyi, *Understanding FACTS*. IEEE Press, 2000.

[6] H. Xie, L. Ängquist, and H. P. Nee, "Active Power Compensation of Voltage Source Converters with Energy Storage Capacitors," in *Proc. of IEEE PES Power Systems Conference & Exposition*, 2006.

[7] H. Xie, L. Ängquist, and H. P. Nee, "Impact of Energy Storage on System Performance under Fault Conditions." Proc. of CIGRÉ International Symposium on Transient Phenomena in Large Electric Power Systems, Zagreb, Croatia, April 2007.

[8] C. R. X.-P. Zhang and B. Pal, *Flexible AC Transmission Systems: Modelling and Control*. Springer, 2006.

[9] J. Verboomen, D. V. V. Hertem, P. H. Schavemaker, W. L. Kling, and R. Belmans, "Border-Flow Control by means of Phase Shifting

Transformers," in *Proc. of IEEE PowerTech*, 2007.

[10] A. Marianakis, M. Glavic, and T. van Cutsem, "Control of phase shifting transformers by multiple transmission system operators," in *Proc. of IEEE PowerTech*, 2007.

[11] E. W. Kimbark, "Improvement of System Stability by Switched Series Capacitors," *IEEE Trans. on Power Apparatus and Systems*, vol. PAS-85, February 1966.

[12] N. Ramarao and D. K. Reitan, "Optimal Control of Transients in a Power System," *Letter in Proceedings of the IEEE*, vol. 57, August 1969.

[13] N. Ramarao and B. Subramanyam, "Optimal Control of Electromechanical Transients in a third-order Power System Model," *Letter in Proceedings of the IEEE*, vol. 61, September 1973.

[14] D. N. Kosterev and W. J. Kolodziej, "Bang-Bang Series Capacitor Transient stability Control," *IEEE Trans. on Power Systems*, vol. 10, May 1995.

[15] J. Chang and J. H. Chow, "Time-Optimal Control of Power Systems Requiring Multiple Switchings of Series Capacitors," *IEEE Trans. on Power Systems*, vol. 13, May 1998.

[16] N. Yang, Q. Liu, and J. D. McCalley, "TCSC Controller Design for damping Interarea Oscillations," *IEEE Trans. on Power Systems*, vol. 13, November 1998.

[17] J. Sanchez-Gasca and J. H. Chow, "Power System Reduction to Simplify the Design of Damping Controllers for Interarea oscillations," *IEEE Trans. on Power Systems*, vol. 11, August 1996.

[18] N. Martins, F. G. Silva, and P. C. Pellanda, "Utilizing Transfer Function Modal Equivalents of Low-Order for the Design of Power Oscillation Damping Controllers in Large Power Systems," in *Proc. of IEEE PES General Meeting*, 2005.

[19] R. Majumder, B. C. Pal, C. Dofour, and P. Korba, "Design and Real-Time Implementation of Robust FACTS Controller for Damping Inter-Area Oscillation," *IEEE Trans. on Power Systems*, vol. 21, May 2006.

[20] B. Chaudhuri, R. Majumder, and B. C. Pal, "Application of Multiple-Model Adaptive Control Strategy for Robust Damping of Interarea Oscillations in Power System," *IEEE Trans. on Power Systems*, vol. 12, September 2004.

[21] M. Klein, G. J. Rogers, and P. Kundur, "A fundamental study of inter-area oscillations in Power Systems," *IEEE Trans. on Power Systems*, vol. 6, August 1991.

[22] R. Sadikovic, P. Korba, and G. Andersson, "Self-tuning Controller for Damping of Power System Oscillations with FACTS devices," in *Proc. of IEEE Power Engineering Society General Meeting*, 2006.

[23] L. Ängquist and C. Gama, "Damping algorithm based on phasor estimation," in *Proc. of IEEE Power Engineering Society Winter Meeting*, pp. 1160–1165, 2001.

[24] K. R. Padiyar and K. U. Rao, "Discrete Control of TCSC for Stability Improvement in Power Systems," in *Proc. of IEEE 4th Conf. on Control Applications*, 1995.

[25] D. N. Kosterev, W. Kolodziej, R. Mohler, and W. Mittelstadt, "Robust Transient Stability Control Using Thyristor-Controlled Series Compensation," in *Proc. of IEEE 4th Conf. on Control Applications*, 1996.

[26] M. H. Hague, "Improvement of First Swing Stability Limit by Utilizing full Benefit of Shunt FACTS devices," *IEEE Trans. on Power Systems*, vol. 19, November 2004.

[27] X. Zhou and J. Liang, "Overview of control schemes for TCSC to enhance the stability of power systems," in *Proc. of IEE Gener. Transm. Distr.*, 1999.

[28] H. Latorre, "TCSC and its application in the interconnection Colombia-Ecuador 230 kV," master thesis report, Royal Institute of Technology), 2002.

[29] P. Kundur, *Power System Stability and Control*, pp. 813–816. McGraw-Hill, 1994.

[30] CIGRÉ, "Long term dynamics - Phase II," final report, CIGRE, March 1995.

[31] O. Samuelsson, *Power Oscillation Damping - Structural aspects of controlling active power*. PhD thesis, LTH, Lund Institute of Technology, 1997.

A Parameter estimation in the DPFC system model

Here, the estimation relations and the power oscillation damping control laws for the extended DPFC system model in Fig. 6.1 are derived.

A.1 Estimation of the parameter X_{eq}

Initially, assume that the average total power transmitted between the grid areas is denoted by P_{tot0} and the average power on the DPFC line is denoted by P_{Xstat}. For convenience, the total reactance of the DPFC line is denoted by $X = X_{PST} + X_{TSSC} + X_{line}$. Let $\Delta\theta$ denote the *advancing (boost)* phase shift of the PST. In order to find an estimation relation for X_{eq}, the relation between the average power transmitted through the DPFC line and the inserted TSSC reactance is derived. Then,

$$P_{tot0} = \frac{U_{1j}U_{2j}}{X_{eq}}\sin(\theta) + \frac{U_{1j}U_{2j}}{X}\sin(\theta + \Delta\theta), \tag{A.1}$$

with

$$\theta = \theta_{1j} - \theta_{2j}. \tag{A.2}$$

The power through the controlled line can be expressed as

$$P_{Xstat} = \frac{U_{1j}U_{2j}}{X}\sin(\theta + \Delta\theta). \tag{A.3}$$

Differentiating Eq. A.1 and Eq. A.3 with respect to X leads to

$$0 = \frac{U_{1j}U_{2j}}{X_{eq}}\cos(\theta)\frac{d\theta}{dX} + \frac{dP_{Xstat}}{dX}. \tag{A.4}$$

Table A.1: Values of R for different values of θ and $\Delta\theta$.

θ	$\Delta\theta = -15°$	$\Delta\theta = +15°$
30	R=1.12	R=0.82
40	R=1.18	R=0.75
50	R=1.27	R=0.65
60	R=1.41	R=0.52
70	R=1.67	R=0.25

$$\frac{P_{Xstat}}{dX} = -\frac{U_{1j}U_{2j}}{X^2}\sin(\theta+\Delta\theta) + \frac{U_{1j}U_{2j}}{X}\cos(\theta+\Delta\theta)\frac{d\theta}{dX}, \tag{A.5}$$

Eliminating $d\theta/dX$ between Eq. A.5 and Eq. A.4 and rearranging gives

$$\frac{dP_{Xstat}}{dX} = \frac{-U_{1j}U_{2j}\sin(\theta+\Delta\theta)}{X^2 + X_{eq}X\cos(\theta+\Delta\theta)/\cos\theta}. \tag{A.6}$$

Using Eq. A.3, this simplifies to

$$\frac{dP_{Xstat}}{dX} = \frac{-P_{Xstat}}{X + X_{eq}\cos(\theta+\Delta\theta)/\cos\theta}. \tag{A.7}$$

If this differential equation in X is solved for the average power on the line $P_{Xstat}(X)$ it yields

$$P_{Xstat}(X_0+\Delta X) = P_{Xstat}(X_0)\frac{X_0 + X_{eq}\cos(\theta+\Delta\theta)/\cos\theta}{X_0 + \Delta X + X_{eq}\cos(\theta+\Delta\theta)/\cos\theta}. \tag{A.8}$$

Here the initial value of X is denoted X_0 and the change in the line reactance is given as ΔX. Here the ratio $R = cos(\theta+\Delta\theta)/cos(\theta)$ was assumed to be constant. If we assume that the PST gives maximum $\pm 15°$ in phase angle shift and that $\theta < 70°$ then R for different angle differences is given by Table A.1 below.

It can be seen that the assumption is valid if the steps in X produce small changes in the angle difference θ. The assumption fails when the steps give large changes in separation angle θ. The assumption is more accurate when the PST has a retarding angle. In order to improve the parameter estimation in the SIMPOW implementation, the separation angle θ before and after the estimation steps is calculated and the average value of the ratio R is used for the estimation.

This expression Eq. A.8 can be compared with the expression of the static step response for the system without the PST,

$$P_{Xstat}(X_0 + \Delta X) = P_{Xstat}(X_0) \left(\frac{X_{eq} + X_0}{X_{eq} + X_0 + \Delta X} \right). \quad \text{(A.9)}$$

It can be noted by comparing the expressions that the X_{eq} variable in Eq. A.9 is replaced by $X_{eq} \cos(\theta + \Delta\theta)/(\cos\theta)$ in the DPFC case.

The relation Eq. A.8 is used by the DPFC controller to determine the value of X_{eq} when the response in the line average power following a step in the TSSC reactance is known.

A.2 Estimation of the parameter X_i

As in the case of the derivation of the estimation relation for the system model with CSC it is interesting to derive the instantanous response of the transmitted power through the DPFC line. To this end, we can assume that the generator electrical angles are constant due to the large inertia. Using this assumption, the peak power transmitted through the line can be calculated. The DPFC system model can then be simplified to the one in Fig. A.1. Here the symmetry has been used to move X_{i1} and X_{i2} to the sending end side. This can be done when the concern is power flow calculations. In this system, the receiving generator voltage is connected directly to X_{eq} and to the right side of the PST. U_S, the sending end generator voltage, U_R, the receiving generator voltage and $U_{R\Delta}$, the receiving generator voltage phase shifted with $\Delta\theta$ are assumed to be constant voltages during the disturbance.

The system can be transformed using a Y-Δ transformation as in Fig. A.2.

This transformation gives

$$X_{SR\Delta} = X_i X \left(\frac{1}{X} + \frac{1}{X_i} + \frac{1}{X_{eq}} \right) = \left(X X_i + X X_{eq} + X_i X_{eq} \right) / X_{eq} \quad \text{(A.10)}$$

$$X_{RR\Delta} = X_{eq} X \left(\frac{1}{X} + \frac{1}{X_i} + \frac{1}{X_{eq}} \right) = \left(X X_i + X X_{eq} + X_i X_{eq} \right) / X_i. \quad \text{(A.11)}$$

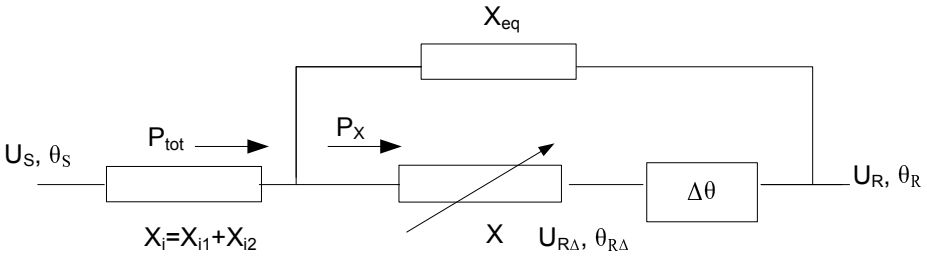

Figure A.1: Reduced DPFC system model.

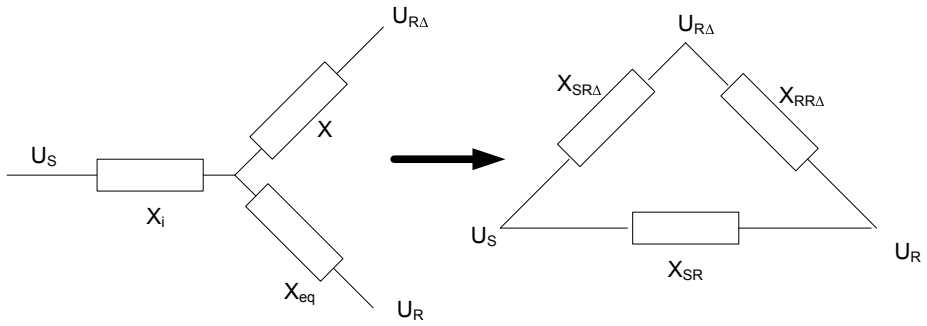

Figure A.2: Y-Δ transformation of reduced DPFC model.

The initial power on the controlled line can now be expressed as

$$P_X = \frac{U_{R\Delta} U_S \sin\theta_\Delta}{X_{SR\Delta}} + \frac{U_{R\Delta} U_R \sin(\Delta\theta)}{X_{RR\Delta}} \tag{A.12}$$

where $\theta_\Delta = \theta_S - \theta_{R\Delta}$ denotes the voltage angle between the U_S and $U_{R\Delta}$ nodes. If a step in X from X to X' is applied, $X_{SR\Delta}$ is changed accordingly from $X_{SR\Delta}$ to $X_{SR\Delta}$'. For the instantaneous response we can assume due to the inertia of the synchronous machines that θ_Δ and $\Delta\theta$ are constant. We also assume that the voltages at the generators are well controlled so that U_S, U_R and $U_{R\Delta}$ can be assumed to be constant. Eq. A.12 is valid both before and after the step in reactance, thus the power transmitted through the controlled line after the step can be expressed as

$$P'_X = \frac{U_{R\Delta} U_S \sin\theta_\Delta}{X'_{SR\Delta}} + \frac{U_{R\Delta} U_R \sin(\Delta\theta)}{X'_{RR\Delta}}. \tag{A.13}$$

Dividing Eq. A.13 with Eq. A.12 and rearranging yields

$$P'_X = P_X \frac{(XX_i + XX_{eq} + X_iX_{eq})}{(X'X_i + X'X_{eq} + X_iX_{eq})}, \tag{A.14}$$

which reduces to

$$P'_X = P_X \frac{X_{tot}(X + X_{eq})}{X'_{tot}(X' + X_{eq})} \tag{A.15}$$

with

$$X_{tot} = X_i + \frac{XX_{eq}}{X + X_{eq}}. \tag{A.16}$$

This expression is the same as the relation derived for the system model with no PST included. Eq. A.15 can be used to estimate the parameter X_i for a particular system once X_{eq} has been estimated from Eq. A.8.

B Derivation of the control law in the DPFC system model

In this section, the oscillation damping control law for the DPFC controller is derived. The goal of the derivation is to find a control law which ideally damps an oscillation and changes the power flow of the line to a specified value by means of two reactance changes separated in time by half an oscillation cycle. The idealized curve-forms of the line power and the total power are illustrated in Fig. 5.6. Provided that the parameters of the system have been established, the necessary reactance steps to damp an oscillation in two discrete steps can be calculated as follows:

Let the initial average power on the DPFC line be denoted by P_{Xstat0}. For convenience, the total reactance of the DPFC line is given by $X = X_{PST} + X_{TSSC} + X_{line}$ with denotations from Fig. 6.1. The initial value of X is X_0, the value after the first reactance step is X_1 and the final value is denoted X_2. Let $\Delta\theta$ denote the *advancing (boost)* phase shift of the PST. We assume that the grid parameters are known as X_i and X_{eq}.

The desired value of the total DPFC line reactance X_2 in order for the average power on the line to equal the given power set-point P_{Xsp} after the two steps can be calculated using Eq. A.8 so that

$$P_{Xsp}(X) = P_{Xstat0}\left(\frac{X_{eqEff} + X_0}{X_{eqEff} + X_2}\right) \tag{B.1}$$

with

$$X_{eqEff} = X_{eq}\frac{\cos(\theta_0 + \Delta\theta)}{\cos\theta_0}. \tag{B.2}$$

Here, $\theta_0 = \theta_{1j} - \theta_{2j}$, the initial average phase angle shift of the DPFC line can be calculated from

$$P_{Xstat0} = \frac{U_{1j} U_{2j} \sin(\theta_0 + \Delta\theta)}{X_0}, \tag{B.3}$$

where we assume the voltage magnitudes at the line ends U_{1j} and U_{2j} to equal the nominal voltage U_0.

Using the denotations given in Fig. 5.6, the power on the line after the first step can be calculated using Eq. 4.47 as

$$P_{Xp1} = P_{Xp0} \frac{X_{tot0}(X_0 + X_{eq})}{X_{tot1}(X_1 + X_{eq})} \tag{B.4}$$

with

$$X_{tot} = X_i + \frac{X X_{eq}}{X + X_{eq}}. \tag{B.5}$$

Here, the peak power on the DPFC line right before the first step is denoted P_{Xp0} and after the first step as P_{Xp1}, the "virtual" total reactance between grid areas calculated by Eq. B.5 is denoted by X_{tot0} initially and X_{tot1} following the first reactance step in the sequence.

The next oscillation peak value in the line power can be calculated as

$$P'_{Xp1} = (P_{Xstat1} - P_{Xp1})\, e^{\sigma T_{osc}/2} + P_{Xstat1}, \tag{B.6}$$

with

$$P_{Xstat1} = P_{Xstat0} \left(\frac{X_0 + X_{eqEff}}{X_1 + X_{eqEff}} \right) \tag{B.7}$$

as the average line power after the first step in reactance. Here it has been assumed that the oscillation is symmetric around the average power value, which is an assumption of linearity of the system equations. The real part of the oscillation mode eigenvalue is given by σ and the cycle time of the oscillation is given by T_{osc}.

In order to damp the oscillation completely after the second step in reactance, the instantaneous value of the active power after the step on the line

must equal the average value, which is known as P_{Xsp}. Hence, by using Eq. 4.47, the following relation can be obtained:

$$P_{Xsp} = P'_{Xp1} \frac{X_{tot1}(X_1 + X_{eq})}{X_{tot2}(X_2 + X_{eq})}. \tag{B.8}$$

Insertion of Eq. B.4 and Eq. B.6 in Eq. B.8 gives:

$$K = A_{p1} \left(\frac{X_{tot1}(X_1 + X_{eq})}{X_1 + X_{eqEff}} \right) - A_{p2} \tag{B.9}$$

with,

$$K = P_{Xsp} X_{tot2}(X_2 + X_{eq}), \tag{B.10}$$

$$A_{p1} = P_{Xstat0} \left(1 + e^{\sigma T_{osc}/2} \right) (X_0 + X_{eqEff}), \tag{B.11}$$

and

$$A_{p2} = P_{Xp0} X_{tot0}(X_0 + X_{eq}) e^{\sigma T_{osc}/2}. \tag{B.12}$$

Solving for X_1 yields the non-linear relation,

$$X_1 = \frac{X_{eqEff}(K + A_{p2}) - A_{p1} X_i X_{eq}}{A_{p1}(X_i + X_{eq}) - K - A_{p2}}. \tag{B.13}$$

Now, the requested reactance values after the first and second step in reactance are known as X_1 and X_2 respectively and the control law is complete.

List of Acronyms

ARX	Auto Regressive with eXternal input
CSC	Controlled Series Compensator
COI	Center Of Inertia
DPFC	Dynamic Power Flow Controller
FACTS	Flexible AC Transmission Systems
FSW	First Swing (transient)
GTO	Gate Turn Off thyristor
IGBT	Insulated Gate Bipolar Transistor
LQR	Linear Quadratic Regulator
MMAC	Multiple Model Adaptive Controller
MPC	Model Predictive Controller
PMU	Phasor Measurement Unit
POD	Power Oscillation Damping
PSDF	Phase Shifter Distribution Factor
PSS	Power System Stabilizer
PST	Phase-Shifting Transformer

RLS	Recursive Least Squares (estimator)
SC	Short Circuit
SNR	Signal to Noise Ratio
SPM	Structure Preserving Model
SSSC	Static Synchronous Series Compensator
STATCOM	Static Synchronous Compensator
SVC	Static Var Compensator
SVS	Static Var System
TCBR	Thyristor Controlled Braking Resistor
TCR	Thyristor Controlled Reactor
TCSC	Thyristor Controlled Series Capacitor
TCSR	Thyristor Controlled Series Reactor
TSSC	Thyristor Switched Series Capacitor
TSSR	Thyristor Switched Series Reactor
UPFC	Unified Power Flow Controller
VSC	Voltage Source Converter

List of Symbols

The symbols are listed in approximative order of appearance in the thesis.

H	Generator constant of inertia.	$[s]$
θ	Generator rotor angle relative to synchronously rotating frame.	$[rad.]$
ω	Angular frequency for rotor oscillations relative to synchronously rotating frame.	$[rad./s]$
ω_0	Nominal electrical AC frequency.	$[rad./s]$
D	Damping constant.	$[p.u./(rad./s)]$
P'_m	Mechanical power delivered to generator.	$[p.u.]$
P'_e	Electrical power delivered from generator.	$[p.u.]$
S_N	Nominal power rating of generator.	$[W]$
W_{kin}	Kinetical energy of generator and turbine at nominal speed.	$[J]$
ω_{0m}	Rated mechanical angular frequency of generator.	$[rad./s]$
J	Combined moment of inertia of generator and turbine.	

		$[kgm^2]$
x'_d	Generator transient d-axis reactance.	$[p.u.]$
x_l	Line reactance to infinite bus in one machine system.	$[p.u.]$
E	Generator voltage magnitude behind transient reactance.	$[p.u.]$
U	Node voltage magnitude.	$[p.u.]$
$\bar{E}$	Generator voltage phasor behind transient reactance.	$[p.u.]$
$\bar{I}$	Generator current phasor.	$[p.u.]$
$\bar{Y}$	Power system admittance matrix.	$[p.u.]$
$\bar{Y}_{ij}$	Admittance matrix element, row i, column j.	$[p.u.]$
$\bar{G}_{ij}$	Real part of admittance matrix element i, j.	$[p.u.]$
$\bar{B}_{ij}$	Imaginary part of admittance matrix element i, j.	$[p.u.]$
P_{L0}	Nominal value of active power load.	$[p.u.]$
Q_{L0}	Nominal value of reactive power load.	$[p.u.]$
U_L	Voltage magnitude at load node.	$[p.u.]$
U_{L0}	Nominal voltage magnitude at load node.	$[p.u.]$
$E'_{qk}\angle\delta$	Generator internal bus voltage at k:th node in SPM model.	

		$[p.u.]$
x'_{dk}	k:th generator node transient reactance, including transformer reactance in SPM model.	$[p.u.]$
$U_k \angle \theta$	Voltage at k:th node in SPM model.	$[p.u.]$
M_k	Inertia constant of k:th machine in SPM model.	$[s^2/rad]$
T'_{dok}	D-axis transient open-circuit time constant of k:th generator in SPM model.	$[s]$
x_{dk}	k:th generator node stationary reactance in SPM model.	$[p.u.]$
E_{fk}	EMF proportional to the field voltage of generator k in SPM model.	$[p.u.]$
$\Delta\theta_{ij}$	Phase shift angle of PST connected between nodes i and j.	$[rad.]$
$\xi_{\Delta\theta}$	Phase shifter distribution factor of PST connected between nodes i an j.	$[p.u./rad.]$
Z_T	PST series impedance.	$[p.u.]$
$\Delta\theta_{adv0}$	Ideal advancing phase angle shift of PST.	$[rad.]$
$\Delta\theta_{adv}$	Actual advancing phase angle shift of PST.	$[rad.]$
$\Delta\theta_{ret0}$	Ideal retarding phase angle shift of PST.	$[rad.]$
$\Delta\theta_{ret}$	Actual retarding phase angle shift of PST.	$[rad.]$
β	Phase retardation angle due to PST impedance.	

		$[rad.]$
X_{TCSC}	Reactive impedance of TCSC unit.	$[p.u.]$
X_L	Reactance of TCR branch in the TCSC.	$[p.u.]$
X_C	Reactance of the fixed capacitor in the TCSC unit.	$[p.u.]$
α	Firing delay angle for TCSC calculated from the zero crossing of the capacitor voltage.	$[rad.]$
P_{tot0}	Total average active power transmitted between two grid areas.	$[p.u.]$
ω_{osc}	Angular frequency of the inter-area oscillation.	$[rad./s]$
f_{osc}	Frequency of the inter-area oscillation.	$[Hz]$
T_{osc}	Period time for the inter-area oscillation.	$[Hz]$
P_m	Excess mechanical power in a grid area.	$[p.u.]$
P_e	Electrical power transmitted between two grid areas.	$[p.u.]$
Z	Impedance of the CSC line including the CSC device in the system model for CSC.	$[p.u.]$
Z_{i1}	Short circuit impedance of area 1 in the system model for CSC.	$[p.u.]$

Z_{i2}	Short circuit impedance of area 2 in the system model for CSC.	$[p.u.]$
Z_{eq}	Parallel impedance in the system model for CSC.	$[p.u.]$
X_i	Total series reactance in the system model for CSC and DPFC.	$[p.u.]$
X_{i1}	Series reactance of area 1 in the system model for CSC and DPFC.	$[p.u.]$
X_{i2}	Series reactance of area 2 in the system model for CSC and DPFC.	$[p.u.]$
X_{eq}	Parallel reactance in the system model for CSC and DPFC.	$[p.u.]$
X	Reactance of the CSC or DPFC line in the system model including the CSC or DPFC device reactance.	$[p.u.]$
X'	Reactance of the CSC or DPFC line in the system model including the CSC or DPFC device reactance after a certain change in line reactance.	$[p.u.]$
U_1	Voltage magnitude at machine equivalent of area 1 in the CSC or DPFC system model.	$[p.u.]$

U_2	Voltage magnitude at machine equivalent of area 2 in the CSC or DPFC system model. $[p.u.]$
θ_1	Voltage phase angle at machine equivalent of area 1 in the CSC or DPFC system model. $[rad.]$
θ_2	Voltage phase angle at machine equivalent of area 2 in the CSC or DPFC system model. $[rad.]$
$U_1 j$	Voltage magnitude at CSC/DPFC line end 1 in the CSC or DPFC system model. $[p.u.]$
$U_2 j$	Voltage magnitude at CSC/DPFC line end 2 in the CSC or DPFC system model. $[p.u.]$
$\theta_1 j$	Voltage phase angle at CSC/DPFC line end 1 in the CSC or DPFC system model. $[rad.]$
$\theta_2 j$	Voltage phase angle at CSC/DPFC line end 2 in the CSC or DPFC system model. $[rad.]$
P_X	Instantaneous power transmitted through the CSC/DPFC line. $[p.u.]$
P'_X	Instantaneous power transmitted through the CSC/DPFC line after a certain change in the line reactance. $[p.u.]$
P_{Xstat}	Average power (averaged over a full oscillation cycle) transmitted through the CSC/DPFC line. $[p.u.]$
P'_{Xstat}	Average power (averaged over a full oscillation cycle) transmitted through the CSC/DPFC line after a certain change in the line reactance. $[p.u.]$

X_{tot}	Total reactance between machine representations in CSC system model or "virtual" total reactance in DPFC system model.	$[p.u.]$
X'_{tot}	Total reactance between machine representations in CSC system model or "virtual" total reactance in DPFC system model after a certain change in the line reactance.	$[p.u.]$
ΔX	Magnitude of a step change in line reactance performed by CSC or DPFC unit.	$[p.u.]$
P_{av}	Average value of the line power estimated by the RLS.	$[p.u.]$
$\Delta \bar{P}$	Phasor describing the power oscillation estimated by the RLS in the synchronously rotating frame.	$[p.u.]$
ΔP_D	Real part of $\Delta \bar{P}$.	$[p.u.]$
ΔP_Q	Imaginary part of $\Delta \bar{P}$.	$[p.u.]$
ω_{CO}	Cut off frequency of the RLS algorithm.	$[rad/s]$
θ_{stat}	Steady-state voltage phase angle between the machines in the CSC system model around which the system equations are linearized.	$[rad.]$
θ'_{stat}	Steady-state voltage phase angle between the machines in the CSC system model around which the system equations are linearized after a certain change in the line reactance.	$[rad.]$

σ	Real part of the eigenvalue corresponding to the inter-area oscillation mode in the system model for the CSC and DPFC.	$[rad/s]$
$\Delta\theta$	Ideal phase angle shift of PST in system model (positive when advancing).	$[deg./rad.]$
X_{line}	Reactance of the DPFC line not including the DPFC itself.	$[p.u.]$
X_{PST}	The tap-dependent series reactance of the PST.	$[p.u.]$
θ_0	The steady-state voltage phase angle difference between the DPFC line ends before a step in the TSSC reactance.	$[rad.]$
θ_{av}	The average of the steady-state voltage phase angle differences between the DPFC line ends before and after a step in the TSSC reactance.	$[rad.]$
X_{eqEff}	A transformed "effective" version of the parallel reactance X_{eq} in the DPFC system model.	$[p.u.]$
P_{Xsp}	Post-contingency set-point for the fast power flow controller used in the CSC and DPFC controller.	$[p.u.]$
X_0	Initial value of the CSC or DPFC line reactance including the controllable device.	$[p.u.]$
X_1	Value of the CSC or DPFC line reactance including the controllable device after the first step in a two-step damping sequence.	$[p.u.]$

X_2 Value of the CSC or DPFC line reactance including the controllable device after the second step in a two-step damping sequence. $[p.u.]$

X_{tot0} Total initial reactance between machine representations in CSC system model or "virtual" total reactance in DPFC system model. $[p.u.]$

X_{tot1} Total reactance between machine representations after the first step in a damping sequence for the CSC or DPFC controller. $[p.u.]$

X_{tot2} Total reactance between machine representations after the second step in a damping sequence for the CSC or DPFC controller. $[p.u.]$

P_{Xstat0} Initial value of the average power (averaged over a full oscillation cycle) on the DPFC line when a damping sequence is started. $[p.u.]$

P_{Xstat1} Value of the average power (averaged over a full oscillation cycle) on the DPFC line after the first step in a damping sequence. $[p.u.]$

P_{p0} Instantaneous value of the total inter-area power before the first step in a CSC damping sequence. $[p.u.]$

P_{p1} Instantaneous value of the total inter-area power after the first step in a CSC damping sequence. $[p.u.]$

P'_{p1} Value of the estimated instantaneous total inter-area power before the second step in a CSC damping sequence. $[p.u.]$

P_{Xp0} Value of the instantaneous CSC or DPFC line power before the first step in a CSC or DPFC damping sequence.

[$p.u.$]

P_{Xp1} Value of the instantaneous CSC or DPFC line power after the first step in a CSC or DPFC damping sequence.

[$p.u.$]

P'_{Xp1} Value of the estimated instantaneous CSC or DPFC line power before the second step in a CSC or DPFC damping sequence. [$p.u.$]

ΔX_1 First desired reactance step in a two-step damping sequence determined by the DPFC or CSC controller.[$p.u.$]

ΔX_2 Second desired reactance step in a two-step damping sequence determined by the DPFC or CSC controller.

[$p.u.$]

ΔX_{tot} Change in the total reactance between areas in the system model due to a change in the controlled line reactance.

[$p.u.$]

δ Voltage phase angle difference between the sending and receiving areas in a COI reference frame. [$p.u.$]

δ_r Voltage phase angle of the receiving area in a COI reference frame. [$p.u.$]

δ_s Voltage phase angle of the sending area in a COI reference frame. [$p.u.$]

$P_{post}(\delta)$ Post-fault $P - \delta$ dependence used for transient stability assessment. [$p.u.$]

$P_{postFC}(\delta)$ Post-fault $P - \delta$ dependence with full series compensation of the CSC or DPFC device. [$p.u.$]

$P_{postHC}(\delta)$	Post-fault $P-\delta$ dependence with half of the maximum capacitive series reactance of the CSC or DPFC device used.	$[p.u.]$
$P_{pre}(\delta)$	Pre-fault $P-\delta$ dependence used for transient stability assessment.	$[p.u.]$
$P_{fault}(\delta)$	$P-\delta$ dependence during the fault used for transient stability assessment.	$[p.u.]$
P_{mPost}	Post-fault excess mechanical power in the grid area transmitting power.	$[p.u.]$
P_{mPre}	Pre-fault excess mechanical power in the grid area transmitting power.	$[p.u.]$
X_{CSC}	CSC reactance value determined by complete CSC controller.	$[p.u.]$
X_{TSSC}	TSSC reactance value determined by complete CSC controller.	$[p.u.]$
X_{CSCmin}	Minimum reactance value (maximum capacitive reactance) of CSC unit.	$[p.u.]$
X_{CSClim}	Maximum reactance value (minimum capacitive reactance) of CSC unit during oscillation damping different from the physical limit of the device.	$[p.u.]$
X_{POD}	POD contribution to X_{CSC} or X_{TSSC}.	$[p.u.]$
X_{FSW}	Transient stability contribution to X_{CSC} or X_{TSSC}.	$[p.u.]$

X_{PI}	Long term power flow control contribution to X_{CSC} or X_{TSSC}.	$[p.u.]$
P_{ref}	Reference value for the line power flow provided to the CSC or DPFC controller.	$[p.u.]$
I_X	CSC or DPFC line RMS current.	$[p.u.]$
γ	Weight factor used in the estimation process for X_i and X_{eq}.	$[-]$
Z_{im}	Imaginary part of the rotating phasor representing the line power oscillation estimated by the RLS estimator.	$[p.u.]$
Z_{re}	Real part of the rotating phasor representing the line power oscillation estimated by the RLS estimator.	$[p.u.]$
P_{av}	Average value of the line power estimated by the RLS estimator.	$[p.u.]$
T_D	Time after a fault until the line power oscillation has an amplitude which is lower than a certain value.	$[s]$
$\Delta X_{initial}$	Actual first reactance step in a damping sequence of the DPFC controller.	$[p.u.]$
R	Term relating X_{eqEff} to X_{eq} in the DPFC system model.	$[p.u.]$
U_S	Voltage magnitude of the sending area machine representation in the derivation of estimation relations in the DPFC system model.	$[p.u.]$

U_R	Voltage magnitude of the receiving area machine representation in the derivation of estimation relations in the DPFC system model. $[p.u.]$
$U_{R\Delta}$	Voltage magnitude of node $R\Delta$ in the derivation of estimation relations in the DPFC system model. $[p.u.]$
θ_S	Voltage phase angle of the sending area machine representation in the derivation of estimation relations in the DPFC system model. $[p.u.]$
θ_R	Voltage phase angle of the receiving area machine representation in the derivation of estimation relations in the DPFC system model. $[p.u.]$
$\theta_{R\Delta}$	Voltage phase angle of node $R\Delta$ in the derivation of estimation relations in the DPFC system model. $[p.u.]$
θ_Δ	Voltage phase angle difference between node S and node $R\Delta$ in the derivation of estimation relations in the DPFC system model. $[p.u.]$
$X_{SR\Delta}$	Initial equivalent reactance between between node S and node $R\Delta$ in the Δ-configuration of the DPFC system model. $[p.u.]$
$X_{RR\Delta}$	Initial equivalent reactance between node R and node $R\Delta$ in the Δ-configuration of the DPFC system model. $[p.u.]$
$X'_{SR\Delta}$	Equivalent reactance between node S and node $R\Delta$ in the Δ-configuration of the DPFC system model after a change in the DPFC line reactance. $[p.u.]$

$X'_{RR\Delta}$ Equivalent reactance between node R and node $R\Delta$ in the Δ-configuration of the DPFC system model after a change in the DPFC line reactance.

$[p.u.]$

X_{SR} Initial equivalent reactance between node S and node R in the Δ-configuration of the DPFC system model.

$[p.u.]$